Nanopartículas magnéticas para aplicaciones biomédicas

Sonia García Jimeno

UNIVERSITAT DE BARCELONA

FACULTAT DE FARMÀCIA

DEPARTAMENT DE FISICOQUÍMICA

NANOPARTÍCULAS MAGNÉTICAS PARA APLICACIONES BIOMÉDICAS

Sonia García Jimeno
Barcelona, 2012

UNIVERSITAT DE BARCELONA

FACULTAT DE FARMÀCIA

DEPARTAMENT DE FISICOQUÍMICA

Programa de Doctorado: “Biotecnología”

Nanopartículas magnéticas para aplicaciones biomédicas

Memoria presentada por Sonia García Jimeno para optar al grado de doctor por la Universidad de Barcelona

Director: Doctoranda:

Joan Estelrich Latrás Sonia García Jimeno

Barcelona, 2012

“Entre libremente, por su propia voluntad,

y deje parte de la felicidad que trae”

A mi familia

Por estar siempre ahí

AGRADECIMIENTOS

La lectura de esta tesis cierra una etapa no solo académica en mi vida. Es un buen momento de mirar hacia atrás, hacer recuento, y agradecer a todas las personas que han contribuido directa o indirectamente en la realización de este trabajo. A ellos están dedicadas estas líneas.

En primer lugar al Dr. Joan Estelrich; director, gracias por apoyarme a lo largo de estos 5 años, por la acogida, el cariño y por haber confiado en mí desde el primer momento y haber sido persistente en conseguirme un futuro.

Gracias a todos los profesores del departamento de Fisicoquímica de la facultad de Farmacia, donde he pasado la mayor parte de mi doctorado, por el buen trato, la ayuda y las sugerencias que me han prestado en muchos momentos, y en especial, a la Dra. María Antonia Busquets, por su cariño, apoyo e interés tanto en el terreno científico como en el personal.

A todos mis compañeros de departamento pero en especial a: Mari, Patricia, Joana, Lucyanna y Eli. Chicas, gracias por todas las alegrías, las lágrimas, los nervios… en definitiva, todos los momentos que hemos compartido. Gracias por haber estado ahí, por la paciencia, por los consejos, porque el haberos conocido es otra de las razones por las cuales ha merecido la pena todo este tiempo… GRACIAS.

Al Dr. Josep Queralt y a la Dra. Elvira Escribano, por todos los ratos que hemos pasado en el estabulario, por la paciencia, por las clases de jardinería, por enseñarme tanto.

Al Dr. José Callejas y Dr. Sándalo Roldán de la universidad de Granada; al Dr. Lorenzo Leija y Dr. Arturo Vera del Cinvestav, Mexico, quisiera agradecerles por haber hecho mis estancias en sus respectivos institutos tan provechosas y agradables.

También me gustaría agradecer todo el apoyo recibido de mi grupo NanoUp, en el recorrido final de esta tesis, por el consuelo, el ánimo y los consejos.

Las últimas líneas las voy a dedicar a aquellas personas que siempre han estado ahí, en los buenos y malos momentos, esa es mi familia… Sin ellos y sin su apoyo constante en todas mis decisiones, no hubiera sido posible llegar hasta aquí. Espero que se sientan orgullosos de mí.

A todos amigos de Barcelona por la alegría, el cariño, palabras de ánimo en los momentos más difíciles y sobre todo por hacerme sentir que en Barcelona tengo a otra nueva familia.

A mis amigos de Donostia y León, por seguir estando ahí y seguir haciéndome partícipe de vuestras vidas, a pesar de la distancia.

A mis padres y hermanos, sois mi vida mi apoyo, los que me habéis enseñado a trabajar y a luchar por las cosas, los que me habéis inculcado unos valores de los que me siento muy orgullosa. Gracias a vosotros he conseguido todo lo que soy. A mis sobrinas Eva y María, por alegrarme la vida.

Índice

1. Introducción

1. Introducción

1.1. Nanotecnología

La nanotecnología constituye la base de la próxima revolución tecnológica, es la continuación de las revoluciones industriales surgidas en los tres últimos siglos: la Primera Revolución Industrial aparecida alrededor de 1750 con la introducción de la máquina de vapor y la obtención del acero, y la Segunda Revolución Industrial, que empezó a finales del s. XIX, como consecuencia de la introducción de la electricidad a escala industrial. Más recientemente, se ha producido la Revolución de la Información, caracterizada por el desarrollo de los sistemas de computación y del desarrollo de internet. Como el desarrollo de los circuitos integrados a gran escala empleados en los procesos de información depende de la reducción del tamaño hasta una escala nanométrica de los componentes individuales de los circuitos, la Revolución de la Información se ha convertido en la Revolución del mundo nanométrico o sea en la Nanotecnología. La nanotecnología es el estudio, diseño, creación, manipulación y aplicación de materiales, aparatos y sistemas funcionales a través del control de la materia a escala nano, así como la explotación de determinados fenómenos y propiedades de la materia a esta escala (1-100 nm). Las nanopartículas son partículas con dimensiones comprendidas entre las moléculas y las estructuras microscópicas (Figura 1). Cuando se manipula la materia a una escala tan minúscula como son los átomos y las moléculas, la materia presenta fenómenos y propiedades totalmente nuevos. En concreto, las propiedades físicas de las nanopartículas son muy distintas de las que se observan en un sólido de tamaño macroscópico con la misma composición química. Así, la investigación del comportamiento de la materia a escala nanométrica abre una prometedora perspectiva de nuevos conocimientos y de aplicaciones en todos los campos científicos y/o tecnológicos. En la vanguardia de estas aplicaciones se encuentran las relacionadas con las Ciencias de la Salud: nanopartículas como sistemas de diagnóstico y de administración de fármacos. Vistas como materiales, las nanopartículas son tan pequeñas que exhiben características no observables en estructuras más grandes (incluso después de alcanzar tamaños de 100 nm); vistas como moléculas, son tan grandes que proporcionan acceso al reino del comportamiento cuántico, que no sería accesible de otra manera [Akbarzadeh et al. 2012].

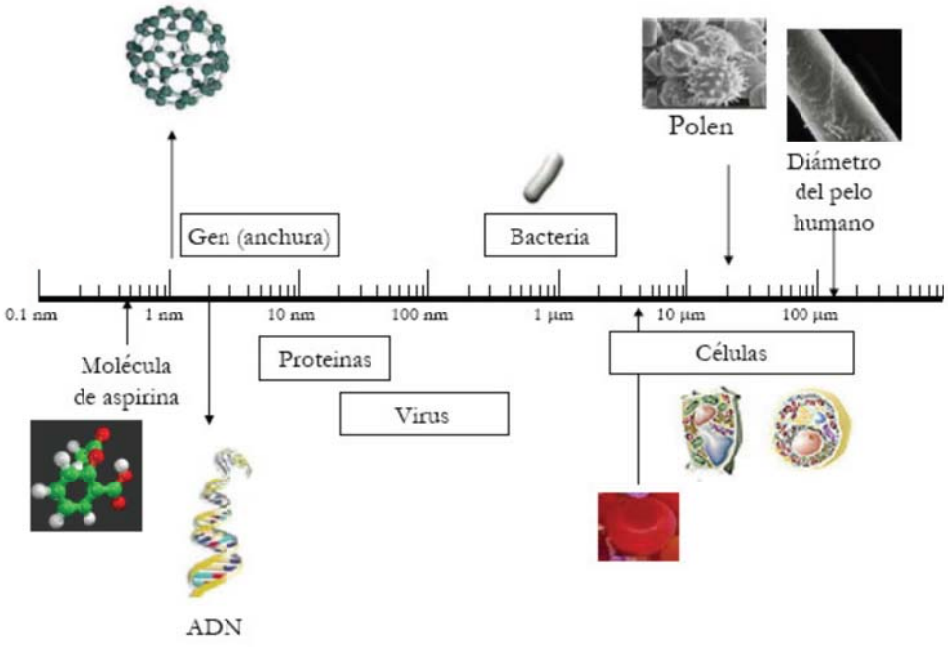

Figura 1. Las nanopartículas presentan un tamaño comprendido entre los organismos micrométricos y las moléculas (Roca 2009).

1.2. Nanopartículas magnéticas

Un tipo de nanopartícula que ha suscitado un elevado interés son las nanopartículas magnéticas (NPMs), nanopartículas que pueden ser manipuladas bajo la influencia de un campo magnético externo (Leslie-Pelecky y Rieke, 1996). Las NPMs están formadas generalmente por elementos magnéticos, tales como hierro, níquel, cobalto y sus óxidos. Presentan numerosas aplicaciones en biotecnología, biomedicina, ciencia de materiales, ingeniería y protección del medio ambiente. Sin embargo, un problema inevitable asociado con las partículas de este tamaño es su inestabilidad intrínseca que se manifiesta a lo largo del tiempo. Las partículas tienden a formar aglomerados a fin de reducir la energía asociada con la elevada relación área superficial/volumen propia de las partículas a escala nano. Además, las partículas sin recubrimiento son muy activas químicamente, y se oxidan fácilmente en el aire, produciendo una pérdida de magnetismo y de su capacidad de dispersarse. En la mayoría de las aplicaciones es, por lo tanto, crucial desarrollar estrategias de protección, durante o después de la síntesis, para estabilizar químicamente las partículas magnéticas contra la degradación. Estas estrategias comprenden la inserción o el recubrimiento con especies orgánicas, tales como tensioactivos o polímeros, o recubriendo con capas inorgánicas, como la sílice o el carbón. Cuando las partículas magnéticas estabilizadas se pueden dispersar fácilmente en un fluido, se ha formado un ferrofluido (Rosenweig 2002; Lu et al. 2007). Las aplicaciones industriales de las nanopartículas magnéticas cubren un amplio espectro. Entre estas, se puede mencionar el uso de ferrofluidos como tintas

magnéticas, sellos magnéticos en motores, instrumentos para memoria óptica, giroscopios, unidades de refrigeración magnética, etc. Cada aplicación potencial de las NPMs requiere tener propiedades diferentes. Por ejemplo, en las aplicaciones de almacenamiento de datos, las partículas requieren poseer un estado magnético estable y cambiante para representar bits de información que no se vean afectados por fluctuaciones de temperatura.

Para usos biomédicos, es necesario que las partículas magnéticas sean estables en agua a pH 7 y, también, en un entorno fisiológico. La estabilidad coloidal del fluido dependerá de la carga y de la química de la superficie, que dará lugar a repulsiones estéricas y/o culombianas. Otro factor importante son las dimensiones de las partículas, que deben ser suficientemente pequeñas para evitar o, como mínimo, enlentecer la precipitación [Akbarzadeh et al. 2012].

1.3. Comportamiento magnético

El comportamiento magnético de un material depende básicamente de los electrones de los átomos que lo constituyen, en concreto del número de electrones desapareados que posea cada átomo, así como del orbital en el que se encuentren. Los efectos magnéticos son causados por los movimientos de aquellas partículas que poseen masa y cargas eléctricas. Una partícula cargada eléctricamente crea, cuando gira, un dipolo magnético, el llamado magnetrón. Al aplicar un campo magnético externo al material, los dipolos magnéticos se ordenan con el campo dando lugar a un momento magnético dentro del material. Un electrón presenta dos tipos de momentos angulares: el momento de orbital y el momento de espín. Ambos pueden interactuar como cualquier par de dipolos y producir un acoplamiento espín-orbital. De las características de este acoplamiento surgen las propiedades magnéticas de los átomos y las moléculas, y los materiales se clasifican según la respuesta a un campo magnético externo en cinco formas básicas de magnetismo: *diamagnetismo*, *paramagnetismo*, *ferromagnetismo*, *antiferromagnetismo* y *ferrimagnetismo* (Cullity 1972; Jilles 1991).

En presencia de un campo magnético aplicado externamente, la corriente atómica creada por el movimiento orbital de los electrones se opone al campo aplicado. Todos los materiales muestran esta repulsión débil como respuesta a un campo magnético, y esta propiedad es la que se conoce como diamagnetismo. Un ejemplo de material diamagnético es el agua y las proteínas (Pankhurst et al. 2003). Como ya se ha indicado, el diamagnetismo es muy débil, y, por consiguiente, cualquier otra forma de comportamiento magnético que el material pueda poseer supera, generalmente, los efectos de la corriente generada por el movimiento de los electrones. En términos de la configuración electrónica, el diamagnetismo se observa en aquellos materiales que tienen completas las subcapas electrónicas, hecho que comporta que los momentos

magnéticos estén apareados y, en conjunto, unos se contrarrestan con los otros. Los materiales diamagnéticos tienen una susceptibilidad magnética negativa ($\chi < 0$), y repelen débilmente un campo magnético aplicado (Figura 3, color rojo). La susceptibilidad magnética es una constante de proporcionalidad adimensional que indica el grado de magnetización en respuesta a un campo aplicado. Matemáticamente, $\chi = M/H$, donde M és la magnetización del material (el momento dipolar magnético por unidad de volumen) y H es la fuerza del campo magnético, ambos expresados en A m^{-1} (Pankhurst et al. 2003).

El resto de comportamientos magnéticos se observan en materiales que tienen algún que otro electrón desapareado en sus capas atómicas, a menudo en las capas *3d* o *4f* de cada átomo. Los materiales cuyos momentos magnéticos atómicos no están apareados muestran paramagnetismo; en éstos, el momento magnético es diferente de cero y adquieren una magnetización cuando se encuentran en un campo magnético (Figura 3, color verde). Un ejemplo de este comportamiento es la hemoglobina, proteína que posee en su interior un ión hierro con electrones desapareados, pero que por encontrarse tan lejos de otros iones hierro no puede interaccionar con ellos (Pankhurst et al. 2003). Las dos propiedades que definen al paramagnetismo son: una susceptibilidad magnética ligeramente positiva ($\chi \sim 0$), que es directamente proporcional al campo magnético, y una magnetización nula en la ausencia de campo magnético. La causa de que estos materiales no presenten una magnetización remanente se debe a que, en un campo magnético, los espines se orientan en la dirección del campo por ser el estado de más baja energía. Sin embargo, en ausencia de campo magnético, la agitación térmica fuerza a los espines a disponerse en una orientación aleatoria. Por esta razón, a bajas temperaturas no se observa paramagnetismo, debido al comportamiento cooperativo entre los espines, que se produce por debajo de una temperatura de transición específica (la llamada *temperatura de Curie*). Por debajo de dicha temperatura, el acoplamiento de los espines produce uno de los tres tipos diferentes de magnetismo colectivo: ferromagnetismo, ferrimagnetismo y antiferromagnetismo.

Los materiales que poseen ferromagnetismo (por ejemplo, el hierro, níquel y cobalto) presentan, por debajo de la temperatura de Curie, momentos magnéticos atómicos de igual magnitud y alineados de manera paralela (en la misma dirección del campo externo, pero incluso en ausencia de campo magnético externo) debido a que sus estructuras cristalinas permiten un acoplamiento directo de las interacciones entre los momentos. Los electrones interaccionan mediante un mecanismo de intercambio (Coey 1998) en el caso de los metales (superintercambio en el caso de óxidos metálicos ya que interaccionan a través de los átomos de oxígeno), hecho que hace aumentar fuertemente la densidad de flujo magnético. Los fuertes acoplamientos de los espines persisten después de eliminar el campo magnético externo, dando lugar a una magnetización permanente (Figura 3, color negro). Los materiales que conservan una

magnetización permanente en ausencia de un campo magnético aplicado se conocen como *imanes duros*. Por el contrario, los materiales que tienen momentos magnéticos atómicos de igual magnitud y dispuestos de manera antiparalela muestran, por debajo de la *temperatura de Néel* (análoga a la temperatura de Curie pero aplicada a este tipo de materiales), el comportamiento conocido como antiferromagnetismo (por ejemplo, la troilita, FeS), caracterizado por poseer una magnetización neta nula. Por encima de la temperatura de Néel, la energía térmica es suficiente para producir que los momentos magnéticos atómicos alineados de manera opuesta fluctúen de manera aleatoria, comportando la desaparición de su ordenación de largo alcance. En este estado, los materiales exhiben comportamiento paramagnético. Si los electrones, por debajo de la temperatura de Curie, están alineados de forma antiparalela, pero el momento magnético resultante no se anula, el material es ferrimagnético (Raikher et al. 1974). Por encima de la temperatura de Curie, la substancia se transforma en paramagnética.

1.3.1. Superparamagnetismo

Debido a que, si todos los momentos magnéticos se orientasen en la misma dirección se generaría una gran cantidad de energía magnetostática, el material agrupa los magnetrones en regiones denominadas dominios magnéticos (Kittel 1946). Un dominio magnético es un volumen de material ferromagnético en el que todos los magnetrones se alinean en la misma dirección (magnetización uniforme). Dentro de cada dominio los espines están orientados en la misma dirección pero distinta a la de otros dominios magnéticos (Figura 2). El concepto de dominio permite distinguir el ferromagnetismo del paramagnetismo. Cada región de magnetización uniforme está separada por una pared. La formación de las paredes de dominio es un proceso condicionado por el equilibrio entre la energía magnetostática, que aumenta proporcionalmente con el volumen de los materiales, y la energía superficial de la pared del dominio, que aumenta proporcionalmente con el área interfacial entre dominios. Aunque se genere energía de interfacial de unos dominios con otros, esta configuración multidominio dentro del material es la más favorable desde el punto de vista energético. Sin embargo, cuando el tamaño de la partícula de material disminuye, el número de dominios magnéticos decrece hasta un valor crítico (D_{CRIT}) en el que el elevado valor de la energía asociada con la pared de los dominios es termodinámicamente desfavorable, y el material se convierte en monodominio (Este tamaño se alcanza cuando se igualan las energía magnetostática con la superficial). Así, el valor D_{CRIT} indica el tamaño de la transición monodominio-multidominio. Por debajo de D_{CRIT}, el material posee todos sus momentos magnéticos orientados en la misma dirección cuando se le aplica un campo magnético. Esto da lugar a un dipolo permanente dentro del material de una magnitud similar a la de los materiales

ferromagnéticos y unas 100 veces mayor que los paramagnéticos (Frenkel y Dorfman 1930; Kittel 1946). En ausencia de campo magnético, este dipolo se mantiene (comportamiento ferromagnético dentro de monodominio). El valor crítico D_{CRIT} para dos de los materiales magnéticos más usados, la magnetita y la maghemita, es de 128 y 166 nm, respectivamente (Butler y Banerjee 1975).

Como conclusión, las partículas ferromagnéticas presentan magnetización uniforme en aquellas partículas de tamaño inferior a un determinado D_{CRIT}, y magnetización no uniforme en las partículas mayores. Las primeras son las consideradas partículas de dominio único o monodominio, mientras que las últimas son partículas de dominio múltiple o multidominio.

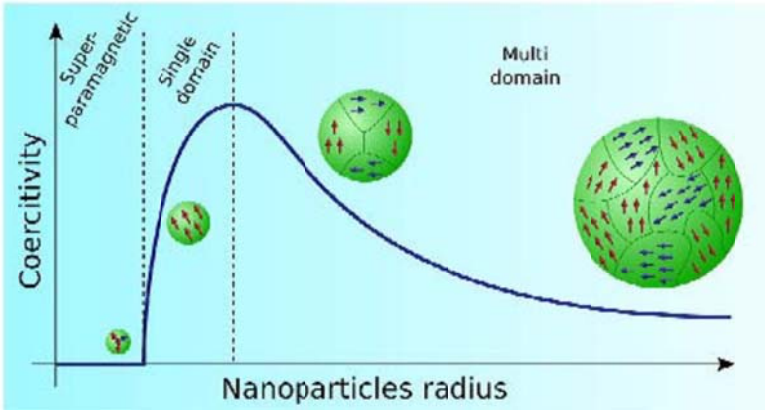

Figura 2. Esquema de la relación entre el tamaño y la coercividad (Akbarzadeh, et al. 2012).

Por otra parte, la respuesta de los materiales ferromagnéticos a la acción de un campo aplicado queda definida por la existencia de un ciclo de histéresis, caracterizado por dos parámetros principales: la remanencia y la coercividad (Figura 3), que, a su vez, está relacionada con la anchura del ciclo de histéresis. La coercividad es la intensidad del campo magnético que se debe aplicar a un material para reducir su magnetización a cero luego de que la muestra ha sido magnetizada hasta saturación (magnetización de saturación). Por lo tanto la coercividad mide la resistencia de un material ferromagnético a ser desmagnetizado. Cuando se trata con partículas de tamaño nano, la coercitividad es la propiedad de mayor interés, y depende enormemente del tamaño. Se ha encontrado que cuando se reduce el tamaño de partícula, aumenta, en un principio, la coercividad, y, a continuación tiende a 0 tal como puede verse en la Figura 2.

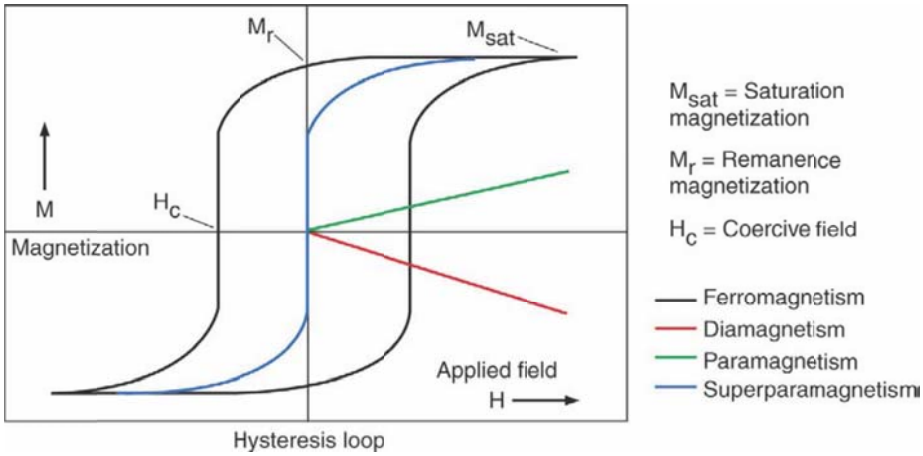

Figura 3. Curva de histéresis (magnetización *M* frente a campo magnético aplicado *H*) característica de nanopartículas ferromagnéticas y superparamagnéticas. Como comparación, también se muestra el comportamiento paramagnético y diamagnético (Arruebo et al. 2007).

Cuando el tamaño de las partículas de monodominio continúa disminuyendo se llega a un segundo valor crítico (D_{SP}) que indica la transición de material ferro a superparamagnético) (Hergt et al. 2008). Por debajo de D_{SP}, los dipolos, en ausencia de campo externo, se orientan al azar ya que la energía térmica es superior a la energía de anisotropía magnética por partícula, que es la energía responsable de mantener los momentos magnéticos de una partícula en una determinada dirección (Batlle y Labarta, 2002). En consecuencia, el momento magnético resultante es nulo, al igual que ocurre en los materiales paramagnéticos. Este comportamiento es propio de los materiales superparamagnéticos. En estos materiales, la coercividad llega a 0 (Figura 3, color azul). La propiedad de superparamagnetismo es un requisito indispensable para el uso de las NPMs en biomedicina. En las partículas superparamagnéticas son lo suficientemente fuertes para desmagnetizar espontáneamente un conjunto previamente saturado; por consiguiente, estas partículas tienen coercividad 0 y no presentan histéresis. Las nanopartículas se convierten en magnéticas en presencia de un imán externo, pero vuelven al estado no magnético cuando deja de actuar el imán externo. Esto evita un comportamiento activo de las partículas cuando no hay ningún campo aplicado. Introducidas en sistemas vivos, las partículas son magnéticas sólo en presencia de un campo externo, hecho que representa una excepcional ventaja al trabajar en entornos biológicos.

1.3.2. Magnetita/Maghemita

Las partículas magnéticas capaces de dar lugar a ferrofluidos con propiedades superparamagnéticas comprenden metales y óxidos metálicos con valores de D_{SP} comprendidos entre 1 a 100 nm. Estos metales y óxidos incluyen Ni, Co, Fe, Fe_3O_4

(magnetita) y γ-Fe_2O_3 (maghemita). Los metales puros presentan los valores más altos de susceptibilidad magnética que los óxidos (Tabla 1).

Substancia	*Magnetización de saturación M_s (emu cm^{-3}) a 298 K*	*Temperatura de Curie (K)*
Ni	485	631
Co (cúbico)	1400-1422	1404
Fe (cúbico)	1700-1714	1043
γ-Fe_2O_3	394	820-986
Fe_3O_4	480-500	858
$MnO{\cdot}Fe_2O_3$	410	573
$CoO{\cdot}Fe_2O_3$	400	793
$NiO{\cdot}Fe_2O_3$	270	858
$CuO{\cdot}Fe_2O_3$	135	728

Tabla 1. Datos magnéticos de metales de transición y óxidos metálicos.

Sin embargo, los metales de transición son fuertemente tóxicos y muy sensibles a la oxidación. Bajo condiciones atmosféricas el Ni, Fe y Co se oxidan dando aleaciones de NiO_2, CoO, y FeO, que son antiferromagnéticos. En la actualidad, no existe ningún método físico o de síntesis que evite el mecanismo de oxidación, lo que constituye un problema de gran importancia en las nanopartículas a causa de la gran área superficial que presentan. Por consiguiente, los óxidos de hierro, a pesar de su inicial magnetización más baja, ofrecen un gran potencial para formar NPMs oxidativamente estables con diversas posibilidades de aplicación en entornos ricos en oxígeno.

Como la magnetita es el material más magnético de todos los minerales naturales existentes en la Tierra, se emplea profusamente en forma de nanopartículas magnéticas para todo tipo de aplicaciones industriales y biológicas. La maghemita, que es el producto de oxidación de la magnetita, es, también, muy empleado.

Estos dos óxidos tienen propiedades físicas y estructuras cristalinas similares (Tabla 2).

	Sistema cristalino	*Dimensiones de la célula (nm)*	*Densidad (kg m^{-3})*	*Color*	*Susceptibilidad Magnética (emu g^{-1})*
Magnetita	cúbico	a_o = 0,8394	5260	negro	84 (a 273 K)
Maghemita	cúbico o tetragonal	a_o = 0,8346	4870	Marrón rojizo	74 (a 273 K)

Tabla 2. Propiedades físicas de la magnetita y de la maghemita.

Ambos óxidos son ferrimagnéticos, aunque la magnetización de saturación de la maghemita es inferior. La maghemita estructuralmente es γ-Fe_2O_3 y está formada solamente por iones Fe^{3+}. Este hecho justifica que la celda de la maghemita sea ligeramente inferior a la de la magnetita ya que los iones Fe^{2+} son de mayor tamaño. En la estructura cristalina de la maghemita, la mitad de los iones Fe^{3+} están coordinados tetraédricamente y la otra mitad están coordinados octaédricamente. La magnetita contiene iones Fe^{2+} i Fe^{3+} en una relación molar 1:2, $FeO{\cdot}Fe_2O_3$, donde la mitad de los iones Fe^{3+} están coordinados tetraédricamente y la otra mitad están coordinados octaédricamente, y todos los iones Fe^{2+} están coordinados octaédricamente. Tanto la magnetita como la maghemita poseen una estructura cristalina cúbica espinela inversa en la cual los iones O^{2-} se encuentran formando un empaquetamiento cúbico compacto centrado en las caras (fcc) a lo largo de la dirección [111] (Azaroff 1968). Cada celda unidad está formada por 8 celdillas (Figura 4).

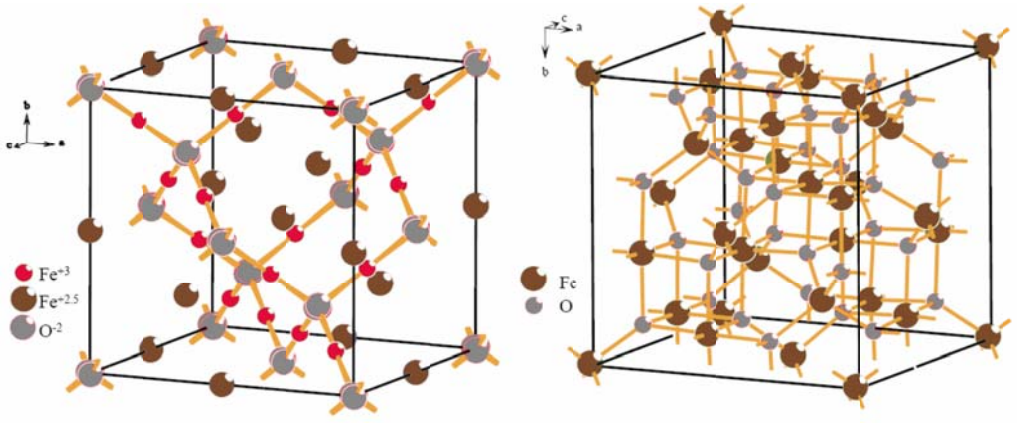

Figura 4. Estructura cristalina tipo espinela de la magnetita (izquierda) y de la maghemita (derecha) (Roca 2009)

En estos óxidos, la disminución de tamaño de las nanopartículas por debajo de los 10 nm es contraproducente. La presencia de iones de hierro en la superficie crece a medida que disminuye el tamaño de la partícula. Los átomos de hierro poseen una naturaleza especial ya que poseen falta de simetría al no encontrarse coordinados en todas las direcciones. Esto da lugar a una disminución de la magnetización de la magnetita y de la maghemita (Cornell y Schwertmann, 1996).

1.4. Síntesis de nanopartículas magnéticas

Durante los últimos años se han descrito diferentes rutas para obtener de manera eficiente NPMs de tamaño controlable, estables, y con una estrecha distribución de tamaños. Estos métodos incluyen la co-precipitación, la microemulsión, la descomposición térmica, la deposición química de vapor, la síntesis por pirolisis, etc. (Una descripción de estos métodos puede encontrarse en Lu et al. (2007)). El método más utilizado, y el seguido en el trabajo experimental de esta tesis, es, por su simplicidad y bajo coste, la co-precipitación de sales de Fe^{3+} y Fe^{2+} en medio altamente alcalino. Es un proceso fácilmente escalable y por ello es utilizado en la industria para el diseño y fabricación de nanopartículas de óxido de hierro como agentes de contraste.

1.5. Nanopartículas magnéticas en biomedicina

La utilización de nanopartículas magnéticas dentro del campo de la biomedicina viene realizándose desde la década de los 90 del s. XX. El hecho de que el hierro sea fácilmente metabolizado dentro del cuerpo, que las partículas tengan tamaños comparables al de las proteínas, células, virus y ADN, que la superficie de estas partículas pueda ser modificada a fin de unir moléculas de interés biológico, que las partículas posean un elevado momento magnético, así como que las líneas de campo puedan atravesar el cuerpo humano, hace que las partículas posean un futuro prometedor en la búsqueda de metodologías poco invasivas de asistencia al diagnóstico y tratamiento de enfermedades (Pankhurst et al. 2003; Huber 2005; Arruebo et al. 2007). Recientemente, han aparecido aplicaciones que combinan tanto la terapéutica como la diagnosis, permitiendo un elevado control de la eficacia de un tratamiento individual. Esta combinación es conocida en la actualidad como *teranosis* (Mornet et al., 2004; Shubayev et al. 2009).

En ausencia de recubrimiento, las NPMs muestran superficies hidrofóbicas que facilitan la fuerza atractiva de Van der Waals y dan lugar a la formación de aglomerados que pueden llegar a alcanzar valores micrométricos. Esta agregación se produce de manera especial en fluidos biológicos, debido a la presencia de sales y

proteínas plasmáticas. En estas circunstancias, las NPMs son incompatibles con su utilización en aplicaciones biomédicas, debido a la alta posibilidad de que se produzca una obstrucción de pequeños capilares.

Las aplicaciones biomédicas de las NPMs pueden clasificarse de acuerdo con si se aplican dentro o fuera del cuerpo (*in vivo*, *in vitro*). El principal uso en aplicaciones in vitro es la selección y separación en aplicaciones diagnósticas y magnetorelaxometría, mientras que las aplicaciones in vivo pueden separarse en aplicaciones terapéuticas (hipertermia/ablación y direccionalización de fármacos, y en aplicaciones de diagnóstico (resonancia magnética nuclear de imagen (RMI). La figura 5 resume estas aplicaciones (Arruebo et al. 2007).

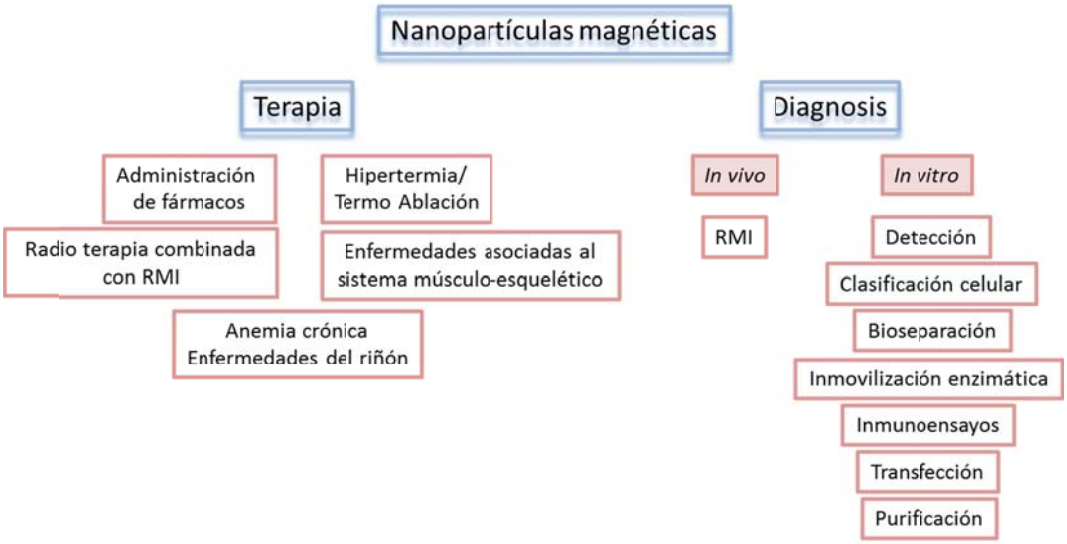

Figura 5. Aplicaciones de las nanopartículas magnéticas en biomedicina (Adaptado de Arruebo et al. 2007).

1.5.1. Aplicaciones in vivo

Para aplicaciones terapéuticas, las NPMs deben ser biocompatibles y de fácil biodegradación en el organismo. En las NPMs formadas por hierro y sus óxidos, después de metabolizarse, los iones de hierro se añaden a los depósitos de hierro del organismo, y finalmente son incorporados por los eritrocitos como parte de la hemoglobina (Weissleder et al. 1989; Mailander y Landfester 2009). De estas partículas apenas se han descrito efectos negativos. Los efectos citotóxicos observados debido a la ingesta de este tipo de partículas sólo ocurren a altas concentraciones (superiores a 100 µg/mL) (Jeng and Swanson 2006; Naqvi et al. 2010).

Se utilizan dos tipos de nanopartículas de óxido de hierro superparamagnéticas: las SPIONs (*SuperParamagnetic Iron Oxide Nanoparticles*) y las USPIONs (*Ultra*

SuperParamagnetic Iron Oxide Nanoparticles), diferenciadas solamente por el tamaño (USPIONs, < 50 nm; SPIONs, > 50 nm) (a partir de este momento, cualquier de los dos tipos se indicará genéricamente con las siglas SPIONs).

El tamaño desempeña un papel clave en la biodistribución in vivo, ya que el tiempo de permanencia en el organismo depende del tamaño de la partícula (Figura 6). Según la finalidad terapéutica de la administración de las NPMs, un parámetro a tener en consideración para que éstas sean de interés desde el punto de vista clínico, es que el tiempo de circulación en sangre tras ser inyectadas en el organismo sea lo suficientemente largo para que puedan alcanzar los objetivos que se desean (Hegt et al. 2008). En caso contrario, se reduciría su eficacia terapéutica. Una partícula cuando entra en el organismo es reconocida por un conjunto de proteínas llamadas opsoninas. Después de unidas, las proteínas sirven de señuelo para la acción de las células del sistema macrófago-fagocítico (SMF) que provocan la internalización vía endocitosis de las NPMs; éstas son agrupadas en los lisosomas donde, presumiblemente, son degradadas, a bajo pH, a iones hierro mediante una serie de enzimas hidrolíticos de acuerdo con las vías endógenas del metabolismo del hierro. El SMF incluye macrófagos del hígado, del bazo y de los nódulos linfáticos, y es el encargado de reconocer y eliminar todas las partículas extrañas que entran en el organismo y por tanto, también provoca la eliminación de las NPMs (Duguet et al. 2006; Hanini et al. 2011). Así, una forma de aumentar la biodisponibilidad de las NPMs es evitando que sean eliminadas por el SMF.

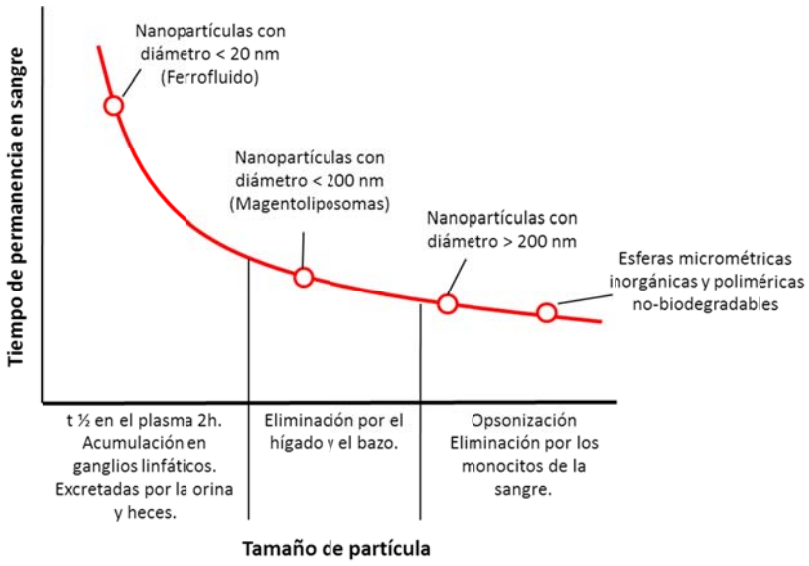

Figura 6. Tiempo de permanencia en sangre en función del tamaño de las NPMs (Adaptado de Arruebo et al. 2007).

El tamaño de las NPMs debe ser suficientemente pequeño para evitar su captura por el bazo, (menor de 200 nm) pero suficientemente grande para evadir la filtración directa

por los riñones (mayor de 5 nm). Por tanto, las NPMs que oscilan entre 10 y 100 nm poseen el tamaño más adecuado para lograr una distribución óptima *in vivo*.

Otra manera de prolongar la vida en el organismo, así como de aumentar su estabilidad coloidal, es recubrir las NPMs con polímeros biocompatibles o encapsularlas en liposomas. La cubierta polimérica o la encapsulación en liposomas, proporciona una barrera física que evita la aglomeración de las nanopartículas y posibilita su fácil dispersión en disoluciones fisiológicas. Las NPMs recubiertas de polímeros biodegradables muestran una menor toxicidad y tienen una mayor biocompatibilidad que las NPMs inorgánicas sin recubrir. Los polímeros más utilizados como recubrimientos de NPMs son el dextrano, utilizado por su alta biocompatibilidad y alta afinidad por el hierro y el polietilenglicol (PEG) (Gupta y Wells 2004; Schipper et al. 2009; Sun et al. 2010; Yue-Jian et al. 2010), con gran capacidad antiadherente que reduce la captación de las partículas por los macrófagos, aumentando su tiempo de circulación en sangre (Choi et al. 2007). Otros polímeros utilizados de forma habitual como recubrimientos para NPMs son el polivinilalcohol (PVA) y el quitosano que proporciona una envoltura biocompatible, catiónica e hidrofílica.

1.5.1.1. Aplicaciones terapéuticas: Hipertermia/Ablación. La hipertermia magnética es el fenómeno que se presenta al exponer una zona que contiene NPMs a ondas electromagnéticas de frecuencia igual a varios centenares de MHz, interacción que genera calor la zona por disipación de la energía (Rosenweig 2002) y permite alcanzar temperaturas entre 42 y 45 ^{o}C durante un período mínimo de 30 minutos. Este aumento de la temperatura produce la muerte celular de la zona a tratar. Es de suma importancia el buen control de la temperatura tanto dentro como fuera del tejido a tratar puesto que se persigue producir el aumento sólo en una zona delimitada (Hildebrandt, et al. 2002). Las células tumorales son más sensibles al incremento de temperatura que las células sanas, así, la principal ventaja de la hipertermia magnética es que permite restringir el calentamiento al área tumoral. La hipertermia se utiliza para potenciar las terapias ya establecidas como la radio o la quimioterapia. Las células tumorales, de naturaleza hipóxica (con bajos niveles de oxígeno) son resistentes a las radiaciones, sin embargo el calor destruye por igual células hipóxicas y células normales. Se ha demostrado que se requiere una dosis menor de radiación para destruir la misma proporción de células tumorales cuando se someten previamente a procesos de hipertermia.

Otro de los requisitos importantes que se deben de considerar es que la temperatura en la zona de atención no se eleve demasiado, ya que si se alcanzase una temperatura mayor a la establecida, se presentaría el fenómeno denominado ablación térmica, que se produce cuando la temperatura alcanzada está alrededor de los 50 ^{o}C (Sayed et al. 2003; Diederich 2005). En este caso, además de muerte celular se produce necrosis. La

ablación térmica se ha empleado como terapia de rescate tras fallos post-radioterapia. La hipertermia, además de la aplicación de campos electromagnéticos, puede producirse mediante ultrasonidos, terapia de perfusión, fotocoagulación de láser intersticial, y administración de calor por contacto externo.

La termoterapia con NPMs es una opción nueva, mínimamente invasiva. La generación de calor depende de las propiedades de magnetización de las formulaciones específicas de las NPMs, así como de la intensidad y frecuencia del campo magnético. Se prefiere el uso de partículas nanométricas (de dominio único) frente a los materiales micrométricos (de dominios múltiples), ya que las nanopartículas absorben mucha más potencia a tolerables campos magnéticos de corriente alterna. Es de cabal importancia, por lo tanto, hacer uso de rutas de síntesis bien establecidas que produzcan partículas uniformes a fin de poder tener un control riguroso de la temperatura.

En esta técnica se inyecta directamente en tumores superficiales o profundos, un fluido que contiene SPIONs con dimensiones entre 10 a 100 nm. A continuación, se aplica un campo magnético alterno de suficiente intensidad y frecuencia que provoca mediante relajaciones de Néel (por rotación del espín) y de Brown (por rotación de la partícula) una disipación de la energía y su transformación en calor, llegando a un sobrecalentamiento del tejido donde se habían dispersado las NPMs. La energía liberada al medio circundante dependerá de la cantidad, del tamaño de las NPMs utilizadas y de la fuerza del campo magnético aplicado (Jordan et al. 1999).

1.5.1.2. Liberación de fármacos. La posibilidad de utilizar atracción magnética externa o la funcionalización de las NPMs con moléculas que reconocen dianas sobre las que actuar, hace que sea posible el guiado de las NPMs hacia las zonas de interés, donde debe producirse la liberación del fármaco. Esta función de liberación focalizada de drogas terapéuticas, conlleva la reducción de la dosis del fármaco y la desaparición de efectos secundarios no deseados sobre otras células o tejidos sanos (Duguet et al. 2006).

El guiado está relacionado con el movimiento y la trayectoria que pueden experimentar las NPMs al aplicárseles un campo magnético estático o alterno, de tal manera que adquieran una velocidad y puedan ser manipuladas controlando dicho campo. El mismo efecto puede lograrse si las partículas están direccionalizadas, por ejemplo si presentan en su superficie un anticuerpo específico para un antígeno presente en las células o tejido que se quieren tratar. Como consecuencia del guiado de las NPMs, éstas pueden focalizarse, o sea, concentrarse en un lugar específico del organismo.

Como ya se ha indicado, se pueden modificar las superficies de las NPMs con polímeros orgánicos para hacerlas biocompatibles y adecuadas para una posterior funcionalización mediante el engarce de moléculas bioactivas, El proceso de localización de fármacos empleando sistemas de liberación magnéticos se basa en la competición entre las fuerzas ejercidas sobre las partículas por el compartimiento sanguíneo y las fuerzas magnéticas generadas por el imán.

1.5.1.3. Aplicaciones diagnósticas: RMI. La RMI es una de las técnicas más utilizadas en la actualidad como herramienta diagnóstica no invasiva (Mitchell y Cohen, 2004). Se basa en la diferencia de las relajaciones magnéticas nucleares de los protones del agua entre los fluidos biológicos y los tejidos sólidos. Un agente de contraste modifica la velocidad de relajación magnética nuclear de los protones de su entorno y cambia el contraste de la señal. Las NPMs se administran a fin de (*a*) aumentar el contraste de la imagen entre el tejido sano y el enfermo, y/o (*b*) indicar el estado funcional de los órganos o del flujo sanguíneo (Corod et al. 2006).

Las NPMs como agentes de contraste para RMI permiten una mejor interpretación de las imágenes obtenidas al aumentar las diferencias entre tejidos normales y tejidos patológicos. Se pueden distinguir dos tipos de agentes de contraste: los agentes de contrate T1 (por ejemplo, iones metálicos paramagnéticos, como el Gd^{3+}), y los agentes de contraste T2 (las NPMs) (Ho et al. 2011). Los contrastes T1 aumentan la brillantez de la imagen mientras que los T2 dan negativos de las imágenes. Los agentes de contraste de RMI convencionales son más efectivos sólo en un modo único de imágenes, T1 o T2. Sin embargo, la combinación del uso simultáneo de ambos agentes en un único agente de contraste puede representar una gran innovación, ya que potencialmente puede proporcionar imágenes más precisas. El fundamento se basaría en el fuerte acoplamiento magnético entre los agentes de contraste T1 y T2 cuando éstos se encuentran próximos, entonces, los procesos de relajación espín-malla de los materiales tipo T1 provocan la disminución de este contraste. Una de las estrategias para alcanzar esta situación es la de preparar nanopartículas que contengan un núcleo superparamagnético y una cubierta paramagnética separada por una capa de material no magnético (Figura 7) (Yoo et al. 2011).

Por otra parte, las NPMs tienden a acumularse en los lugares donde existe una alteración de la vasculatura del tejido, caso de los tumores (Maeda, et al. 2000). Este fenómeno, unido al hecho de que en el tejido tumoral existe un sistema de drenaje linfático defectuoso, provoca la acumulación en las zonas tumorales de aquellas NPMs con de tamaños entre 10 y 100 nm. Actualmente, también se están sintetizando nuevas NPMs para realizar el diagnóstico de enfermedades inflamatorias, con una futura aplicación en enfermedades tan comunes como aterosclerosis, esclerosis múltiple o artritis reumatoide, en las que los macrófagos juegan un papel fundamental.

Para detectar estas enfermedades mediante imagen de RM se aprovecha la avidez que poseen los macrófagos por las NPMs. Por tanto, la fagocitosis de NPMs por los macrófagos actúa como un potente marcador de zonas de inflamación perfecto para visualizar placas de aterosclerosis mediante imagen de resonancia magnética.

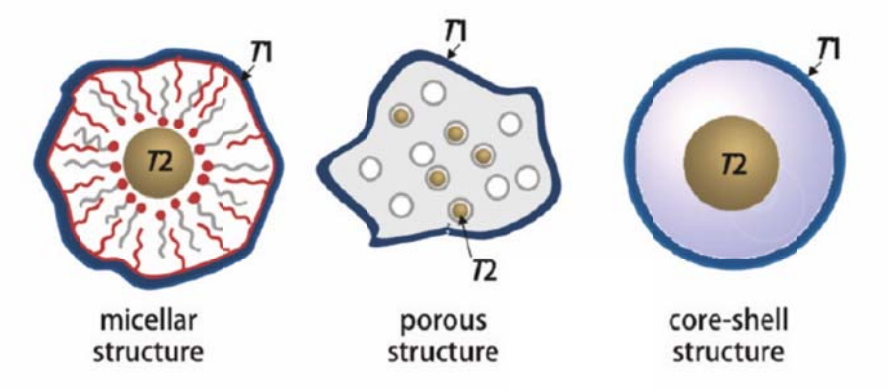

Figura 7. Estructuras posibles de nanopartículas candidatas a ser utilizadas como agentes de contraste duales T1/T2 (Adaptada de Yoo et al., 2011).

1.5.2. Aplicaciones in vitro

1.5.2.1. Separación y selección. En la actualidad la extracción en fase sólida (EFS) goza de mucho predicamento ya que es un sistema eficaz de aislar y preconcentrar los componentes deseados de una muestra analítica, suponiendo una alternativa excelente a los métodos convencionales de concentración tales como la extracción líquido-líquido. Por ejemplo, la EFS es un método rutinario de extracción para determinar los contaminantes a nivel de trazas en muestras medioambientales. Sin embargo, la separación y preconcentración de una substancia presente en grandes volúmenes de disolución consume mucho tiempo cuando se usa una columna estándar de EFS. Es aquí donde toma importancia el uso de adsorbentes magnéticos o magnetizables, formados por NPMs, dando lugar a la llamada extracción en fase sólida magnética. En este procedimiento, se añade el adsorbente magnético a la disolución o suspensión que contiene la substancia a separar. Ésta se adsorbe sobre el adsorbente magnético, y entonces, el adsorbente con la substancia adsorbida es recuperado de la fase líquida empleando un separador magnético apropiado. Para separar y seleccionar, la ventaja de hacer uso de NPMs en lugar de micropartículas magnéticas radica en poder preparar suspensiones que son estables frente a la sedimentación en ausencia de un campo magnético externo.

Como ejemplos de bioseparación mediante partículas magnéticas se puede citar la selección fenotípica de diferentes tipos celulares (células madre, neuronas sensoriales, etc.). Ésta se consigue con esferas magnéticas revestidas de estreptavidina. Por otra

parte, se han usado NPMs conjugadas a anticuerpos para descontaminar la sangre de agentes infecciosos (Weber y Falkenhagen 1997). También se han utilizado los principios de bioseparación magnética en tecnologías de biosensores integrales. Por ejemplo, con la estrategia basada en la amplificación *bio-barcode* se pueden detectar analitos proteicos (como los oligómeros asociados a la enfermedad de Alzheimer) empleando anticuerpos unidos a NPMs (Nam et al. 2003).

1.5.2.2. Magneto-relaxometría. Se introdujo como método de evaluación de inmunoensayos. La magnetorelaxometría mide la viscosidad magnética, esto es, la relajación del momento magnético neto de un sistema de NPMs después de quitar el campo magnético. Existen dos tipos diferentes de relajación. En una muestra seca de NPMs monodominio, la relajación de Néel es el tiempo requerido para volver al equilibrio de la magnetización después de una perturbación. La relajación de Brown caracteriza la rotación viscosa de las partículas en su conjunto. La figura 8 muestra los dos componentes de la relajación magnética de un ferrofluido. El hecho que la magnetorelaxometría dependa del tamaño del núcleo magnético, del radio hidrodinámico y de la anisotropía, posibilita, en base a su comportamiento magnético diferente, distinguir entre conjugados unidos y libres, y, por consiguiente, emplearse como herramientas analíticas en la evaluación de inmunoensayos. Para esta aplicación, los beneficios de reducir el tamaño de partícula a escala nano son similares a los indicados para aplicaciones de separación y selección.

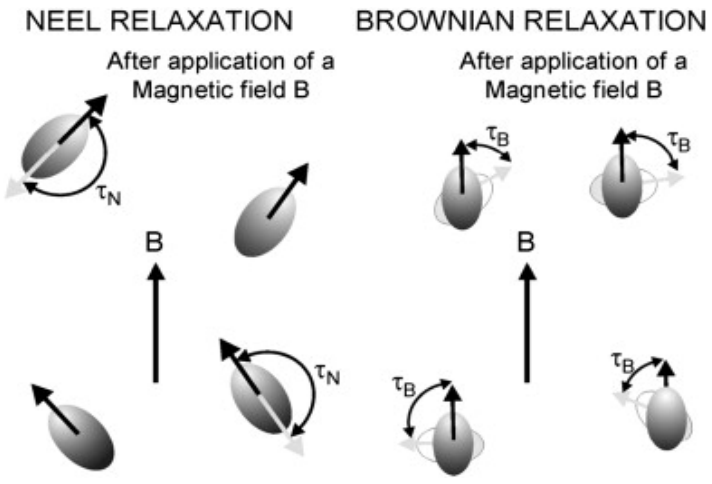

Figura 8. Ilustración de los dos componentes de la relajación magnética de un fluido magnético (Figura 2 de Laurent et al., 2011).

2. Objetivos

2. Objetivos

El objetivo general que se ha planteado en este trabajo de tesis ha sido la *obtención de NPMs que pudiesen ser empleadas en aplicaciones biomédicas*. El tipo de NPMs desarrolladas han sido, por una parte, magnetoliposomas, y, por otra, un ferrofluido estabilizado con polietilenglicol. Como objetivos específicos, se destacaría: a) la síntesis sistemática y reproducible de estas partículas, b) su caracterización, y c) la aplicación de las nanopartículas sintetizadas como agentes terapéuticos, concretamente como sistemas capaces de llevar a cabo una terapia hipertérmica, o de, mediante la direccionalidad magnética, transportar fármacos a zonas de interés.

La consecución de estos objetivos queda reflejada en los cuatro artículos que se presentan (Figura 9), que describen la preparación, caracterización y biodistribución de los magnetoliposomas en ratones CD-1 (artículo 1), la aplicación de estos magnetoliposomas y de un ferrofluido en terapia hipertérmica (artículo 2) y en ablación térmica (artículo 3), y, finalmente, el efecto de un campo magnético externo sobre magnetoliposomas administrados intravenosamente en ratones CD-1.

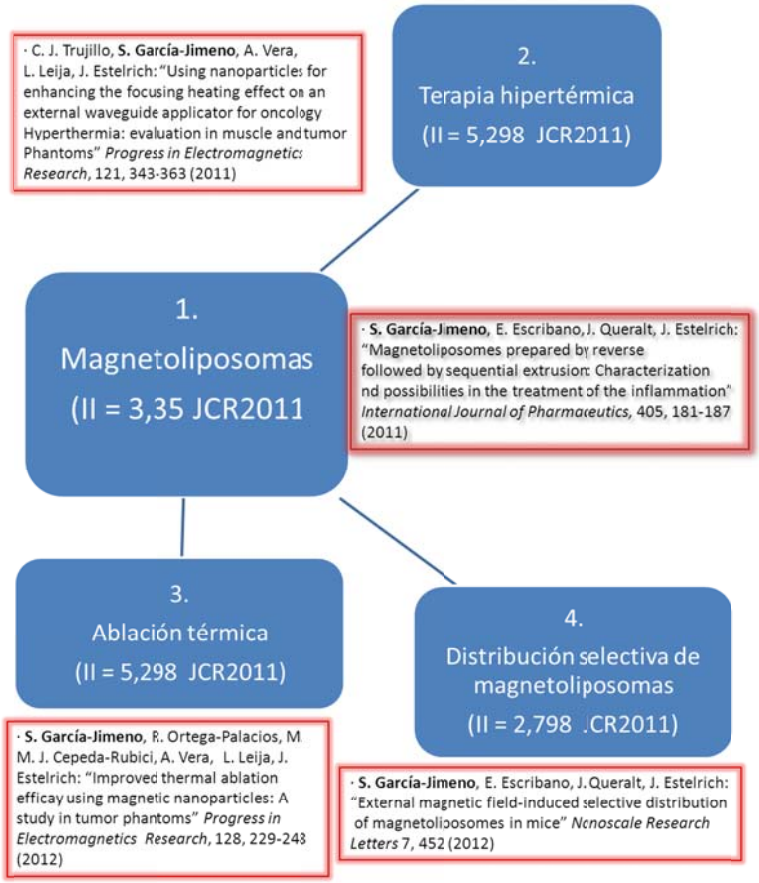

Figura 9. Esquema de los artículos publicados con los resultados obtenidos en el trabajo experimental de esta tesis doctoral (II = Índice de Impacto según el Journal Citation Records de 2011)

3. Resultados

3. Resultados

Los resultados de la presente tesis están reflejados en los siguientes artículos científicos, los cuales se presentan a continuación acompañados por un breve resumen en castellano.

Artículo 1. García-Jimeno, S., Escribano, E., Queralt, J., Estelrich, J., (2011). Magnetoliposomes prepared by reverse-phase followed by sequential extrusion: Characterization and possibilities in the treatment of inflammation. International Journal of Pharmaceutics, 405, 181–187.

Artículo 2. C. J. Trujillo-Romero, S. García-Jimeno, A. Vera, L. Leija, J. Estelrich. (2011). Using nanoparticles for enhancing the focusing heating effect of an external waveguide applicator for oncology hyperthermia: evaluation in muscle and tumor phantoms. Progress In Electromagnetics Research, 121, 343–363.

Artículo 3. S. García-Jimeno, R. Ortega-Palacios, M. F. J. Cepeda-Rubio, A. Vera, L. Leija, J. Estelrich. (2012). Improved Thermal Ablation Efficacy Using Magnetic Nanoparticles: A Study in Tumor Phantoms. Progress In Electromagnetics Research, 128, 229-248.

Artículo 4. S. García-Jimeno, Elvira Escribano, Josep Queralt, Joan Estelrich, (2012). External magnetic field-induced selective distribution of magnetoliposomes in mice. Nanoscale Research Letters, 7 (1): 452.

Artículo 1.

Magnetoliposomes prepared by reverse-phase followed by sequential extrusion: Characterization and possibilities in the treatment of inflammation.

International Journal of Pharmaceutics, 405, 181–187.

Se ha realizado una optimación en la eficiencia de encapsulación de ferrofluido en liposomas, utilizando dos métodos: el de fase reversa y el de extrusión simple. Se describe la cuantificación y la optimización de la encapsulación de ferrofluido en liposomas mediante una modificación del método de fase reversa con la posterior extrusión, para obtener liposomas unilamilares de 200 nm. Para determinar qué relación de Fe_3O_4/fosfolípido es la más adecuada, el film de fosfolípido es hidratado con diferentes diluciones de FF que van desde 1.28 - 32.11 mg de Fe_3O_4 por mL de suspensión. Una vez que se forma la suspensión de magnetoliposomas, se purifican eliminando el ferrofluido no encapsulado mediante columna cromatografía de separación de tamaños (SEC), con Sepharosa 4B. La cantidad de Fe_3O_4 encapsulada se determinó midiendo la cantidad de hierro que se obtienen de las primeras fracciones, mediante un método colorimétrico usando o-phenantroline. El contenido en fosfolípido se determinó mediante el método de Steward-Marshall. Así es calculado el porcentaje de encapsulación, mediante la relación Fe_3O_4/fosfolípido. En ambos casos, se ha utilizado una relación de 0.056 g de hierro por mmol de fosfolípido. En el método de extrusión simple, se obtienen después de la purificación por cromatografía, 15.0 ± 1.7 mg de hierro/mmol PC (n=4) y en el método de fase reversa obtenemos 23.8 ± 1.7 mg de hierro/mmol PC (n=4). El análisis estadístico indica que la encapsulación es significantemente diferente (P=0.0002).

Se ha valorado la biodistribución de nanopartículas en el foco inflamatorio inducido en el lomo de ratón. Se utilizaron ratones hembra CD-1 de 7-8 semanas de edad (28-32 g de peso). Los MLs se administraron por vía intravenosa a ratones sanos y con inflamación inducida, una dosis expresada en contenido de hierro de 0.5 mg/mL. Se ha valorado la concentración de hierro, a los 20 minutos de ser administrados, en el exudado inflamatorio, plasma, hígado y bazo, mediante la técnica, espectrometría de emisión óptica con fuente de plasma de acoplamiento inductivo (ICP-OES), previa digestión acida de la materia orgánica. Se observa que los MLs son acumulados en la zona de inflamación, lo que sugiere que estas partículas podrían contener medicamentos para tratar algunos de los procesos inflamatorios. El estudio realizado esta aprobado por el comité ético de la universidad de Barcelona.

International Journal of Pharmaceutics 405 (2011) 181–187

Contents lists available at ScienceDirect

International Journal of Pharmaceutics

journal homepage: www.elsevier.com/locate/ijpharm

Pharmaceutical Nanotechnology

Magnetoliposomes prepared by reverse-phase followed by sequential extrusion: Characterization and possibilities in the treatment of inflammation

Sonia García-Jimeno[a], Elvira Escribano[b], Josep Queralt[c], Joan Estelrich[a,*]

[a] Departament de Fisicoquímica, Facultat de Farmàcia, Universitat de Barcelona, Avda. Joan XXIII, 08028 Barcelona, Catalonia, Spain
[b] Departament de Farmàcia i Tecnologia Farmacèutica, Facultat de Farmàcia, Universitat de Barcelona, Avda. Joan XXIII, 08028 Barcelona, Catalonia, Spain
[c] Departament de Fisiologia, Facultat de Farmàcia, Universitat de Barcelona, Avda. Joan XXIII, 08028 Barcelona, Catalonia, Spain

ARTICLE INFO

Article history:
Received 16 September 2010
Received in revised form
17 November 2010
Accepted 24 November 2010
Available online 1 December 2010

Keywords:
Biomaterials
Inflammation
Liposomes
Magnetic properties
Magnetic materials

ABSTRACT

Anionic ferrofluid was encapsulated in 200 nm-diameter liposomes. The process involved phase-reverse evaporation followed by sequential extrusion. Magnetoliposomes were characterized by transmission electron microscopy, Doppler laser electrophoresis, SQUID magnetometry, dynamic light scattering and iron content by atomic absorption spectrophotometry. The absence of hysteresis of the magnetic power of particles at room temperature is characteristic of a material with superparamagnetic properties. The encapsulation efficiency was determined for several iron/phospholipid ratios, and this parameter ranged from 0.016 to 0.024 mg iron per mmole of phospholipids, depending on the initial magnetite concentration. In comparison with magnetoliposomes that were obtained solely by extrusion, this method afforded significantly better encapsulation ($P = 0.0002$). Magnetic particles were intravenously administered to healthy or inflammation-induced mice. After 1 h, the content of iron was determined in exudates, liver, spleen and plasma. Magnetoliposomes accumulated in the exudates collected from the inflammation site, which suggests that these particles could be loaded with the drugs needed to treat some inflammatory processes.

1. Introduction

Nanoparticles offer exciting opportunities for technologies at the interfaces between chemistry, physics and biology, as they form a bridge between bulk materials and atomic or molecular structures. A bulk material should have constant physical properties regardless of its size, but this is often not the case at nanoscale. For bulk materials larger than a few μm, the percentage of atoms at the surface is rather insignificant relative to the total number of atoms of material. However, when the size of the material approaches the nanoscale, the percentage of atoms at the surface becomes significant. Magnetic nanoparticles show considerable promise for a wide range of applications, provided the monodispersity of nanoparticles and the surface properties are controlled (Craig, 1995). The use of magnetic nanoparticles as non-volatile data storage media offers certain advantages over other forms of storage. Moreover, magnetic nanoparticles are or may soon be used in several biomedical applications. For example, the combination of biomolecules with a single magnetic nanoparticle is expected to open new avenues in medical diagnostics, drug targeting or innovative cancer therapies (Reiss and Hütten, 2005; Arruebo et al., 2007). The movements of magnetic nanoparticles can be deliberately controlled and magnetic fields can penetrate human tissues without impediment. Consequently, magnetic nanoparticles can be used to deliver packages, such as anticancer drugs or radionuclide atoms, to a targeted area of the human body. Additionally, magnetic nanoparticles respond strongly to time-modulated magnetic fields, and hence enable dynamic methods of cancer treatment. Alternatively, they could be used to enhance the contrast in magnetic resonance imaging. The ability of such particles to convert magnetic energy into heat by relaxation and hysteresis effects has also gained much attention in antitumor therapy. This simple physical effect could be used to destroy cells directly or to induce a modest rise in temperature that could increase the efficacy of chemotherapy or radiotherapy (Schmitt, 2007). Finally, the viscoelastic architecture inside living cells can be studied by controlled positioning of magnetic nanoparticles inside the internal skeleton of cells. The response of such particles to dynamic magnetic fields can then be followed.

For most of these applications, magnetic nanoparticles are formed by ferromagnetic material such as cobalt, iron or nickel, and particularly by ferrimagnetic iron oxides (maghemite, γ-Fe_2O_3, and magnetite, Fe_3O_4). The magnetic material presents different properties according to particle size. Macroscopic materials (of the order of one micron or more) tend towards the formation of magnetic domains that are characterized by the parallel alignment of magnetic moments on the atomic scale within the

* Corresponding author. Tel.: +34 934024559; fax: +34 934035987.
E-mail address: joanestelrich@ub.edu (J. Estelrich).

0378-5173/$ – see front matter © 2010 Elsevier B.V. All rights reserved.
doi:10.1016/j.ijpharm.2010.11.044

domain, and the relative arrangement of the domains in such a way that the net outer magnetization in the absence of outer fields is minimized. However, in the nanometer range, the formation of magnetic domains is not favoured energetically, and the particles form a single domain, that is, every spin in the particle has the same direction. Hence, the total magnetic moment of the particle is the sum of all spins. The critical diameter for single domain formation is approximately 150 nm for magnetite (Leslie-Peleckie and Rieke, 1996). Data storage media and biomedical sensor systems require a single domain. Particles with this property are called thermally blocked particles. They have long magnetic relaxation times in comparison with the typical time scale of measurements used to study the system. If these nanoparticles are placed in a solid matrix, they exhibit both remanence and coercivity. Medical applications require superparamagnetism at room temperature. This property is displayed in small single domain particles (of the order of tens of nanometers or less, 10–15 nm for magnetite). This phenomenon arises from finite size and surface effects, which dominate the magnetic behaviour of individual nanoparticles. Superparamagnetic particles have fast relaxation times and, consequently, show neither remanence nor coercivity. Thus, these nanoparticles are non-magnetic in the absence of an external magnetic field, but they do develop a mean magnetic moment in an external magnetic field. The advantages of superparamagnetic particles are easy suspension, a large surface area, slow sedimentation and a uniform distribution of the particles in the suspension media (Pankhurst et al., 2003). In biology and medicine, superparamagnetic oxide nanoparticles have been used for cell selection and as magnetic resonance imaging (MRI) contrast agents (Mailänder and Landfester, 2009).

While thermal energy efficiently prevents particles of about 10 nm from sedimentation in a gravitational field or from agglomeration due to magnetic dipole interaction, it does not prevent coagulation due to van der Waals attraction (Odenbach, 2003). To overcome this problem, a protective shell must be created for each particle. This can be achieved using two basic approaches to colloidal stabilization: electrostatic stabilization and/or steric stabilization. In general, nanoparticles are coated with surfactants, polymers, or derivatized lipids. The small size of the stabilized particles results in dispersions, known as ferrofluids, which remain suspended indefinitely in gravitational and moderate magnetic fields (Rosenweig, 1985; Blums et al., 1997).

As demonstrated some decades ago, liposomes comprise colloidal structures which are easy to synthesize, biocompatible and nontoxic (Barenholz, 2001). They can be rendered magnetic by encapsulating magnetic nanoparticles to develop a new type of liposomes known as magnetoliposomes (Bulte and De Cuyper, 2003). Magnetoliposomes can be prepared by trapping the material inside the liposomal aqueous interior during membrane formation by extrusion (Martina et al., 2005; Sabaté et al., 2008; Plassat et al., 2007; Laurent et al., 2008), reverse-phase evaporation (Wijaya and Hamad-Schifferli, 2007), or sonication (Dandamundi and Campbell, 2007) methods, or by means of a completely different strategy. In the latter case, the nanoparticles are stabilized by a surfactant coat. Then, the surfactant molecules are exchanged for phospholipid molecules (De Cuyper and Joniau, 1988; De Cuyper et al., 2003, 2006).

In this study, we encapsulated an anionic ferrofluid in magnetoliposomes by means of a double technique: first, the liposomes were prepared by reverse-phase evaporation using a suspension of ferrofluid as the aqueous medium. Then, the resulting liposomes were extruded through 200-nm pore membranes. After purification, a physicochemical characterization was performed, which included transmission electron microscopy, magnetization analysis, size distribution and encapsulation efficiency. Subsequently, the nanoparticles were tested in mice, with or without an induced inflammatory focus on their back, to follow their biodistribution.

2. Materials and methods

2.1. Materials

Soybean phosphatidylcholine, a zwitterionic phospholipid, (Lipoid S-100) (PC) was donated by Lipoid (Ludwigshafen, EU). Nanoparticles of magnetite stabilized with anionic coating (EMG 707) were purchased from FerroTec (Bedford, NH, USA). The particles had a nominal diameter of 10 nm that was determined by transmission electron microscopy (TEM), a coefficient of viscosity of less than 5 mPa s at 27 °C, and a 1.8% volume content in magnetite. A strong neodymium–iron–boron ($Nd_2Fe_{12}B$) magnet (1.2 T) was obtained from Halde GAC (Barcelona, EU). Reagents were of analytical grade.

2.2. Preparation of magnetoliposomes

Magnetoliposomes were obtained using a modified version of the phase-reverse method (Szoka and Papahadjopoulos, 1978). Phospholipids (100 μmol) dissolved in chloroform/methanol (2:1, v/v) were placed in a round-bottom flask and dried in a rotary evaporator under reduced pressure at 40 °C to form a thin film on the inner surface of the flask. The film was hydrated with 9 mL of diethyl ether and 3 mL of FerroTec suspended in saline solution (0.16 mol L^{-1} NaCl) (diluted from 25% to 1% of the original suspension). The mixture was sonicated for 5 min in a bath sonicator (Transsonic Digital Bath sonifier, Elma, EU) at 0 °C. Once the emulsion had been formed, it was placed in a round-bottom flask and the organic solution was removed at −420–440 mmHg at room temperature. The emulsion became a gel and, finally, this gel transformed into a suspension of liposomes. Once this had been obtained, one mL of saline solution was added and the suspension was rotated at −760 mmHg to remove the ether. Liposomes were diluted with saline solution until a final phospholipid concentration of 20 mmol L^{-1} was obtained. They were then extruded at room temperature into a Liposofast device (Avestin, Canada) through two polycarbonate membrane filters of 0.2 μm pore size a minimum of 9 times both ways (MacDonald et al., 1991).

2.3. Characterization of magnetic particles

The morphology of magnetoliposomes was observed by TEM using a Jeol 1010 microscope (Jeol, Japan) operating at 80,000 kV. Previous to the preparation of the samples, magnetoliposomes were separated from empty liposomes by means of a MACS separation column (Miltenyi Biotech, Bergisch Gladbach, EU). Samples were prepared by placing a drop of the particle suspension onto a 400-mesh copper grid coated with carbon film (in some preparations, the magnetoliposomes were stained with uranyl acetate), and they were allowed to air dry before being inserted into the microscope. Images were recorded with a Megaview III camera. The acquisition was accomplished with Soft-Imaging software (SIS, EU). The iron content of magnetic particles was determined by atomic absorption spectrophotometry in a UNICAM PU 939 flame absorption spectrometer equipped with an acetylene/air (1:1) burner and a selenium hollow cathode lamp (Hereaus), which was operated at 248.3 nm with a 0.5 nm band pass. A reference iron solution (50 μg mL^{-1}) was prepared by dilution of a 1000 μg mL^{-1} solution (Merck, Titrisol, Darmstadt, EU) with double distilled water containing 1% of nitric acid. The measurement of iron was highly linear ($R^2 > 0.997$) over the concentration range of 0.3–3.0 μg mL^{-1}. The reproducibility of the assay was determined by repeated measurements of the reference solution as part of a run or from run to

run. The value (93 ± 2 mg Fe^{3+} per mL of ferrofluid) was the average of three replicates. In the case of magnetoliposomes, iron was measured by atomic absorption spectrophotometry as previously described, and by a colorimetric method based on the titration of ferrous ion by *o*-phenanthroline (Kiwada et al., 1986). Both results coincided. The magnetization of magnetoliposomes and ferrofluid was measured as a function of the applied external magnetic field in a SQUID Quantum Design MPMS XL magnetometer. The external magnetic field was swept from +5000 to −5000 Oe, and then back to +5000 Oe. Measurements were taken at room temperature. The hydrodynamic diameter of magnetoliposomes was determined by dynamic light scattering at 90° with a Zetasizer Nano (Malvern, EU) at 25 °C. The particle size distribution was designated by the polydispersity index (PI), which ranged from 0.0 for an entirely monodisperse sample to 1.0 for a polydisperse sample. The ζ-potential measurements of magnetoliposomes were performed at 25 °C using a Zetasizer Nano ZS (Malvern, EU).

2.4. Encapsulation efficiency determination

To establish the best magnetite/phospholipid ratio, we prepared liposomes hydrated with 1.28–32.11 mg of magnetite per mL of suspension. Non-entrapped ferrofluid particles were removed by size exclusion chromatography (SEC) on Sepharose 4B (GE Healthcare, EU). A total of 250 μL of magnetoliposomes were applied to a 1×30 cm column saturated with lipids before sample elution and eluted with bidistilled water. The amount of encapsulated magnetite was determined on the basis of the ferrous ion using *o*-phenanthroline (Kiwada et al., 1986). The phospholipid content was determined by the Steward-Marshall method (Steward-Marshall, 1980). At high magnetite concentrations, the colour of the ferrofluid is added to the colour developed in the chemical reaction. Consequently, the magnetite must be separated from the phospholipids prior to the phospholipid determination. For this purpose, a MACS separation column was used. If a powerful magnet is placed in the system, iron oxide particles pass through the liposomal membrane. Once it has been verified that phospholipid is recovered at 100% in the effluent, the percentage of encapsulation can be calculated from the magnetite/phospholipid ratio.

2.5. Animal and biological methods

We used twenty-seven eight-week-old female CD-1 mice with a body weight of 28–32 g (Harlam Ibérica, Sant Feliu de Codines, Barcelona, EU). The study was conducted under a protocol approved by the Animal Experimentation Ethics Committee of the University of Barcelona.

The mice were randomly divided into four groups (five animals per group): (a) healthy control-saline (*C*): animals with a back air pouch that received saline intravenously (i.v.) (0.1 mL/10 g body weight); (b) healthy control-magnetoliposomes (*CM*): animals with a back air pouch that received magnetoliposomes i.v. (10 mg of iron/kg body weight); (c) an inflammation-control group (*I*): animals with carrageenan-induced inflammation in the air pouch; and (d) inflammation-magnetoliposomes (*IM*): animals with carrageenan-induced inflammation in the air pouch that received magnetoliposomes i.v. (10 mg of iron/kg body weight).

The method used to induce acute inflammation is similar to that described by Romano et al. (1997). Briefly, sterile air pouches were produced by injecting 5 mL of air subcutaneously into the back of the mouse. Then, 1 mL of sterile saline (groups C and CM) or 1 mL of the phlogogen, 1.2% carrageenan lambda (Sigma–Aldrich, Saint Louis, MO) in saline (groups I and IM), was injected into the air pouch. Five hours later, saline (groups C and I) or magnetoliposomes in saline (groups CM and IM) was administered through the jugular vein to anesthetized (isoflurane, Dr Esteve S.A., Barcelona, EU) mice. The mice were sacrificed twenty min after the saline or magnetoliposome administration.

The iron content in plasma, exudates (pouch) and organs were analyzed by inductively coupled plasma atomic emission spectroscopy (ICP-AES, Perkin-Elmer Optima 3200RL, Massachusetts, USA) after acid digestion of the organic material. The statistical significance of iron concentrations was analyzed using ANOVA. Statistical significance was accepted at the 5% level ($P \leq 0.05$). Values are expressed as mean ± SEM.

3. Results and discussion

3.1. Characterization of magnetic particles

A TEM micrograph of magnetoliposomes is shown in Fig. 1. The size of the magnetoliposomes ranged from 130 to 180 nm and they were full of clusters of particles of ferrofluid. The magnetization curve of the magnetoliposomes is shown in Fig. 2. The saturation magnetization (taken as magnetization at the maximum field of 5 kOe, that is, 0.025 emu g^{-1} or 0.028 emu cm^{-3}; the volume magnetization was calculated by assuming that the density of the overall solution was 1.1 g cm^{-3}) was lower than the theoretical value for the bulk Fe_3O_4 of 96.43 emu g^{-1} (4), but was nevertheless consistent with a magnetic colloid in water (1.8 vol% Fe_3O_4, according to the technical information on the ferrofluid) and encapsulated in liposomes. The magnetization curve also showed negligible remnant magnetization at zero field, which is also characteristic of a soft ferromagnetic material of small dimensions such as magnetite. However, the absence of hysteresis at room temperature demonstrated the superparamagnetic behaviour of the magnetite powder of the magnetic particles.

The dependence of the ζ-potential on pH was investigated in magnetoliposomes. Buffer solutions of pH ranging from 2.25 to 11.30 were prepared with phosphate, citrate and borate solutions. Samples were prepared by adding 1.5 μL of magnetoliposomes to aliquots of 3 mL of each pH solution. The ζ-potential results are shown in Fig. 3. The external phospholipid monolayer conferred a negative charge to the magnetoliposomes for the 3.9–11.30 range of pH, as evidenced by the negative values of ζ-potential determined. At pH 7.4, a ζ-potential value of −26.3 mV was obtained (the pH of

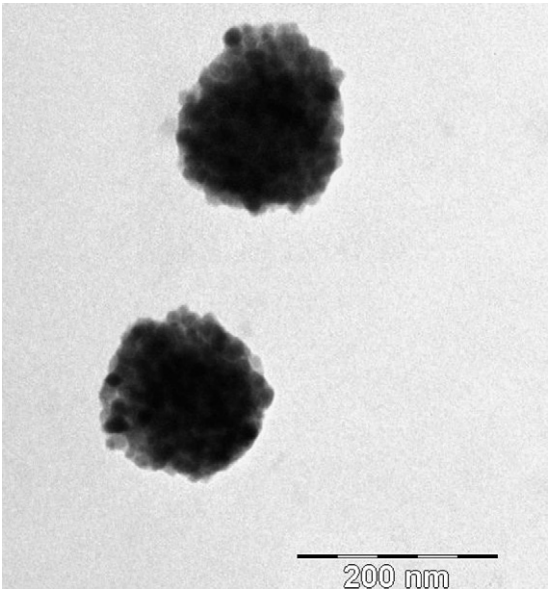

Fig. 1. TEM micrograph of magnetoliposomes. In this figure, the magnetoliposomes were not stained.

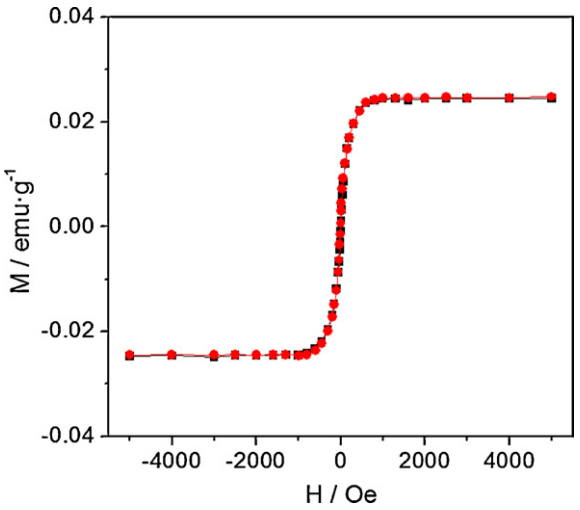

Fig. 2. Mass magnetization as a function of the external magnetic field for magnetoliposomes at ~300 K. The external magnetic fluid was swept from +5000 to −5000 Oe (circles) and then back to +5000 Oe (squares).

the saline suspension of magnetoliposomes is 6.7). Under the same conditions, the ferrofluid gave a maximal value of −41.8 mV at a pH of 3.5. Electrostatic stabilization was confirmed by the fact that no sedimentation was observed when magnetoliposomes at pH 7.4 were centrifuged at ~50,000 × *g* for 15 min at room temperature.

The influence of salts on ζ-potential was also checked in magnetoliposomes. In water, magnetoliposomes presented a ζ-potential of −33.2 mV. When a 1:1 electrolyte was added (KBr or $NaNO_3$), the ζ-potential was greatly reduced at the lowest salt concentration used (Fig. 4). After this reduction, the values of ζ-potential underwent a slight, but continuous, variation with salt concentration: an increase in salt concentration was concomitant with less negative values of ζ-potential. A different effect was observed with divalent salts ($Ca[NO_3]_2$ or $Mg[NO_3]_2$). These salts reversed the negative initial values of the charge to the positive values. This finding can be explained by the adsorption of the counter ions on the external layer of the phospholipid. Since positive values were observed at salt concentrations of less than 0.01 mol L^{-1}, such divalent ions clearly have high adsorption ability. Whereas monovalent ions do not produce any aggregation on liposomes, divalent ions, namely calcium and magnesium, result in the aggregation of charged liposomes (Roldán-Vargas et al., 2009).

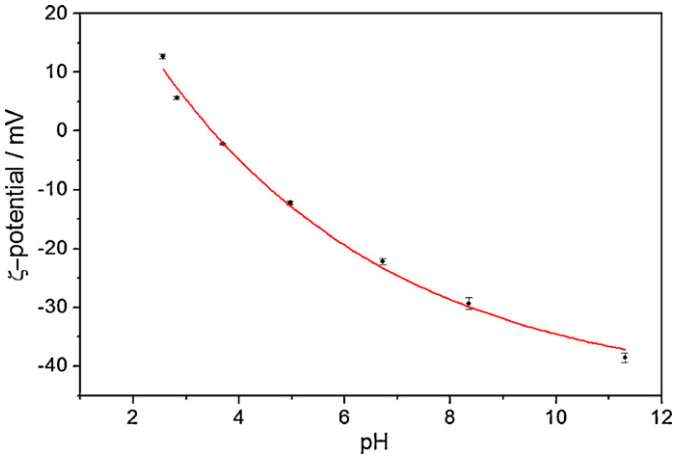

Fig. 3. The ζ-potential of magnetoliposomes as a function of pH. Buffer solutions with an ionic strength of 0.002 were used. Lines are given as a guide (*n* = 3).

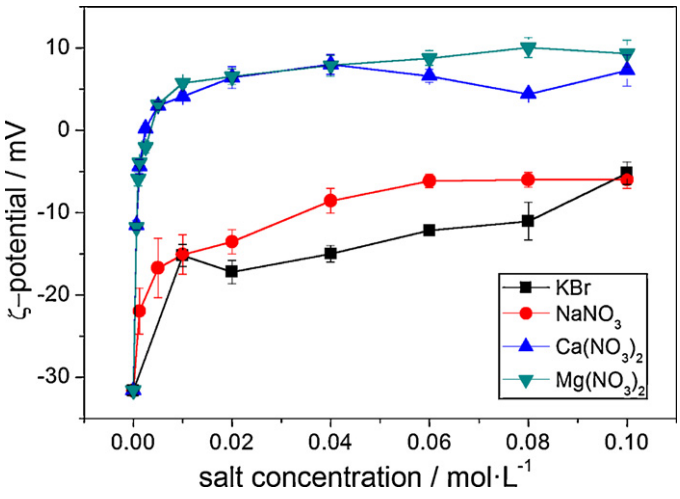

Fig. 4. Influence of electrolytes (monovalent and divalent ions) on electrophoretic properties of magnetoliposomes (*n* = 3).

Fig. 5 shows the profiles of multilamellar magnetoliposomes and extruded magnetoliposomes before and after the SEC purification of a liposomal sample containing 0.140 g of Fe^{3+} per mmole of phospholipids. The size distribution of ferrofluid is displayed in the inset in Fig. 5. This distribution was centred at 104 nm, and, although monomodal, it was polydisperse (PI = 0.291). The hydrodynamic radius of ferrofluid exceeded the radius of the magnetite particle (10 nm) that was obtained by TEM. Thus, a ferrofluid particle may contain more than one particle of magnetite. The clustering of magnetic nanoparticles has also been observed in magnetite stabilized surfactants (Ditsch et al., 2005; Sabaté et al., 2008). Multilamellar magnetoliposomes obtained after solvent evaporation that did not undergo the extrusion step exhibited a bimodal distribution, with a peak centred at 369 nm (76.2% of the entire intensity) corresponding to magnetoliposomes, whereas the minor peak at 80.5 nm (23.8% of the intensity) corresponded to the non-encapsulated ferrofluid. This pattern was observed for all the iron concentrations tested. After extrusion, a wide, unique peak with maxima between 160 and 190 nm was observed. A value of 187 nm was found for the preparation described above. Purification by size exclusion chromatography afforded a narrower peak with a *z*-mean diameter shifted to approximately 200 nm (in this case, 218 nm). This value is in agreement with the diameter obtained by TEM. These

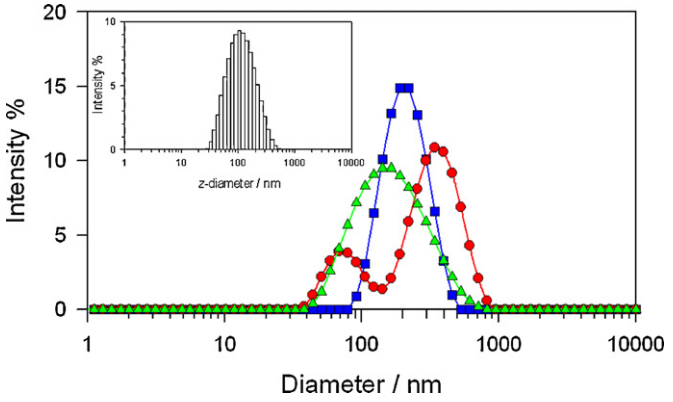

Fig. 5. Distribution of hydrodynamic diameters expressed as *z*-diameters at 298 K of multilamellar magnetoliposomes (red circles), unpurified extruded magnetoliposomes (green triangles), and purified extruded magnetoliposomes (blue squares). The concentration of the samples was 0.140 g Fe^{3+} by mmol of phospholipid. Inset: size distribution of ferrofluid particles. (For interpretation of the references to colour in this figure legend, the reader is referred to the web version of the article.)

Table 1
Encapsulation efficiency of magnetoliposomes.

Initial iron/phospholipid ratio (g/mol) for preparing magnetoliposomes	Final iron/phospholipid ratio (g/mol) for preparing magnetoliposomes after their purification by SEC	Percentage of Fe_3O_4 encapsulated
0.028 + 0.001	0.016 + 0.001	57.1 + 0.1
0.037 + 0.001	0.018 + 0.001	48.6 + 0.1
0.056 + 0.001	0.024 + 0.002	44.6 + 0.1
0.140 + 0.006	0.016 + 0.001	11.4 + 0.1

values imply that the recovered magnetoliposomes were mainly free of contaminating external magnetite, and that the distribution obtained with non-purified magnetoliposomes was the result of overlapping of the ferrofluid and liposome distributions.

3.2. Encapsulation efficiency determination

The encapsulation efficiency was determined in liposomes with varying initial weight/mol ratios of magnetite to phospholipids, ranging from 0.028 g iron/mmol PC to 0.140 g iron/mmol PC. In all set ups, an identical amount of phospholipid was used initially. Magnetite and phospholipid concentrations were determined before extrusion and after purification by chromatography. Table 1 shows the results obtained for encapsulation efficiency.

The amount of encapsulated iron steadily increases as the starting iron/phospholipid ratio increases from 0.028 to 0.056 g iron/mmol PC. The low percentage of encapsulation from 0.140 g iron/mmol PC can be explained by the loss of magnetite during the extrusion process, since the polycarbonate membrane is completely covered by a dark film of magnetite. Although mag-

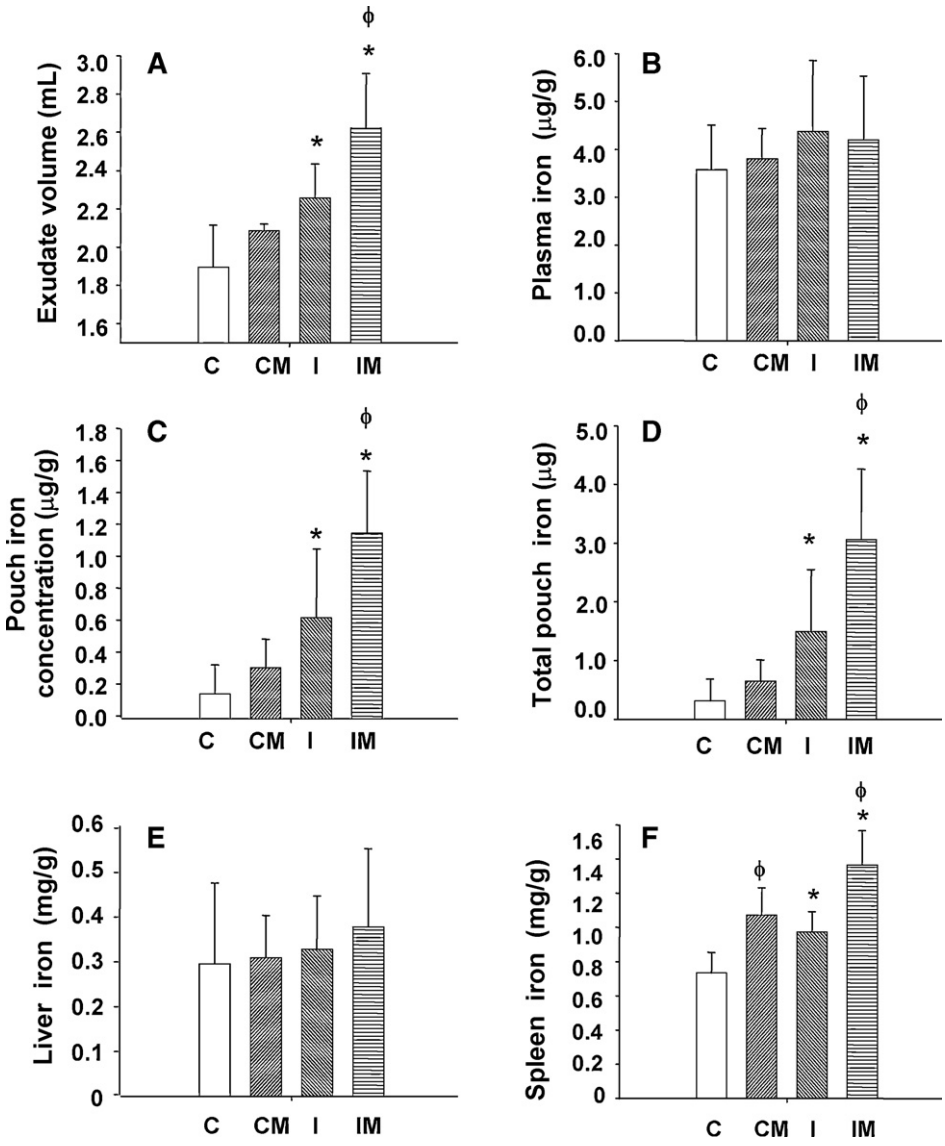

Fig. 6. (A) Pouch volume (mL); (B) plasma iron concentration (μg/mL); (C) pouch (exudates) iron concentration (μg/g); (D) pouch total iron (μg); (E) liver iron concentration (mg/g), and (F) spleen iron concentration (mg/g). Bars represent mean ± SD. From left to right bars correspond to: healthy control mice (C, □), control mice that received magnetoliposomes i.v. (CM, ▨), mice with inflammatory pouch (I, ▧) and mice with inflammatory pouch with magnetoliposomes i.v. (IM, ▤). $P < 0.05$ between control and inflammation groups of mice with or without magnetoliposomes (inflammatory effect). $^{\phi}P < 0.05$ between control and inflammation groups of animals with or without magnetoliposomes (effect of magnetoliposomes).

netite is much smaller than the magnetoliposomes, the formation of clusters of ferrofluid particles could explain the presence of magnetite on the surface of membranes.

As we wanted to determine whether the reverse-phase evaporation presented an improvement in the encapsulation of magnetite, we compared the encapsulation in magnetoliposomes prepared using this method with that obtained by a simple extrusion. In both cases, we used initial ratios of 0.056 g of iron per mmole of phospholipid. After SEC purification, we obtained the following encapsulations: 15.0 ± 1.0 mg iron/mmol PC ($n = 4$) for the extruded magnetoliposomes and 23.8 ± 1.7 mg iron/mmol PC ($n = 4$) for the reverse-phase extruded magnetoliposomes. A statistical analysis of the corresponding means indicated that the encapsulation was significantly different ($P = 0.0002$).

3.3. Biological results

Fig. 6 summarizes the biodistribution of iron after the administration of magnetoliposomes i.v. in mice with or without induced inflammation. Fig. 6A shows the effects of the experimental inflammation on the volume of the exudates. As could be expected, the volume of the pouch exudates in the inflammation control group (I) increased ($P = 0.0255$) in comparison with the healthy control group (C). The volume of exudates in the inflammation-magnetoliposomes group (IM) was also higher than that of the control magnetoliposomes group (CM) ($P = 0.0188$). In the control group, the administration of magnetoliposomes did not increase the volume of exudates. However, an increase in exudate volume was observed in the inflammation group after magnetoliposomes administration ($P = 0.0009$). There was no increase in iron plasma levels (Fig. 6B) after the injection of magnetoliposomes into both healthy and inflammation groups. Plasmas from animals that received magnetoliposomes and those that received saline appeared clear, with no hemolysis.

The iron concentration and total iron in the inflamed air pouch (I) was higher than that of the healthy control non-inflamed air pouch (C) ($P = 0.040$ and $P = 0.056$, respectively) (Fig. 6C and D). This indicates that inflammation produces an increase in iron levels. The same behaviour was observed in animals that received magnetoliposomes: the iron concentration and total iron in the inflamed pouch of animals that received magnetoliposomes (IM) was higher than that of the control animals that received magnetoliposomes (CM) ($P = 0.000$ and $P = 0.003$). In this case, the increase of iron in the inflamed zone (pouch) is a consequence of the inflammation and of the presence of liposomes in this area: the acute inflammatory phase that was produced is characterized by local vasodilatation and enhanced vascular permeability, which facilitates the passage of magnetoliposomes to the inflammatory pouches. As far as the effect of magnetoliposomes on iron levels in the pouch is concerned (Fig. 6C and D), there was no significant increase in iron concentration or total iron in healthy control animals after the administration of magnetoliposomes (C, CM). However, a clear increase in iron concentration and total iron was observed after the administration of magnetoliposomes to animals with air pouch inflammation (I, IM) ($P = 0.018$ and $P = 0.011$).

We did not find any changes that could be attributed to inflammation or magnetoliposomes in the iron concentration in liver (Fig. 6E). However, spleen iron levels increased due to inflammation. Thus, animals with inflammation (with or without magnetoliposomes) had higher iron levels than control animals (without magnetoliposomes [$P = 0.053$] or with them [$P = 0.012$], respectively) (Fig. 6F). After the administration of magnetoliposomes to control animals, the iron levels increased ($P = 0.007$) as they did when magnetoliposomes were administered to animals with inflammation ($P = 0.027$).The levels of basal iron that were found in our study were similar to those reported by Jones et al. (2007). Usually, the highest concentration of magnetic nanoparticles is observed in the liver and spleen (Kim et al., 2006). However in our study, there was no increase in iron concentration in the liver (an organ of the mononuclear phagocytic system) after intravenous administration, whereas there was a clear increase in the spleen compared to the control group (Fig. 6E and F). A similar feature was observed after intraperitoneal administration of magnetic nanoparticles (Kim et al., 2006). Clearly, some factors, such us liposome size, charge and the physical state of the phospholipids used, must determine the specificity of any tissue for magnetoliposomes, and, consequently, for magnetic nanoparticles.

4. Conclusions

Magnetic nanoparticles were encapsulated in liposomes with dimensions of about 200 nm elaborated by reverse-phase evaporation followed by sequential extrusion. The magnetic nanoparticles had superparamagnetic properties. Due to their electrostatic stabilization, we avoided the sedimentation of the magnetic nanoparticles under a gravitational field. Despite the loss of magnetite during the extrusion process, the encapsulation efficiencies achieved with this method were significantly higher than those obtained for magnetoliposomes prepared by simple extrusion.

However, the results of the iron biodistribution study in mice indicate that the magnetic nanoparticles accumulated mainly in the inflammation zone, without the need of a magnet to potentiate the migration of magnetoliposomes to the target site. This suggests that this kind of magnetoliposomes could be used as a system for delivering anti-inflammatory drugs.

Acknowledgment

The authors are grateful for the financial support given by the Spanish Ministerio de Ciencia e Innovación (MICINN) to the project MAT2009-13155-C04-03.

References

Arruebo, M., Fernández-Pacheco, R., Ibarra, M.R., Santamaría, J., 2007. Magnetic nanoparticles for drug delivery. NanoToday 2, 22–32.
Barenholz, Y., 2001. Liposome application: problems and prospects. Curr. Opin. Colloid Interface Sci. 6, 66–77.
Blums, E., Cebers, A., Mairov, M.M., 1997. Magnetic Fluids. Walter de Gruyter, Berlin.
Bulte, J.W.M., De Cuyper, M., 2003. Magnetoliposomes as contrast agents. Methods Enzymol. 373, 175–198.
Craig, D., 1995. Magnetism-Principles and Applications. Wiley, Chichester.
Dandamundi, S., Campbell, R.B., 2007. Development and characterization of magnetic cationic liposomes for targeting tumor microvasculature. Biochim. Biophys. Acta 1768, 427–438.
De Cuyper, M., Joniau, M., 1988. Magnetoliposomes. Formation and structural characterization. Eur. Biophys. J. 15, 311–319.
De Cuyper, M., Müller, P., Lueken, H., Hodenius, M., 2003. Synthesis of magnetic Fe_3O_4 particles covered with a modifiable phospholipids coat. J. Phys.: Condens. Matter. 15, S1425–S1436.
De Cuyper, M., Caluwier, D., Baert, J., Cocquyt, J., Van der Meeren, P., 2006. A successful strategy for the production of cationic magnetoliposomes. Z. Phys. Chem. 220, 133–141.
Ditsch, A., Laibinis, P.E., Wang, D.I.C., Hatton, T.A., 2005. Controlled clustering and enhanced stability of polymer-coated magnetic nanoparticles. Langmuir 21, 6006–6018.
Jones, B.C., Beard, B.L., Gibson, J.N., Unger, E.L., Allen, R.P., McCarthy, K.A., Early, C.J., 2007. Systems genetic analysis of peripheral iron parameters in the mouse. Am. J. Physiol. Regul. Integr. Comp. Physiol. 293, 116–124.
Kim, J.S., Yoon, T.-J., Yu, K.N., Kim, B.G., Park, S.J., Kim, H.W., Lee, K.H., Park, S.B., Lee, J.-K., Cho, M.H., 2006. Toxicity and tissue distribution of magnetic nanoparticles in mice. Toxicol. Sci. 89, 338–347.
Kiwada, H., Sato, J., Yamada, S., Kato, Y., 1986. Feasibility of magnetic liposomes as a targeting device for drugs. Chem. Pharm. Bull. 34, 4253–4258.
Laurent, S., Vander Elst, L., Thirifays, C., Muller, R.N., 2008. Paramagnetic liposomes: inner versus outer membrane relaxivity of DPPC liposomes incorporating gadolinium complexes. Langmuir 241, 4347–4351.
Leslie-Peleckie, D.L., Rieke, R.D., 1996. Magnetic properties of nanostructured materials. Chem. Mater. 8, 1770–1783.

MacDonald, R.C., MacDonald, R.I., Menco, B.P., Takeshita, K., Subbarao, N.K., Hu, L.R., 1991. Small-volume extrusion apparatus for preparation of large, unilamellar vesicles. Biochim. Biophys. Acta 1061, 297–303.
Mailänder, V., Landfester, K., 2009. Interaction of nanoparticles with cells. Biomacromolecules 10, 2379–2400.
Martina, M.S., Fortin, J.P., Ménager, C., Clément, O., Barratt, G., Grabielle-Madelmont, C., Gazeau, F., Cabuil, V., Lesieur, S., 2005. Generation of superparamagnetic liposomes revealed as highly efficient MRI contrast agents in vivo imaging. J. Am. Chem. Soc. 127, 10676–10685.
Odenbach, S., 2003. Ferrofluids – magnetically controlled suspensions. Colloid Surf. A 217, 171–178.
Pankhurst, Q.A., Connolly, J., Jones, S.K., Dobson, J., 2003. Applications of magnetic nanoparticles in biomedicine. J. Phys. D 36, R167–R181.
Plassat, V., Martina, M.S., Barratt, G., Ménager, C., Lesieur, S., 2007. Sterically stabilized superparamagnetic liposomes for MR imaging and cancer therapy: pharmacokinetics and biodistribution. Int. J. Pharm. 344, 118–127.
Reiss, G., Hütten, A., 2005. Magnetic nanoparticles. Applications beyond data storage. Nat. Mater. 4, 725–726.
Roldán-Vargas, S., Barnadas-Rodríguez, R., Quesada-Pérez, M., Estelrich, J., Callejas-Fernández, J., 2009. Surface fractals in liposome aggregation. Phys. Rev. E. 79, 011905-1–011905-14.
Romano, M., Faggioni, R., Sironi, M., Sacco, S., Echtenacher, B., Di Santo, E., Salmona, M., Ghezzi, P., 1997. Carrageenan-induced acute inflammation in the mouse air pouch synovial model. Mediators Inflamm. 6, 32–38.
Rosenweig, R.E., 1985. Ferrohydrodynamics. Cambridge University Press, London.
Sabaté, R., Barnadas-Rodríguez, R., Callejas-Fernández, J., Hidalgo-Álvarez, R., Estelrich, J., 2008. Preparation and characterization of extruded magnetoliposomes. Int. J. Pharm. 347, 156–162.
Schmitt, A.M., 2007. Thermoresponsive magnetic colloids. Colloid Polym. Sci. 285, 953–966.
Steward-Marshall, J.C., 1980. Colorimetric determination of phospholipids with ammonium ferrothiocyanate. Anal. Biochem. 104, 10–14.
Szoka, F., Papahadjopoulos, D., 1978. Procedure for preparation of liposomes with large internal aqueous phase and high capture by reverse-phase evaporation. Proc. Natl. Acad. Sci. U.S.A. 75, 4194–4198.
Wijaya, A., Hamad-Schifferli, K., 2007. High-density encapsulation of Fe_3O_4 nanoparticles in lipid vesicles. Langmuir 23, 9546–9550.

Artículo 2.

Using nanoparticles for enhancing the focusing heating effect of an external waveguide applicator for oncology hyperthermia: evaluation in muscle and tumor phantoms.

Progress In Electromagnetics Research, 121, 343–363.

Un reto en la hipertermia es lograr un calentamiento local de la región del tumor hasta alcanzar la temperatura apropiada para destruir las células cancerosas, sin dañar el tejido sano circundante. La hipertermia magnética, es una nueva terapia mínimamente invasiva destinada a concentrar el calor en los tejidos cancerosos. Esta terapia se basa en la inyección de nanopartículas superparamagnéticas dentro del tumor. En nuestro estudio, las nanopartículas superparamagnéticas, que hemos desarrollado y caracterizado, se componen de nanopartículas de óxido de hierro estabilizado con polietilenglicol. Además, se presenta una nueva técnica especialmente diseñada para hipertermia magnética utilizando como aplicador externo, una guía de ondas electromagnéticas. Se han utilizado 3 concentraciones de magnetita diferentes que se colocaron, dentro de los phantoms de músculo (simulan tejidos), a 3 distancias diferentes del aplicador. Además, se ensayaron dos volúmenes de tumor 2,5 ml y 5,0 mL. La determinación de las curvas de temperatura en función del tiempo, permitieron establecer la concentración de nanopartículas más apropiada para obtener el valor de temperatura adecuada para la terapia de hipertermia. Los resultados que se muestran en este artículo, confirmar la viabilidad del uso de nanopartículas como agentes para la focalización de la energía en el tumor, sin dañar tejidos sanos. Además, estos experimentos han concluido que mediante el uso de este aplicador en combinación con nanopartículas, también es posible controlar localmente los incrementos de temperatura en los tejidos.

Progress In Electromagnetics Research, Vol. 121, 343–363, 2011

USING NANOPARTICLES FOR ENHANCING THE FOCUSING HEATING EFFECT OF AN EXTERNAL WAVEGUIDE APPLICATOR FOR ONCOLOGY HYPERTHERMIA: EVALUATION IN MUSCLE AND TUMOR PHANTOMS

C. J. Trujillo-Romero [1, *], S. García-Jimeno [2], A. Vera [1], L. Leija [1], and J. Estelrich [2, 3]

[1]Electrical Engineering Department, Bioelectronics Section, CINVESTAV-IPN, Mexico D.F., Mexico

[2]Departament de Fisicoquímica, Facultat de Farmàcia, Universitat de Barcelona, Avda. Joan XXIII, Barcelona 08028, Catalonia, Spain

[3]Institut de Nanociència i Nanotecnologia, IN^{2}UB, Universitat de Barcelona, Spain

Abstract—A technical challenge in hyperthermia therapy is to locally heat the tumor region up to an appropriate temperature to destroy cancerous cells, without damaging the surrounding healthy tissue. Magnetic fluid hyperthermia (MFH) is a novel, minimally invasive therapy aiming at concentrating heat inside cancerous tissues. This therapy is based on the injection of different superparamagnetic nanoparticles inside the tumor. In our study, superparamagnetic nanoparticles, which we developed and characterized, consisted of iron oxide nanoparticles stabilized with polyethylene glycol. Moreover, a new technique for MFH using a specially designed external electromagnetic waveguide as applicator is presented. Three magnetite concentrations were used for making the tumor phantoms, which were embedded in muscle phantoms. The phantoms were radiated and located at three different distances from the applicator. Furthermore, two volumes of tumor (2.5 mL and 5.0 mL) were assayed. Heating curves, as a function of time, allowed the establishment of a more appropriate nanoparticle concentration for obtaining the temperature increase suitable for hyperthermia therapy. The results shown in this

Received 29 September 2011, Accepted 19 October 2011, Scheduled 1 November 2011

* Corresponding author: Citlalli Jessica Trujillo-Romero (ctrujillo@cinvestav.mx).

The technical contribution of the second author to this work was as significant as the first author.

paper confirm the feasibility of using nanoparticles as agents to focus the energy over the tumor, without creating hot spots in healthy tissue. In addition, the experiments validated that by using this applicator in combination with nanoparticles, it is also possible to locally control the increments of temperature in tissues.

1. INTRODUCTION

The biological effectiveness of heating for cancer treatment, so-called hyperthermia, has been known for decades [1, 2]. Hyperthermia, which is an increase of temperature up to 42°C to 45°C, can be artificially induced by using drugs, particles, or medical devices [3, 4]. One kind of hyperthermia therapy is the magnetic fluid hyperthermia (MFH), which exploits the magnetic properties of nano-size iron oxides to destroy tumor cells; these nanoparticles might also be used as agents to enhance chemotherapy and radiotherapy [5, 6]. It has been shown that ferrofluid-mediated hyperthermia can be synergistically enhanced and improved by chemotherapy using magnetic nanoparticles functionalized with various anticancer drugs [7, 8]. The most used nano-size iron oxides are maghemite (γ-Fe_2O_3) and magnetite (Fe_3O_4). The reasons for this choice are: (i) both the iron oxides are biocompatible; (ii) they can be synthesized on a large scale; and (iii) their magnetization is significantly high, thus allowing these particles to be easily controlled by an external magnetic fields [9]. When magnetic nanoparticles are exposed to an appropriate AC magnetic field, the magnetic energy is converted into heat [10, 11]. The transformation of the magnetic energy into heat is due to the Néel relaxation, which is caused by the rapidly alternating magnetic dipole moments, and the Brownian relaxation, which is due to nanoparticle rotation, resulting in friction of the particles with the fluid [13]. For ferrofluids, which are stabilized magnetic nanoparticles, the Brownian and Néel relaxations depend on the particle size ($\sim$20 nm) [14]. If magnetic nanoparticles are inserted inside a tumor, as magnetic fields can penetrate the body, the application of an external electromagnetic (EM) field in the desired range of radiofrequencies will generate a thermal shock which will destroy the cells of the tumor without damaging the surrounding healthy tissues noninvasively. This is achieved by increasing the susceptibility of carcinogenic cells in environments of 42–45°C temperature, leading to apoptotic reactions [12]. The heat generated by the nanoparticles has a therapeutic effect similar to that obtained by conventional hyperthermia treatments but with the advantage that it is concentrated only at the tumor.

Nowadays, several studies concerning ferrofluid behavior in hyperthermia treatments have been performed by using coils to generate alternating magnetic fields, which excite nanoparticles implanted in tumors [15, 16]. Magnetic fields at low frequencies (e.g., 153 kHz) are used in most of the studies carried out in hyperthermia treatments [10]. Even if coils are the typical devices to generate alternating magnetic fields, there are other devices that are able to generate such fields, and one of them is the waveguide (WG).

In hyperthermia, WGs radiate EM waves into the patient. The TE mode is the most often used in hyperthermia treatments [17–19]. The TE waveguide primarily generates an electric field perpendicular to the propagation axes; the electrical field interacts with the dielectric properties of the tissue thereby causing heating. WGs also generate a magnetic field; however, the permeability of biological tissues is equal to that of free space, and, in consequence, biological tissues are considered for this application as nonmagnetic [20]. Hence, the magnetic field generated by the applicator cannot cause heating in the tissue. For this reason, hyperthermia studies carried out with WGs only took into account the electric field generated by the applicator.

At present, the use of magnetic nanoparticles as an agent to focus EM energy is one of the most promising techniques in hyperthermia. In this paper, we use magnetic nanoparticles coated with polyethylene glycol (PEG) as a system of nanoparticles for exploiting the magnetic field generated by a WG. PEG stabilizes the nanoparticles thereby avoiding aggregation and conferring biostability to them because the *in vivo* clearance of the nanoparticles is significantly delayed [15]. Because of their high flexibility and hydrophilicity, PEG macromolecules are good stabilizing agents. In the cited studies, the magnetic particles have been stabilized by substances different than PEG. According to our information, this is the first time that an unmodified PEG has been used to obtain a ferrofluid suitable for hyperthermia studies. In unpublished studies, we have checked the stability of ferrofluid performed with several amounts and molecular weights of PEG. The use of PEG 6000 afforded a material with a great stability. And, furthermore, the obtained ferrofluid is wholly biocompatible and biodegradable. The used concentration of magnetite is similar to that found in literature.The synergic use of a rectangular WG and magnetic nanoparticles allows taking advantage not only of the effect of the electric field but also of the effect of the magnetic field in a hyperthermia therapy. With this approach, the area of energy deposition can be locally controlled, thereby potentiating the heating effect in the tumor. On the other hand, it is also possible to reduce the time of treatment, as well as the input power used in the hyperthermia

treatment.

Nowadays, different equations describe the interaction of EM fields with tissue; this interaction causes heating in biological tissues. Bioheat transfer equation (BHTE) is used to describe the temperature evolution in biological tissues. The BHTE proposed by Pennes [21] can be written as:

$$\rho_t C_t \frac{\partial T}{\partial t} = \text{div}\,(k\nabla T) + \omega_b \rho_b C_b\,(T_b - T) + Q_{met} + Q_{ext}, \qquad (1)$$

where ρ_t, C_t, and k, are the density, specific heat and thermal conductivity of the tissue, respectively; ρ_b, C_b, and ω_b are the density, specific heat and perfusion rate of blood, respectively; T_b is the arterial blood temperature; Q_{met} is the heat source from metabolism, and Q_{ext} is the absorbed power density which can be written as:

$$Q_{ext} = \frac{1}{2}\sigma_t\,|E|_{,}^{2} \qquad (2)$$

where σ_t is the electrical conductivity of the tissue and E is the electric field generated by the WG applicator. By analyzing Eq. (2), it is evident that only the E field is taken into account to achieve the temperature increase in tissues and tumors. Although the WG applicator generates E and H fields, the last one is neglected because tissues are considered in these studies as nonmagnetic. However, when magnetic nanopartices are injected into tumors, their magnetic properties are intensified, and consequently, the H field also is involved in the heating process.

On the other hand, if magnetic nanoparticles are concentrated inside tumors the absorbed power density is given by [22]:

$$Q_{ext} = \pi\mu_0\chi'' f H^2 \qquad (3)$$

where μ_0 is the permeability of free space, χ'' is the imaginary part of the magnetic susceptibility, f is the frequency of the alternating magnetic field, and H is the magnetic field amplitude. From Eq. (3), it is observed that temperature increments are proportional to the square of the amplitude of the H field intensity [20]. In which case, the E and H fields can be used as sources for heating, by substituting Eqs. (2) and (3) by Eq. (1), the BHTE can be rewritten in other terms as:

$$\rho_t C_t \frac{\partial T}{\partial t} = \text{div}\,(k\nabla T) + \omega_b \rho_b C_b\,(T_b - T) + Q_{met} + \frac{1}{2}\sigma_t |E|^2 + \pi\mu_0\chi'' f H^2 \qquad (4)$$

From Eq. (4), it can be observed that the heating effect is produced by both the electric and magnetic fields generated by the external applicator; i.e., the heating effect produced by the WG applicator depends not only of the square of E field but also of the square of

H field. For this reason, the heating efficiency is higher compared with that obtained with a coil; in which just the magnetic field is taken into account for heating. In this sense, to test the hyperthermic effect of magnetic nanoparticles, and to observe the behavior of temperature increase in the deep regions and the dependence of the concentration of magnetic particles in the tumor tissue, the distribution of temperature increases, along the depth of agarose phantoms with different concentrations of magnetic particles, has been analyzed.

2. MATERIALS AND METHODS

2.1. Materials

All chemicals were of reagent grade and used without purification. Ferric chloride hexahydrate ($Cl_3Fe.6H_2O$) and ferrous chloride tetrahydrate ($Cl_2Fe.4H_2O$) were purchased from Sigma-Aldrich (St. Louis, MO). Agarose (Ultrapure^{TM} agarose) was purchased from Invitrogen (Mexico, D.F.). Polyethylenglycol (PEG) of 6000 Da molecular weight was from VWR International (Barcelona, EU). Ammonium hydroxide (NH_4OH, 25%) was from Panreac (Barcelona, EU). Deionized Millipore Milli-Q water was used in all experiments. A strong neodymium — iron — boron ($Nd_2Fe_{12}B$) magnet (1.2 T) was obtained from Halde GAC (Barcelona, EU).

2.2. Synthesis and Characterization of Ferrofluid

The ferrofluid was prepared by using a co-precipitation method in the presence of excess PEG. Briefly, once the polymer was dissolved in water, $FeCl_2/FeCl_3$ at 1 : 2 molar ratio were added. When the PEG and iron salts were well dissolved, a 25% (v/v) NH_4OH solution was added with vigorous mechanical stirring. Later, the ferrofluid was poured into a beaker and the vessel was placed onto the permanent magnet. The ferrofluid was washed four times with water by decanting the supernatant so as to eliminate excess PEG. Finally, water was added until the desired concentration was obtained. The final suspension was sonicated (Transsonic Digital Bath sonifier, Elma, EU). The morphology of the ferrofluid was studied by transmission electron microscopy (TEM_i) by using a Jeol 1010 microscope at an accelerating voltage of 80 kV. Images were recorded with a Megaview III camera. The acquisition was accomplished with Soft-Imaging software (SIS, EU). Samples were prepared by deposition of one drop of an appropriately diluted solution onto a copper grid coated with carbon film with a Formvar membrane and drying it in air before it was loaded onto the microscope. The hydrodynamic diameter of the

magnetic particles was determined by dynamic light scattering at 90° with a Zetasizer Nano (Malvern, EU) at 25°C. The Fe_3O_4 content of ferrofluid was determined by a colorimetric method based on the titration of ferrous ion by *o*-phenanthroline. Magnetic measurements were made in a superconducting quantum interference device (SQUID) magnetometer (Quantum design MPMS XL) at room temperature. The external magnetic field was swept from +5,000 to −5, 000 Oe, and then back to +5,000 Oe.

2.3. Agarose Muscle and Tumor Phantoms with Different Concentrations of Ferrofluid

2.3.1. Solid Muscle Phantom

A phantom based on agarose (17.8 g), tri-distilled water (1 L), ethanol (1 L), and NaCl (12 g) [23] was made to simulate the relative permittivity and electrical conductivity [24, 25] of muscle tissue at 224 MHz (the work frequency of the RF applicator). Muscle relative permittivity, reported in the literature at 224 MHz, is 60.7 and electrical conductivity is 0.743 S/m. Tri-distilled water, ethanol, and NaCl were mixed and heated at ∼80°C. When this mixture reached 80°C, agarose was added and it was totally dissolved. The final mixture was poured into a special methacrylate container. Phantom permittivity was measured by using a dielectric probe kit (85070C, Hewlett Packard, USA), whereas the electrical conductivity was obtained by means of Eq. (5)

$$\sigma = \varepsilon'' \varepsilon_0 \omega \tag{5}$$

where σ is the electrical conductivity, ε'' is the loss factor, ε_0 is the permittivity of free space, and $\omega = 2\pi f$ is the angular frequency. The final volume of muscle phantom was approximately 2.85 L.

2.3.2. Tumor and Ferrofluid Concentration

The ferrofluid was concentrated in small spheres of agarose (∼18 mm diameter). Each sphere was made with 0.006 g/mL of agarose and several amounts of ferrofluid. Such spheres simulated a cancerous tissue, a carcinoma in this case. Permittivity of carcinomas at 224 MHz is 59, and its electrical conductivity 0.9 [25, 26]. Two sizes of spheres were used: 2.5 mL and 5.0 mL. For the spheres of 2.5 mL, three different concentrations of ferrofluid were used: 4.4 mg/mL, 8.8 mg/mL, and 13.3 mg/mL of magnetite. These spheres were introduced inside the muscle phantom at 2 cm, 3 cm and 4 cm depths before it was totally solidified. For the spheres of 5 mL, which mimic bigger tumors, only one concentration of ferrofluid (8.8 mg/mL of magnetite) was used.

2.4. RF WG Applicator

The applicator is a radiofrequency (RF) WG which works in TE_{10} mode ($m = 1$, $n = 0$) [27]. TE_{10} is a dominant propagation mode, i.e., only one wave travels inside the WG. To propagate only the TE_{10} mode, the WG dimensions must be calculated at a specific

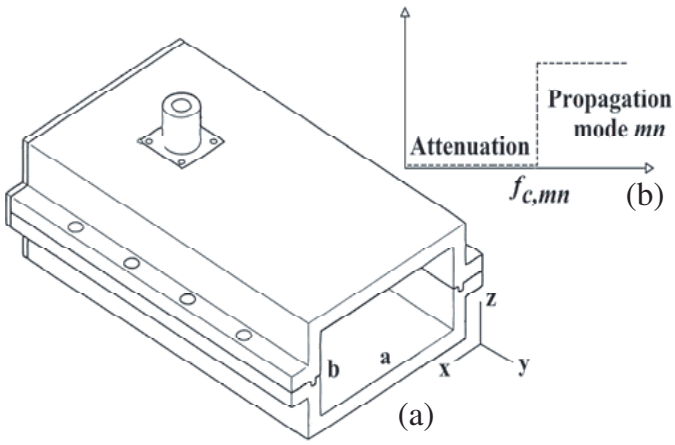

Figure 1. (a) x-, y-, and z-axes of a rectangular WG and WG apertures a and b. (b) TE_{mn} propagation mode due to the cutoff frequency.

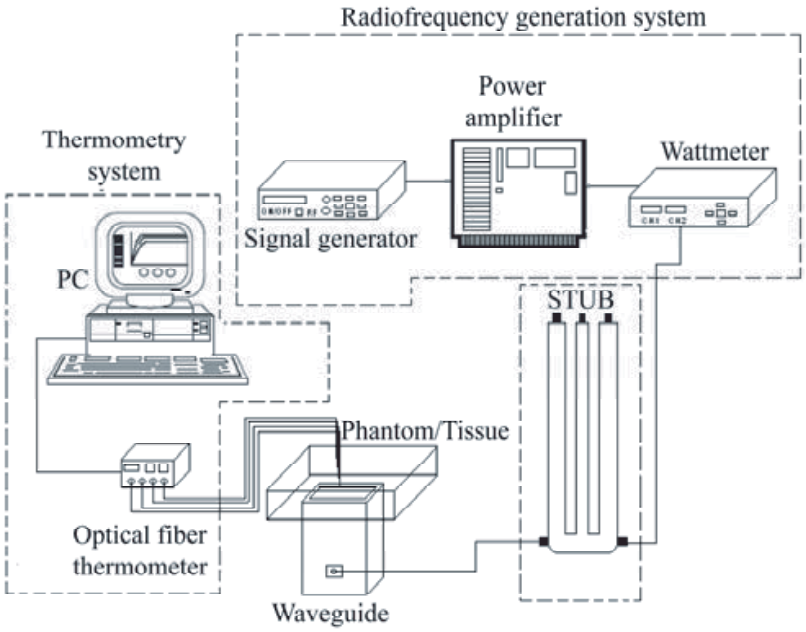

Figure 2. The experimental setup needed to carry out the thermal tests.

cutoff frequency. The cutoff frequency assures that waves at other low frequencies cannot propagate inside the WG as is depicted in Fig. 1(b). This applicator was specially designed to work at 224 MHz; its dimensions were $a = 7.9$ cm and $b = 3.9$ cm (Fig. 1(a)).

2.5. RF System

The RF system consists of a radiofrequency generation system comprising a signal generator (SML03, Rohde&Schwartz, Germany), a power amplifier (500A250, Amplifier Research, USA), and a power meter (PM2002, Amplifier Research, USA). Finally, so as to match the RF system with the applicator, a stub (matching coupler) was used. Fig. 2 shows the complete experimental setup for inducing and measuring the temperature increase.

2.6. Temperature Measurements

Four non-EM interfering temperature sensors (M3300, Luxtron, USA), based on optical fiber, were used to record temperature increases. These temperature measurements were recorded inside the muscle phantom and ferrofluid, just above the central point of the aperture of the applicator (Fig. 3). The input power used in each test was 66 W. Each tests lasted 960 s; this time was chosen in order to study the response as a function of time and to simulate more real conditions.

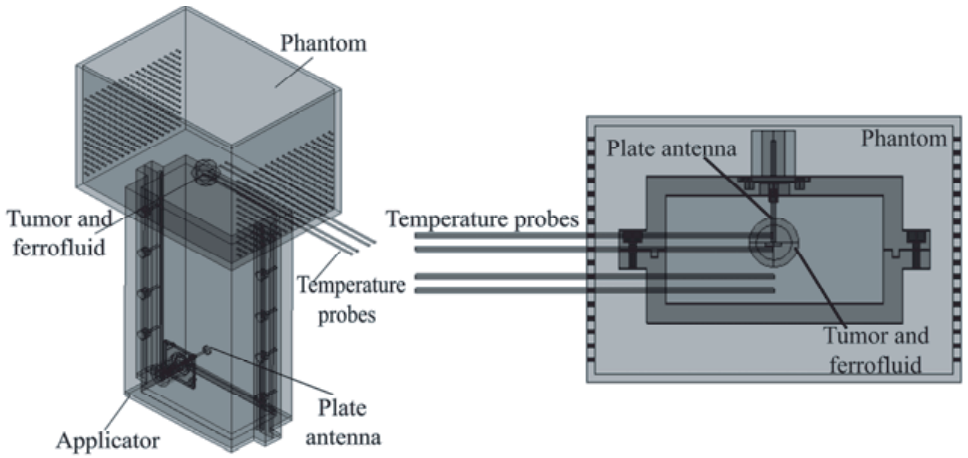

Figure 3. Experimental setup to measure temperature increments inside the muscle phantom and the tumor. (a) Tridimensional view of the setup. (b) Top view of the setup.

Optical fiber sensors were chosen because they do not modify the radiation pattern of the applicator. One sensor was placed approximately at the center of the sphere (tumor); another one was placed at 0.5 cm from the first sensor (inside the tumor). Finally, both remaining sensors were placed at 1.5 cm and 2 cm from the first sensor, respectively. The last two sensors were placed outside the ferrofluid (when spheres of 2.5 mL were used). For the spheres of 5.0 mL, only the sensor at 2 cm was out of the tumor, just in contact with the muscle phantom. The final phantom (muscle and tumor phantom) was irradiated for 20 min; at 16 min all sensors were displaced by 0.5 cm, and after every 30 s they were displaced to cover a distance of 4 cm at one side. Temperature experiments were recorded at 2 cm, 3 cm and 4 cm depths, where the spheres (tumor and ferrofluid) were placed so as to simulate tumors at different depths; this analysis was carried out to know the viability of our applicator to treat tumors localized at different depths. The initial temperature of the muscle phantom was controlled at 25°C. The radiation was applied five times to all the phantoms and the temperatures were acquired every second during the experiments using True Temp software (Luxtron, USA).

3. RESULTS AND DISCUSSION

3.1. Synthesis and Characterization of Ferrofluid

Figure 4 shows a transmission electron microscopy (TEM_i) micrograph from which the spherical shape and an average diameter of 15 nm of the particles of ferrofluid were observed. The z-average diameter of particles obtained by dynamic light scattering was $51.7\,\text{nm} \pm 1.2\,\text{nm}$; this value was much larger than that found from TEM_i. This was because even in the absence of any external magnetic field, the magnetostatic (magnetic dipole-dipole) interactions among the particles can cause their agglomeration. The particle size distribution was designated by the polydispersity index (PI) (0.181 ± 0.003), which varied from 0.0 for an entirely monodisperse sample to 1.0 for a polydisperse sample. The Fe_3O_4 concentration of ferrofluid determined spectrophotometrically was 22 mg/mL. The magnetic hysteresis loop of the ferrofluid measured at room temperature is shown in the inset of Fig. 4. The saturation magnetization of magnetic nanoparticles was about 52 emu/g, and the coercive field was closed to zero. This means that the sample exhibited superparamagnetic behavior and had high magnetization that determines the heating power in magnetic heating experiments.

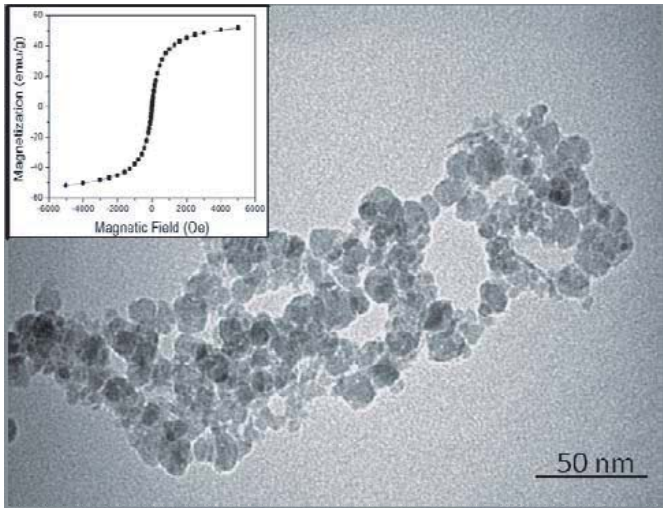

Figure 4. TEM$_i$ image of the ferrofluid used in the experiment. Inset: magnetization curve for ferrofluid as a function of the applied magnetic field.

Table 1. Dielectric properties of muscle, carcinoma, and their equivalent phantoms.

Dielectric properties	Muscle tissue (literature)	Carcinoma (literature)	Muscle phantom (measured)	Carcinoma phantom (measured)
Relative permittivity	60.70	∼59.00	61.13 ± 0.98	62.80 ± 2.00
Electrical conductivity (S/m)	0.74	∼0.90	0.50 ± 0.03	0.52 ± 0.06

3.2. Agarose Muscle and Cancer Tumor Phantoms with Various Concentrations of Ferrofluid

For the developed phantoms (Fig. 5), their relative permittivity and electrical conductivity have to be similar to that of the tissues the phantoms mimic. Table 1 shows the values for the dielectric properties of muscle and carcinomous tissues (obtained from the literature) [23, 26] as well as the experimentally measured values in our phantoms. As can be seen, dielectric properties achieved in the muscle phantom showed similar values to those reported in the literature; the differences in the relative permittivity and conductivity observed between phantoms and carcinomas were 3.8 units and 0.375 S/m, respectively.

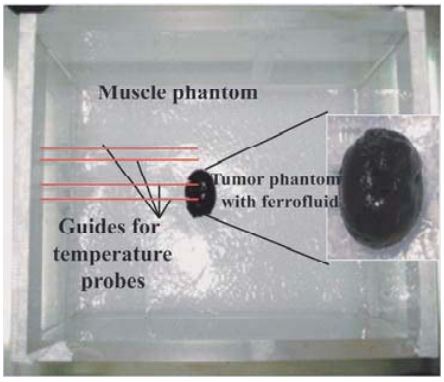

Figure 5. Muscle and carcinoma phantoms; the latter contains the ferrofluid.

3.3. Temperature Measurements

Figure 6 depicts the time-dependent temperature increments obtained for each of the three different concentrations of magnetite analyzed. Fig. 6(a) shows the temperature behavior for a concentration of 4.4 mg/mL of magnetite when the tumor phantom is located at 2 cm, 3 cm and 4 cm depths from the WG. When the tumor phantom was located at 2 cm, the temperature increment recorded by the probe inserted in the middle point of the tumor was approximately 10°C, whereas the other probes recorded lower increments of temperature. The temperature difference between the probe inside the tumor and the one located 2 cm away from the middle was 2.7°C; this means that the heat is concentrated inside the tumor. As a general rule, the increases in temperature were progressively smaller with the depth increasing. At 3 cm depth, the increase of temperature recorded by the central probe was ∼7°C and, at the same depth, but 2 cm away, the increase was just ∼4°C. From Fig. 6, it can be concluded that at 2 cm and 3 cm depths, the obtained increments can be considered within the therapeutic hyperthermia range (∼7°C), whereas the heating at 4 cm depth reached only an increment of 2°C.

Figures 6(b) and (c) show the temperature tendency as a function of time for 8.8 mg/mL and 13.3 mg/mL of magnetite, respectively. The concentration of 8.8 mg/mL shows that when the tumor is at 2 cm depth (red lines), the obtained heating is similar over the whole tumor because the difference of temperature is only 0.22°C between the probe located in the inner and that at 0.5 cm, whereas the differences with the other sensors were 2.5°C and 5°C, respectively. Finally, Fig. 6(c) shows that a concentration of 13.3 mg/mL of magnetite tends to saturation; that is, the amount of magnetite is higher than the maximum concentration which can be excited by the magnetic

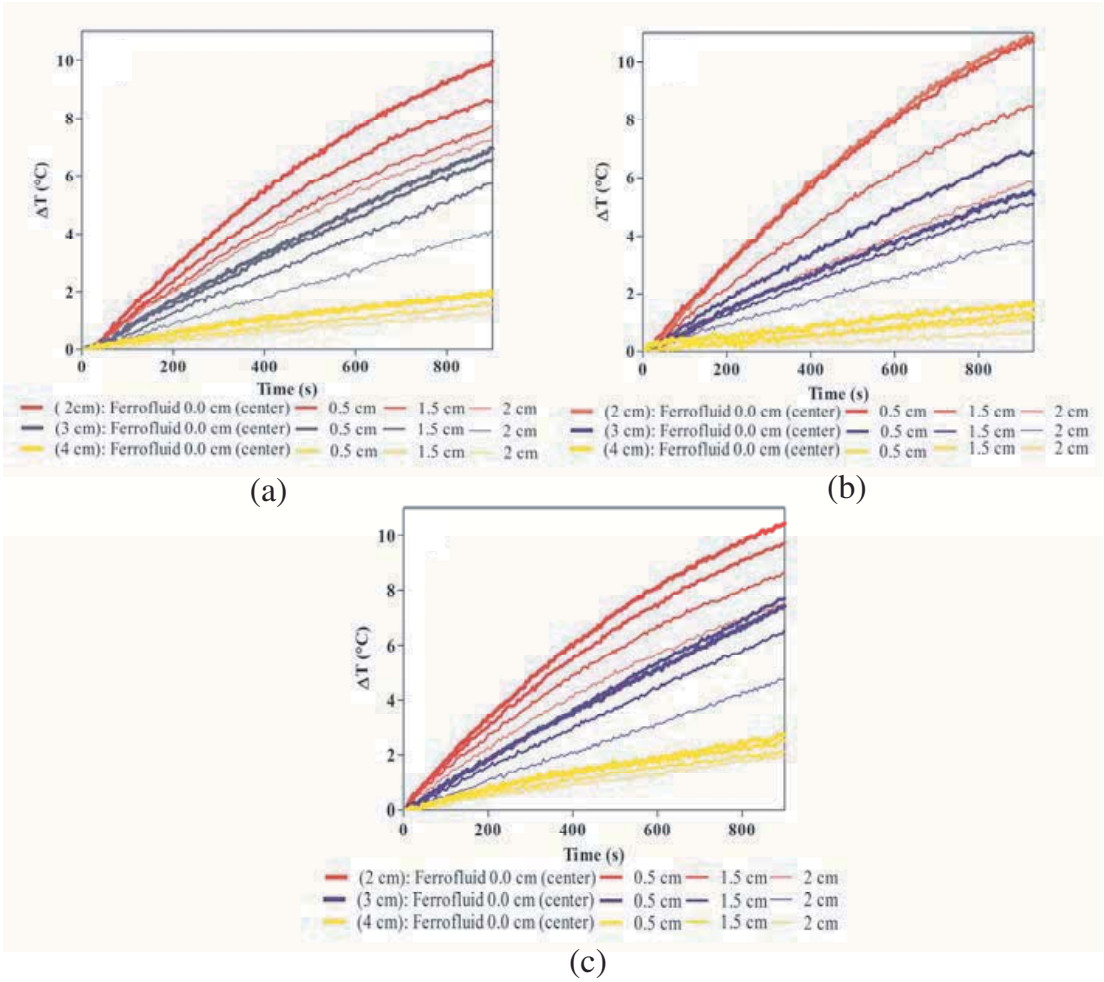

Figure 6. Temperature increments obtained with. (a) 4.4 mg/mL of magnetite. (b) 8.8 mg/mL of magnetite. (c) 13.3 mg/mL of magnetite. For each concentration, 12 time-dependent curves are displayed. They can be grouped in three series, each one indicated by a different color: red lines represent the temperature increments when the tumor is at 2 cm depth from the applicator; blue lines when the tumor is at 3 cm depth; and yellow lines when it is at 4 cm depth. For each tumor at a determined depth, the temperature was determined at the center of the tumor phantom, at 0.5 cm from the center (but still inside the tumor), and at 1.5 cm and 2.0 cm from the center (both outside the tumor).

field generated by the WG applicator. As a consequence, though the concentration of magnetite is higher, the temperature increments achieved were similar to those obtained with a concentration of 8.8 mg/mL of magnetite.

Table 2 summarizes the temperature increments recorded at the end of each test. As can be observed, the three concentrations of

Table 2. Maximum temperature increment obtained at the end of the tests (960 s) with each concentration of ferrofluid at 2 cm, 3 cm and 4 cm depths.

Ferrofluid concentration (mg/mL)	$\Delta T(^\circ C)$ *Probe 1 (inside the tumor)*	$\Delta T(^\circ C)$ *Probe 2 (0.5 cm inside the tumor)*	$\Delta T(^\circ C)$ *Probe 3 (1.5 cm outside the tumor)*	$\Delta T(^\circ C)$ *Probe 4 (2 cm outside the tumor)*
4.4 at 2.0 cm	10.20	8.94	7.28	7.49
4.4 at 3.0 cm	7.18	6.90	5.83	4.35
4.4 at 4.0 cm	2.05	2.13	1.64	1.22
8.8 at 2.0 cm	11.14	10.92	8.65	6.06
8.8 at 3.0 cm	4.65	5.78	4.18	3.21
8.8 at 4.0 cm	1.68	1.36	1.20	0.72
13.3 at 2.0 cm	11.11	10.20	9.07	7.59
13.3 at 3.0 cm	7.80	8.13	6.87	5.11
13.3 at 4.0 cm	2.90	2.62	2.28	2.10

ferrofluid reached a temperature increase suitable for hyperthermia therapy when the tumor was at 2 cm from the applicator. In contrast, the temperature increments are lower in the case where the tumor was at 4 cm depth ($\sim$3°C). Concerning the 4.4 mg/mL concentration, at 3 cm depth, the heat was more concentrated inside the tumor, because the temperature difference between both probes in the tumor was 0.28°C, whereas temperature differences with the other probes outside the tumor were 1.35°C and 2.83°C, respectively. The concentration of 8.8 mg/mL at 2 cm depth shows a high capacity of focusing heat. In this way, the temperature difference inside the tumor was 0.22°C, whereas temperature differences with the other probes were 2.49°C and 5.08°C; that is, at 2 cm away from the tumor, the temperature decreased approximately by 5°C. For a concentration of 13.3 mg/mL (at 2 cm depth), the temperature difference inside the tumor was 0.91°C whereas with the other probes were 2.04°C and 3.52°C, respectively. Finally, at 3 cm depth, the temperature difference in the tumor was 0.28°C and temperature differences with the other probes were 1.26°C and 3.02°C, respectively. In conclusion, each concentration presented a tendency to localize temperature rise within the tumor. These results were corroborated by the thermograms shown

in Figs. 7(a) and 7(e); here, the temperature distributions obtained without ferrofluid are shown. The uniform temperature distribution generated by the WG is not concentrated just over the tumor phantom (agarose with ferrofluid), while in the other case, when we use the ferrofluid, the heat was concentrated inside the tumor (See Figs. 7(b)–(d) and Figs. 7(f)–(h).

Figures 7(a)–(l) depict the thermal distributions obtained with each concentration of magnetite. From these figures the focusing effect produced by the ferrofluid could be observed. Figs. 7(a)–(d) show the temperature distributions for 4.4 mg/mL, 8.8 mg/mL, and 13.3 mg/mL of the magnetite when the tumor was located at 2 cm depth, and the temperature distributions in the absence of magnetite, 0.0 mg/mL. Such temperature distributions clearly demonstrate the focusing effect of the heat produced by the ferrofluid. As observed in Fig. 7(a), in a muscle phantom without ferrofluid, the surface that presented temperature increments of at least 7°C, which is needed to induce hyperthermia, was of approximately 3 cm × 4 cm; that is to say, the temperatures reached in this area were suitable for hyperthermia therapy. The highest temperatures were measured at the center of the WG aperture (in each figure, the gray dashed line represents the aperture of the applicator). The shapes of the temperature distributions changed when the concentration of magnetite in the ferrofluid varied. For 4.4 mg/mL of the magnetite (if the tumor is at 2 cm depth) (Fig. 7(b), the therapeutic heating area was approximately 2 cm × 2 cm with a maximum increment of 9.37°C. In the temperature distribution obtained with 8.8 mg/mL (Fig. 7(c)), the therapeutic heating region was approximately 1 cm × 3 cm with a maximum increment of 9.43°C, whereas for a distribution with 13.3 mg/mL (Fig. 7(d)) this region was quite bigger, 2 cm × 4 cm, and the increment achieved was 8.49°C. By analyzing these results, dependence among the concentrations of magnetite, temperature, and size of the heating region was observed. It is true that for a concentration of 13.3 mg/mL of magnetite, the temperature achieved was lower than for that obtained with 8.8 mg/mL, but, as previously noted, the amount of magnetite is higher than that which can be excited by the applicator. Of the three concentrations, the optimal results were obtained with the concentration of 8.8 mg/mL of magnetite, because the temperature achieved was the highest, and the generated therapeutic heating area was focused in a small region, just inside the tumor.

Figures 7(e)–(h) show the temperature distributions for the mentioned concentrations but at 3 cm depth. In a muscle phantom without ferrofluid, the area of the therapeutic heating region was approximately 3 cm × 4 cm and the temperature increment achieved

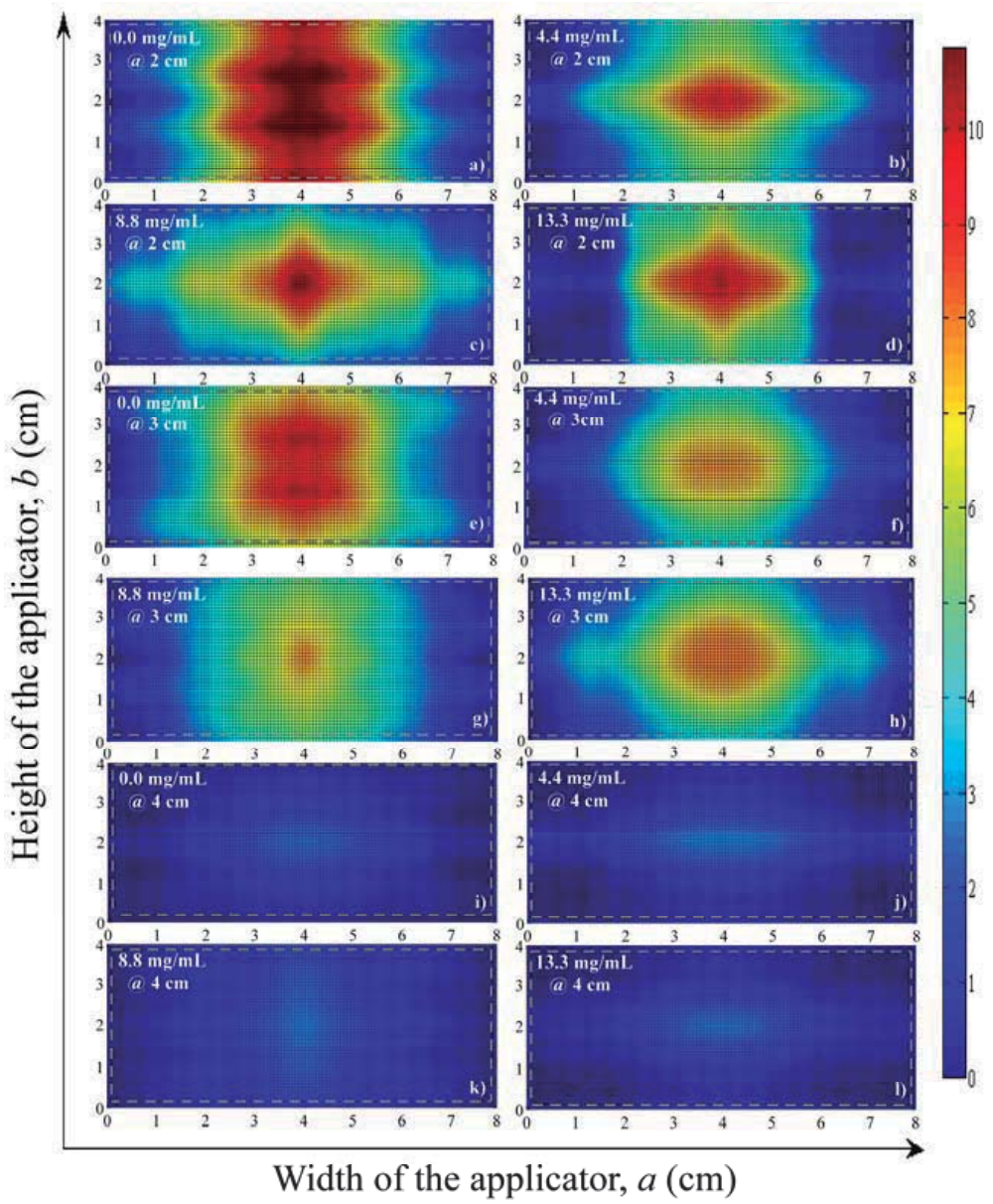

Figure 7. Thermograms obtained after applying the EM radiation on a muscle phantom containing a carcinoma phantom, whose volume is 2.5 mL, at several depths (Figs. 4(a)–(d), 2 cm; Figs. 4(e)–(h), 3 cm; Figs. 4(i)–(l), 4 cm). The carcinoma phantom contained the following concentrations of magnetite: 0.0 mg/mL (Figs. 4(a), (e), (i), 4.4 mg/mL.) (Figs. 4 (b), (f), (j), 8.8 mg/mL.) (Figs. 4(c), (g), (k), and 13.3 mg/mL.) (Figs. 4(d), (h), (l). On the right, the color scale of temperature increments.)

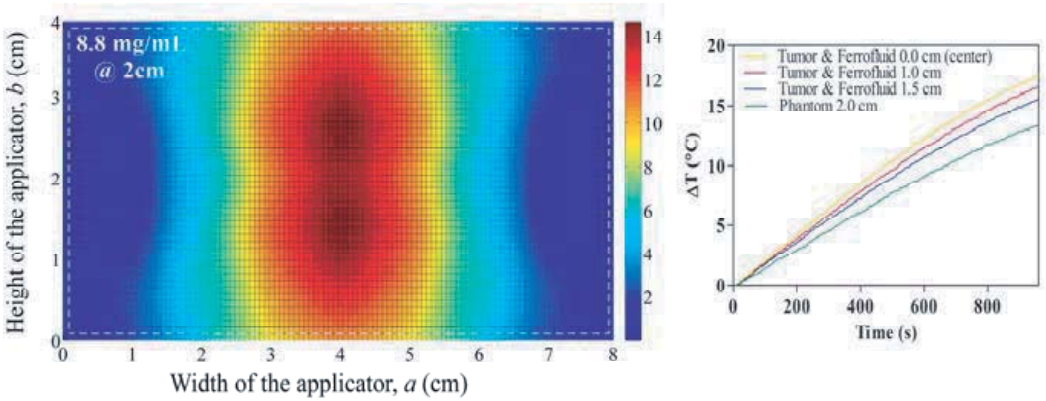

(a) (b)

Figure 8. Temperature increments obtained for a tumor phantom with a volume of 5 mL. (a) Temperature distributions obtained at 2 cm depth with a concentration of 8.8 mg/mL magnetite. (b) Temperature increments obtained with 8.8 mg/mL of magnetite. Probes 1, 2, and 3 are inside the tumor, whereas probe 4 is just in contact with the muscle phantom.

was 9.8°C (Fig. 7(e)). A therapeutic heating region of ∼2.5 cm × 2 cm and a temperature increment of 7.7°C were obtained when the carcinoma contained magnetite at a concentration of 4.4 mg/mL (Fig. 7(f)). The thermal distribution obtained with 13.3 mg/mL showed a therapeutic heating region of approximately 3 cm × 3 cm and the maximum temperature achieved was 8.3°C (Fig. 7(h)). The concentration of 8.8 mg/mL provided a rather special distribution of heating (Fig. 7(g)); the pattern of the distribution of temperatures showed a small focus of heat with a maximum temperature increment of 8.1°C. The therapeutic heating region, 1 cm × 4 cm, was smaller than that obtained with other conditions. This singular effect was observed repeatedly in all the analyzed samples. Finally, temperature distributions at 4 cm depth obtained with each concentration of magnetite are shown in Figs. 7(i)–(l). As observed previously (Fig. 6), at this depth, the temperature increments were not enough elevated to produce hyperthermia effects. However, the heat focusing effect of the ferrofluid over the tumor was clearly visible (we can observe a light blue color at the center of the thermogram, corresponding to increments of 3–4°C, on a dark blue color, which comprises increments of temperature only up to 1°C). Table 3 summarizes the heating area and the maximal increment of temperature achieved with each concentration at each analyzed depth.

Table 3. Area comprising the increments of temperature higher than 7°C (therapeutic temperature) and the maximal temperature increments achieved.

Concentration of magnetite (mg/mL)	Therapeutically useful area	Maximal temperature increment (°C)
0.0 at 2.0 cm	3.0 cm × 4.0 cm	10.8°C.
4.4 at 2.0 cm	2.0 cm × 2.0 cm	9.4°C
8.8 at 2.0 cm	1.0 cm × 3.0 cm	9.4°C
13.3 at 2.0 cm	2.0 cm × 4.0 cm	8.5°C
0.0 at 3.0 cm	3.0 cm × 4.0 cm	9.8°C
4.4 at 3.0 cm	2.5 cm × 3.0 cm	7.7°C
8.8 at 3.0 cm	1.0 cm × 4.0 cm	8.1°C
13.3 at 3.0 cm	3.0 cm × 3.0 cm	8.3°C
0.0 at 4.0 cm	-	2.7°C
4.4 at 4.0 cm	-	2.9°C
8.8 at 4.0 cm	-	2.9°C
13.3 at 4.0 cm	-	2.9°C

To determine the influence of the size of the tumor on the temperature distribution, a tumor with a volume of 5 mL was used. The tumor contained ferrofluid of 8.8 mg/mL and it was located at 2 cm depth. Fig. 8(a) shows the obtained thermal distribution, where a maximal increment of 14.60°C was observed. In this case, the area with a minimal temperature increment of 7°C was approximately 3 cm × 4 cm. Here, we can observe that the heated area was dependent on the mass occupied by the ferrofluid. Fig. 8(b) shows the temperature increments as function of time. Due to the higher size of the tumor, now, probes 1, 2, and 3 recorded temperatures inside the tumor, whereas probe 4 recorded the temperature inside the muscle phantom. Temperature differences among probe 1, and probes 2 and 3 were 0.99°C and 2.1°C, respectively, and between probe 1 and probe 4 was 4.21°C. These differences show that the heat was concentrated especially inside the tumor.

4. CONCLUSION

A technical challenge in hyperthermia treatment is to locally heat the tumor region up to the appropriate therapeutic temperature without damaging the surrounding healthy tissue. This paper presents a study concerning the heating and focusing effect of the combination of a radiofrequency applicator (RF WG) and a ferrofluid as an alternative to focus the EM energy over a localized zone of the body. In our experiments, the EM energy is transformed into heat which leads to an increase of temperature; any increase equal or higher than 7°C is considered as suitable for hyperthermia therapy. The RF applicator used in this work generates electric and magnetic fields; the electric field interacts with the electrical properties of tissue, i.e., permittivity and conductivity. The magnetic properties of the tissue are extremely weak, the presence of superparamagnetic nanoparticles used in this work permits that, through the interaction of magnetic components of nanoparticles and radiation, an additional amount of heat is generated, i.e., the nanoparticles act as enhancers of the heating effect of our RF applicator.

The results shown in this paper confirm that the use of nanoparticles as agents to localized temperature rise in the whole tumor volume is feasible. Hence, by using this applicator in combination with nanoparticles it is possible: (i) to focus the energy over the tumor without creating hot spots in healthy tissue (the therapeutic region is determined by the volume occupied by the ferrofluid), (ii) to provide higher temperatures to tissues depending on the ferrofluid concentration (this fact is an advantage because the power used by the hyperthermia system could be reduced), and (iii) to control the increments of temperatures in tissues. We also found that there is a maximum magnetite concentration that the magnetic field, generated by the applicator, can excite; this concentration determines the maximum temperature reached inside the tumor phantom. On the other hand, from this study it can be concluded that the amount of magnetic nanoparticles which should be injected to obtain suitable thermal levels will depend on the depth and size of the tumor. Finally, we conclude that it is possible to use higher power inputs and reduce the radiation time or to use lower power inputs and increase radiation time.

ACKNOWLEDGMENT

The authors are grateful for the financial support given by the Spanish Ministerio de Ciencia e Innovación (MICINN), project MAT2009-

13155-C04-03. The authors thank J. H. Zepeda for his invaluable technical assistance. We also thank Ruben Pérez Valladares for the revision of the manuscript.

REFERENCES

1. Falk, M. H. and R. D. Issels, "Hyperthermia in oncology," *International Journal of Hyperthermia*, Vol. 17, 1–18, Jan. 2001.
2. Hildebrandt, B., P. Wust, O. Ahlers, et al., "The cellular and molecular basis of hyperthermia," *Crit. Rev. Oncology/Hematology*, Vol. 43, 33–56, Jul. 2002.
3. Gupta, R. C. and S. P. Singh, "Elliptically bent slotted waveguide conformal focused array for hyperthermia treatment of tumors in curved region of human body," *Progress In Electromagnetics Research*, Vol. 62, 107–125, 2006.
4. Gong, Y. and G. Wang, "Superficial tumor hyperthermia with flat left-handed metamaterial lens," *Progress In Electromagnetics Research*, Vol. 98, 389–405, 2009.
5. Arruebo, M., R. Fernádez-Pacheco, M. R. Ibarra, and J. Santamaría, "Magnetic nanoparticles for drug delivery," *Nano Today*, Vol. 2, No. 3, 22–32, 2007.
6. Pankhurst, Q. A., J. Connolly, S. K. Jones, and J. Dobson, "Applications of magnetic nanoparticles in biomedicine," *Journal of Physics D: Applied Physics*, Vol. 36, No. 13, 167, 2003.
7. Babincová, M., P. Cičanec, V. Altanerová, C. Altaner, and P. Babinec, "AC-magnetic field controlled drug release from magnetoliposomes: Design of a method for site-specific chemotherapy," Bioelectrochemistry, Vol. 55, No. 1–2, 17–19, 2002.
8. Babincová, M., V. Altanerova, C. Altaner, C. Bergemann, and P. Babinec, "In vitro analysis of cisplatin functionalized magnetic nanoparticles in combined cancer chemotherapy and electromagnetic hyperthermia," *IEEE Transactions on Nanobioscience*, Vol. 7, No. 1, 15–19, 2008.
9. Luong, T. T., T. P. Ha, L. D. Tran, M. H. Do, T. T. Mai, N. H. Pham, H. B. T. Phan, G. H. T. Pham, N. M. T. Hoang, Q. T. Nguyen, and P. X. Nguyen, "Design of carboxylated fe3o4/poly(styrene-co-acrylic acid) ferrouids with highly efficient magnetic heating effect," *Colloids and Surfaces A: Physicochemical and Engineering Aspects*, Vol. 384, No. 1–3, 23–30, 2011.
10. Hiergeist, R., W. Andra, N. Buske, R. Hergt, I. Hilger, U. Richter, and W. Kaiser, "Application of magnetite ferrouids

for hyperthermia," *Journal of Magnetism and Magnetic Materials*, Vol. 201, 420–422, 1999.

11. Duguet, E., S. Vasseur, S. Mornet, and J.-M. Devoisselle, "Magnetic nanoparticles and their applications in medicine," *Nanomedicine*, Vol. 1, No. 2, 157–168, 2006.
12. Thomas, L. A., L. Dekker, M. Kallumadil, P. Southern, M. Wilson, S. P. Nair, Q. A. Pankhurst, and I. P. Parkin, "Carboxylic acid-stabilised iron oxide nanoparticles for use in magnetic hyperthermia," *J. Mater. Chem.*, Vol. 19, 6529–6535, 2009.
13. Laurent, S., D. Forge, M. Port, A. Roch, C. Robic, L. Vander Elst, and R. N. Muller, "Magnetic iron oxide nanoparticles: Synthesis, stabilization, vectorization, physicochemical characterizations, and biological applications," *Chemical Reviews*, Vol. 108, No. 6, 2064–2110, 2008.
14. Rovers, S. A., R. Hoogenboom, M. F. Kemmere, and J. T. F. Keurentjes, "Relaxation processes of superparamagnetic iron oxide nanoparticles in liquid and incorporated in poly(methyl methacrylate)," *The Journal of Physical Chemistry C*, Vol. 112, No. 40, 15643–15646, 2008.
15. Ingrid, H., et al., "Magnetic nanoparticles for selective heating of magnetically labelled cells in culture: preliminary investigation," *Nanotechnology*, Vol. 15, 1027, 2004.
16. Rudolf, H., et al., "Magnetic particle hyperthermia: Nanoparticle magnetism and materials development for cancer therapy," *J. Phys.: Condens. Matter*, Vol. 18, 2919, 2006.
17. Wiersma, J. and J. D. V. Dijk, "RF hyperthermia array modelling; validation by means of measured em-field distributions," *International Journal of Hyperthermia*, Vol. 17, No. 1, 63–81, 2001.
18. Nilsson, P., T. Larsson, and B. Persson, "Absorbed power distributions from two tilted waveguide applicators," *International Journal of Hyperthermia*, Vol. 1, No. 1, 29–43, 1985.
19. Gardner, R., H. Vargas, J. Block, C. Vogel, A. Fenn, G. Kuehl, and M. Doval, "Focused microwave phased array thermotherapy for primary breast cancer," *Annals of Surgical Oncology*, Vol. 9, 326–332, 2002.
20. Durney, C., C. Johnson, P. Barber, H. Massoudi, M. Iskander, S. Allen, and J. Mitchell, *Radiofrequency Radiation Dosimetry Handbook*, USAF School of Aerospace Medicine, 1986.
21. Pennes, H. H., "Analysis of skin, muscle and brachial arterial blood temperatures in the resting normal human forearm," *Am.*

J. Med. Sci., Vol. 215, No. 3, 354, 1948.

22. Skumiel, A., A. Jozefczak, M. Timko, P. Kopcansky, F. Herchl, M. Koneracka, and T. N., "Heating effect in biocompatible magnetic fluid," *International Journal of Thermophysics*, Vol. 28, No. 5, 1461–1469, 2007.
23. Gabriel, C., "Compilation of the dielectric properties of body tissues at RF and microwave frequencies," Report N.AL/OE-TR-1996-0037, Occupational and environmental health directorate, Radiofrequency Radiation Division, Brooks Air Force Base, Texas, USA, Jun. 1996.
24. Iero, D., T. Isernia, A. F. Morabito, I. Catapano, and L. Crocco, "Optimal constrained field focusing for hyperthermia cancer therapy: A feasibility assessment on realistic phantoms," *Progress In Electromagnetics Research*, Vol. 102, 125–141, 2010.
25. Lai, J. C. Y., C. B. Soh, E. Gunawan, and K. S. Low, "Homogeneous and heterogeneous breast phantoms for ultra-wideband microwave imaging applications," *Progress In Electromagnetics Research*, Vol. 100, 397–415, 2010.
26. Yoo, D.-S., "The dielectric properties of cancerous tissues in a nude mouse xenograft model," *Bioelectromagnetics*, Vol. 25, 492–497, 2004.
27. Trujillo-Romero, C. J., L. Leija, and A. Vera, "FEM modeling for performance evaluation of an electromagnetic oncology deep hyperthermia applicator when using monopole, inverted T, and plate antennas," *Progress In Electromagnetics Research*, Vol. 120, 99–125, 2011.

Articulo 3.

Improved thermal ablation efficacy using magnetic nanoparticles: A study in tumor phantoms

Progress In Electromagnetics Research, 128, 229-248.

El uso de NPMs en hipertermia y ablación térmica, es especialmente prometedor en la lucha contra el cáncer, siempre que la temperatura terapéutica se mantenga constante en todo el tejido diana. El presente estudio muestra como varía la temperatura a lo largo de tiempo, después de la radiación mediante una antena de microondas a una frecuencia de 2,45 GHz, en función de la concentración de NPMs (ferrofluido y magnetoliposomas). Se colocaron sensores de temperatura dentro y fuera del phantom tumor (simula tejido mamario canceroso), para evaluar el efecto de la focalización de calor en el tumor. Los resultados han demostrado que al aumentar la concentración de NPMs, aumenta la temperatura alcanzada, obteniendo, un incremento de temperatura de más de 56˚C con una concentración de ferrofluido de 13.2 mg/mL, mientras que en el phantom de referencia (sin NPMs) sólo fue de ≈ 21˚C. En cuanto a los magnetoliposomas, la temperatura alcanzada fue similar a la obtenida con ferrofluido, para una concentración de las nanopartículas inferior. De los resultados, se puede confirmar, la factibilidad de uso de nanopartículas como agentes para centrar la energía sobre el tumor sin necesidad de calentar el tejido sano.

Progress In Electromagnetics Research, Vol. 128, 229–248, 2012

IMPROVED THERMAL ABLATION EFFICACY USING MAGNETIC NANOPARTICLES: A STUDY IN TUMOR PHANTOMS

S. García-Jimeno[1], R. Ortega-Palacios[2], M. F. J. Cepeda-Rubio[2], A. Vera[2], L. Leija[2], and J. Estelrich[1, 3, *]

[1]Departament de Fisicoquímica, Facultat de Farmàcia, Universitat de Barcelona, Avda. Joan XXIII, 08028 Barcelona, Catalonia, (Spain)

[2]Electrical Engineering Department, Bioelectronics Section, CINVESTAV-IPN, Mexico D.F., Mexico

[3]Institut de Nanociència i Nanotecnologia, IN^{2}UB, Universitat de Barcelona, (Spain)

Abstract—Magnetic heating used for inducing hyperthermia and thermal ablation is particularly promising in the treatment of cancer provided that the therapeutic temperature is kept constant during the treatment time throughout the targeted tissue and the healthy surrounding tissues are maintained at a safe temperature. The present study shows the temperature increment produced by different concentrations of magnetic nanoparticles (ferrofluid and magnetoliposomes) inside a phantom, after irradiating tissue-mimicking materials (phantoms)with a minimally invasive coaxial antenna working at a frequency of 2.45 GHz. This frequency was chosen because maximum dielectric loss of water molecules begins at 2.4 GHz and because this is an ISM (industrial, scientific and medical) frequency. Temperature sensors were placed inside and outside the tumor phantom to assess the focusing effect of heat produced by nanoparticles. Results have shown that the temperature increments depend on the nanoparticles concentration. In this way, a temperature increment of more than 56°C was obtained with a ferrofluid concentration of 13.2 mg/mL, whereas the increment in the reference phantom was only of $\approx$ 21°C. Concerning the magnetoliposomes, the temperature achieved was similar to that obtained with the ferrofluid but at a lesser concentration of nanoparticles. These results

Received 1 February 2012, Accepted 27 March 2012, Scheduled 30 May 2012

* Corresponding author: Joan Estelrich (joanestelrich@ub.edu).

demonstrate that it is possible to achieve higher temperatures and to focus energy where the nanoparticles are located.

1. INTRODUCTION

Magnetic nanoparticles (MNPs) for medical applications have been developed in recent years. Since MNPs have magnetic features that are not present in most biological materials, they can be applied in special medical techniques such as cell separation, separation of biological materials using magnetically labeled beads, immunoassays, magnetic resonance imaging (MRI), drug delivery, thermal marking to improve the tumor detection capacity of thermography, and hyperthermia therapy [1–7].

Hyperthermia is a cancer treatment used to enhance the effects of already established therapies, such as radiotherapy and chemotherapy. The most important requirement for the use of hyperthermia in cancer therapy is to locally increase and maintain temperature within cancer cells above 41°C while surrounding healthy tissues remain at safe temperatures. Under this general concept of hyperthermia, one can distinguish between hyperthermia (when temperature is between 40°C and 44°C) [8, 9] and thermal ablation if temperature exceeds 50°C [10]. When thermal energy increases the tissue temperature above 40°C, normal cellular processes become deactivated in a dose-dependent manner, which eventually may result in the death of cells. In thermal ablation, in contrast, cells or tissues show areas of extensive necrosis [11].

Electromagnetic radiation can be used to induce hyperthermia. The electromagnetic energy must be directed from an external source and it must penetrate normal tissue. Minimally invasive antennas can be also used in electromagnetic hyperthermia; in this case, the antenna is inserted in the tissue and is in direct contact with the tissue. Although the efficacy of electromagnetic hyperthermia has been proven in numerous clinical trials, it has not gained wide acceptance. The major technical problem with electromagnetic hyperthermia is the difficulty of heating the target tumor at the desired temperature without damaging the surrounding tissues. MNPs of various types may address this issue through intracellular hyperthermia or ablation; i.e., by driving submicron magnetic particles inside the tumor and then making them generate heat under an alternating magnetic field [12].

In order to generate heat, as described above, nanoparticles with superparamagnetic properties are inserted into the tumor and then they are exposed to an electromagnetic field (EMF) which operates at radio frequencies (RF) or in the microwave (MW) range. In this

way magnetic and electrical energy is transformed into heat. Polar molecules interact with electric fields and cause frictional heating while magnetic loss is attributed to Néel relaxation due to rapidly alternating magnetic dipole moments. Brownian relaxation, which occurs due to nanoparticle rotation, results in friction between particles and surrounding fluids. In MNPs, Brownian and Néel relaxation depends on particle size (an average value of $\sim 15\,\mathrm{nm}$)and composition [13, 14].

Different equations describe the interaction of electromagnetic fields with tissue; this interaction causes heating in biological tissues under certain conditions (applied power, exposure time). The bioheat transfer equation (BHTE) is used to describe the temperature evolution in biological tissues. The BHTE can be written as:

$$\rho_t C_t \frac{\partial T}{\partial t} = \mathrm{div}\left(k\nabla T\right) + \omega_b \rho_b C_b \left(T_b - T\right) + Q_{met} + Q_{ext}, \tag{1}$$

where ρ_t, C_t, and k, are the density, specific heat and thermal conductivity of the tissue, respectively; ρ_b, C_b, and ω_b are the density, specific heat and perfusion rate of blood, respectively; T_b is the arterial blood temperature; Q_{met} is the heat source from metabolism, and Q_{ext} is the absorbed power density which can be written as:

$$Q_{ext} = \frac{1}{2}\sigma_t \left|E\right|^2, \tag{2}$$

where σ_t is the electrical conductivity of the tissue and E is the electric field generated by the electromagnetic source, in our case the antenna. By analyzing Eq. (2), it is evident that only the E field is taken into account to achieve the temperature increment in tissues and tumors. Although the antenna generates E and H fields, the last one is neglected because tissues are considered as nonmagnetic. However, when magnetic nanoparticles are injected into tumors, nanoparticle magnetic properties are intensified, and consequently, the H field also is involved in the heating process.

On the other hand, if magnetic nanoparticles are concentrated inside tumors, the absorbed power density is given by [15]:

$$Q_{ext} = \pi \mu_0 \chi'' f H^2, \tag{3}$$

where μ_0 is the permeability of free space, χ'' is the imaginary part of the magnetic susceptibility, f is the frequency of the alternating magnetic field, and H is the magnetic field amplitude. From Eq. (3), it can be seen that temperature increments are proportional to the square of the amplitude of the H field intensity. In this case, the E and H fields can be used as sources for heating. Substituting Eqs. (2) and (3) in Eq. (1), the BHTE can be rewritten as:

$$\rho_t C_t \frac{\partial T}{\partial t} = \mathrm{div}\left(k\nabla T\right) + \omega_b \rho_b C_b \left(T_b - T\right) + Q_{met} + \frac{1}{2}\sigma_t \left|E\right|^2 + \pi \mu_0 \chi'' f H^2 \tag{4}$$

From Eq. (4), it can be observed that the heating effect is produced by both the electric and magnetic fields generated by the applicator; i.e., the heating effect produced by the antenna depends not only on the square of E field but also on the square of H field. For this reason, the heating efficiency of the approach being reported here is expected to be higher compared with that obtained without using nanoparticles, where just the magnetic field is taken into account for heating [16]. The distribution of temperature increment in phantoms with different concentrations of magnetic particles has been analyzed in this study in order to test the hyperthermic effect of magnetic nanoparticles, and to observe the behavior of temperature increment in the deep regions of the tumor tissue as well as the dependence of the concentration of magnetic particles in it.

Currently, MNPs consisting of iron oxide nanoparticles are widely used. Among the materials potentially suitable for use in thermal therapy, magnetite has been considered the best from the standpoint of magnetic properties and biocompatibility [17]. To a large extent, the morphological, structural, and magnetic profiles of nanoparticles determine their suitability as magnetic hyperthermia/ablation agents. Such information is therefore of paramount importance when attempting to produce the temperatures required with a minimal magnetic particle concentration and also to avoid damaging surrounding normal tissue through overheating.

As mentioned above, one important issue for hyperthermia treatment is to know how the temperature increases in tumor tissue, as well as whether the heat is focused inside the tumor. One challenge of assessing induced energy generation in animal tissue is the technical difficulty of visualizing MNPs. To date, gel phantoms have been the only transparent porous materials that are equivalent to animal tissue for *in vitro* studies, despite the fact that gels are homogeneous in comparison to the complicated morphology of a tumor.

In this study, increments of temperature and heat focusing were determined by using a phantom as a tumor model and MNPs based on ferrofluid and magnetoliposomes (MLs) at different concentrations. The phantom was made of a mixture of different components in order to represent the thermal and electromagnetic properties of human tissues [14, 18]. The ferrofluid was based on magnetite stabilized by polyethylene glycol (PEG), and the MLs were liposomes encapsulating the ferrofluid. A minimally invasive coaxial antenna was used to irradiate the phantom.

2. MATERIALS AND METHODS

2.1. Materials

Soybean phosphatidylcholine (PC), a zwitterionic phospholipid (Lipoid S-100), was a gift from Lipoid (Ludwigshafen, EU). Ferric chloride hexahydrate ($Cl_3Fe.6H_2O$), ferrous chloride tetrahydrate ($Cl_2Fe.4H_2O$) and cholesterol (CHOL)were purchased from Sigma-Aldrich (St. Louis, MO, USA). PEG of 6000 Da molecular weight was from VWR International (Barcelona, EU). Agarose (Ultrapure^{TM} agarose) was purchased from Invitrogen (Mexico, D.F.). All other reagents were of analytical grade and were from Panreac (Barcelona, EU). Deionized Millipore Milli-Q water was used in all the experiments. A strong neodymium-iron-boron ($Nd_2Fe_{12}B$) magnet (1.2 T) was obtained from Halde GAC (Barcelona, EU).

2.2. Preparation and Characterization of Magnetic Nanoparticles

Ferrofluid was prepared using the co-precipitation method in the presence of excess PEG. Briefly, once the polymer was dissolved in water, a 1:2 molar ratio mixture of $FeCl_2/FeCl_3$ was added. When the PEG and iron salts were well dissolved, an ammonia solution was added drop-wise while being stirred. After this, the ferrofluid was poured into a beaker and the vessel was placed on a permanent magnet. The ferrofluid was washed with water by decanting the supernatant in order to eliminate excess PEG. Finally, PEG coated particles were dispersed in water and the resulting suspension was sonicated for 10 min at room temperature and 100% of the ultrasonic power (Transsonic Digital Bath sonifier, Elma, EU).

MLs were obtained by extrusion [19]. A mixture of PC/CHOL (4:1 molar ratio) dissolved in chloroform/methanol (2:1, v/v) was evaporated until a film was formed. This film was hydrated with the appropriate amount of a mixture of water and ferrofluid (FF) to give a lipid concentration of 16 mmol/L. Multilamellar liposomes were formed by gentle sonication and vortexing. After this, multilamellar liposomes were extruded at room temperature in a Liposofast device (Avestin, Canada) through two polycarbonate membrane filters of 0.2-µm pore size, a minimum of 9 times. Finally, unilamellar MLs were obtained.

The morphology of the samples was studied by transmission electron microscopy (TEM) using a Jeol 1010 microscope at an accelerating voltage of 80 kV. Images were recorded with a Megaview III camera, and acquisition was accomplished with Soft-Imaging software (SIS, Münster, EU). The hydrodynamic diameter of the MNPs

was determined by dynamic light scattering (DLS) at 90° with a Zetasizer Nano (Malvern, EU) at 25°C. Particle size distribution was designated using the polydispersity index (PI), which ranged from 0.0 for an entirely monodisperse sample to 1.0 for a polydisperse sample. Iron content of the ferrofluid and MLs was determined by inductively-coupled plasma-optical emission spectrometry (ICP-OES) using Perkin Elmer equipment (Optima 3200RL). Magnetic measurements were made on a superconducting quantum interference device (SQUID) magnetometer (Quantum design MPMS XL) at room temperature. The external magnetic field was swept from +5000 to −5000 Oe, and then back to +5000 Oe.

2.3. Preparation and Characterization of Agarose Tumor Phantoms

A phantom was prepared by dispersing agarose, tridistilled water, ethanol and NaCl (0.1 M) to obtain a permittivity near to the values of breast carcinoma at 2.45 GHz. At this frequency, tumor permittivity is around 60 and its conductivity is about 2.5 S/m; the phantom mimicking the tumor had a permittivity of 55.88 and a conductivity of 2.88 S/m. The mixture was then heated to 80°C, until the agarose was completely dissolved. The solution was then poured into a transparent container and cooled to room temperature (25°C) until solidification occurred.

In order to maintain the MNPs in a specific place inside the phantom, they were concentrated in small spheres of agarose. Each sphere was made of tridistilled water, 0.006 g/mL of agarose and several concentrations of magnetite. Two sizes of spheres were used: some with a volume of 2.5 mL and 1.68 cm in diameter, and others with a volume of 5 mL and 2.12 cm in diameter. For the spheres of 2.5 mL, the following concentrations of magnetite were used: 0.0 (reference phantom), 2.2, 4.4, 5.5, 8.8 and 13.2 mg/mL (for the ferrofluid) and 1.2 mg/mL when the sphere was made with MLs. For spheres of 5 mL, only one concentration of magnetite in ferrofluid (8.8 mg/mL) and MLs (1.2 mg/mL) was used. The spheres were introduced inside the phantom before it was totally solidified.

Electrical properties of the phantom were measured in order to compare them with those of human tissues. Figure 1 shows the experimental setup used to characterize the phantoms that was subjected to a radiation process with the microcoaxial antenna. The phantom permittivity was measured using a dielectric probe kit (85070C, Hewlett Packard, USA). The dielectric probe kit software provided real (ε) and imaginary (ε'') permittivity. Phantom electrical conductivity was obtained from the equation: $\sigma = \varepsilon'' \varepsilon_0 \omega$, where $\omega =$

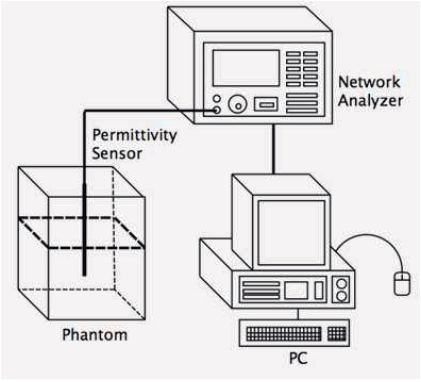

Figure 1. Experimental setup used to measure the electrical properties of the phantom.

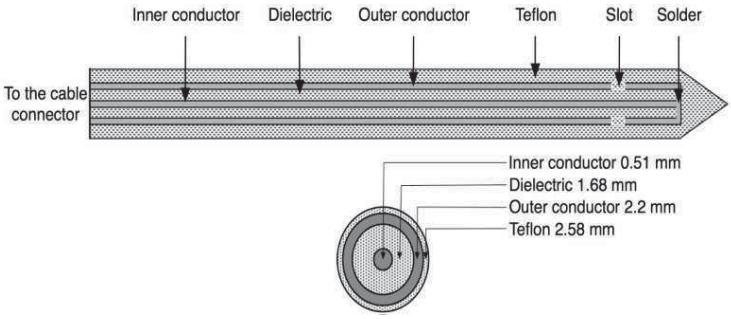

Figure 2. Structure and dimensions of the coaxial antenna.

$2\pi f$ is the angular frequency and f is the frequency of the radiation. It is important to remark that the dielectric probe measurements assume that the sample under test has a permeability of 1 (non-magnetic);this is not true for samples with MNPs, and, in consequence, such values are valid in a qualitative sense. It is important to know the values of the electrical properties because those values are related to the temperature increase (it is possible to enhance heat generation by changing the dielectric properties of tissues).

2.4. Antenna Design

The antenna worked at 2.45 GHz and was based on a 50-Ω UT-085 semi rigid coaxial cable. The entire outer conductor was made of copper and a small ring-shaped slot was carved in it, close to the short-circuited distal tip of the antenna, to allow electromagnetic wave propagation into the tissue. Our antenna had a 1-mm-wide slot, in order to get minimal power reflection. The inner conductor was made of silver-plated copper wire (SPCW) and the coaxial dielectric used was low-loss polytetrafluoroethylene (PTFE). The length of the antenna tip affected power reflection and the shape of the SAR (specific absorption rate)

pattern, and it was adjusted to provide a good trade-off between power reflection and SAR pattern. In addition, the antenna was encased in a PTFE catheter to prevent adhesion of ablated tissue [20]. Figure 2 shows the structure of the antenna, and its inner diameters. It is important to mention that when this kind of antenna is used in clinical trials, it is introduced inside tissues so it is considered as a minimally invasive applicator.

2.5. Microwave Ablation System

The experimental setup consisted of a radiation system and a thermometry system (Figure 3). The radiation system employed a power amplifier SSPA 1.0-2.5-50 W (Aethercomm, Carlsbad, CA, USA) and a microwave generator SML03 2.45-GHz (Rohde & Schwarz, Germany). The thermometry system used fiber-optic thermal probes (Luxtron, Santa Clara, CA, USA) to measure the real-time

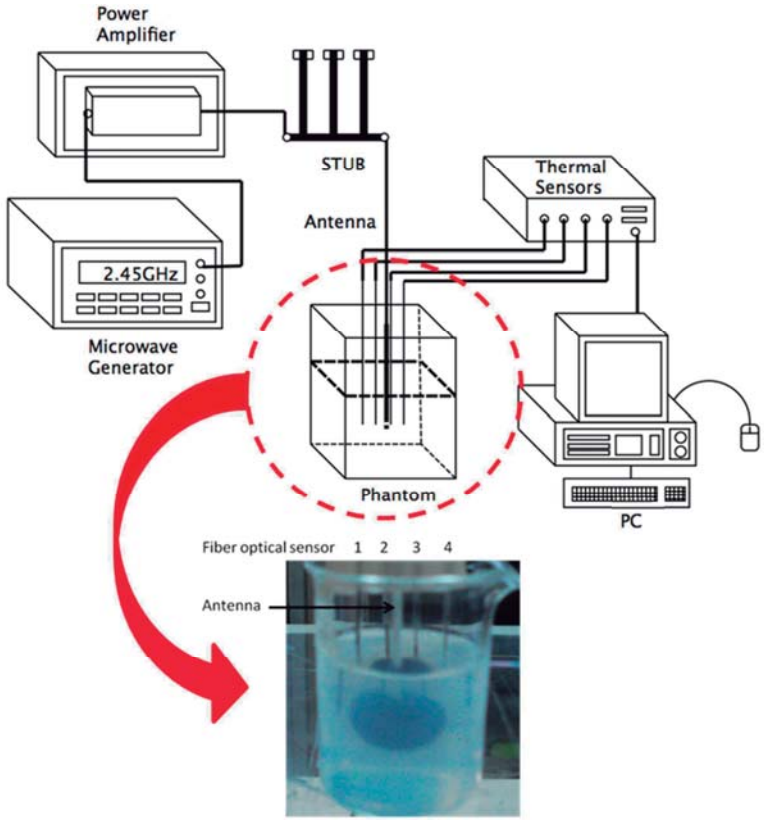

Figure 3. Schematic representation of the radiation and thermometry system. An image of an actual tumor phantom, with FF inside, is shown. Fiber-optic sensors and antenna are embedded in the tumor phantom.

temperature during the microwave ablation (MWA) experiments. The fiber-optic thermal sensors were connected to the M3300 Fluoroptic thermometer (Luxtron) and had a communication link to a computer via an RS-232 serial cable. This experimental setup, used to measure temperature increments inside the muscle phantom and the tumor, has been used in previously described hyperthermia studies [21].

The temperature sensors were placed alongside the antenna, at 0.0 cm, 0.5 cm, 1.0 cm and 1.5 cm, for every experiment. We used a stub between the power amplifier and the antenna to get the best standing wave ratio (SWR), which was measured by a network analyzer (Agilent Technologies, Santa Clara, CA, USA). SWR measurements were carried out with the antenna embedded in the phantom.

The radiation power during the experiments was 10 W and was applied for 5 min. Transmission and reflection power levels were monitored by a power meter PM2002 (Amplifier Research, Souderton, PA, USA). The stub was adjusted so that the reflected power was minimal (SWR near 1.0) and incident power was maximal (10 W). The frequency was fixed at 2.45 GHz. Data was stored every second by using a computer connected to the fluoroptic thermometer.

2.6. Temperature Measurements in Agarose Tumor Phantoms

When the tumor phantom was solid, the glass capillaries and the coaxial antenna were inserted inside the phantom. Once they were placed at the desired position, temperature probes were placed inside the phantom through the glass capillaries. Four temperature sensors were inserted in a horizontal line, with a distance of $\sim$ 0.5 cm between them. The coaxial antenna was inserted at the center of the sphere. A temperature sensor was placed next to the antenna; another sensor was positioned at 0.5 cm from the antenna and the other two sensors were situated at 1.0 cm and 1.5 cm respectively. For the small sphere, diameter of 1.68 cm, the last two sensors were placed outside the MNPs sphere, only in contact with the tumor phantom. For the big sphere, diameter of 2.12 cm, only the outermost sensor was placed outside the MNPs sphere. The antenna was then connected to the stub until coupling between the antenna and power amplifier was achieved; we considered that coupling was attained when measured SWR was near 1.0. Once the coupling was adjusted, microwave radiation was applied for 5 min. The initial temperature of the phantom was controlled at $\sim$25°C, and temperature increments were recorded. Measured temperature was compared for each concentration of magnetite. To find out the difference between the concentration of magnetite and the increase of temperature, we

generated thermographs. The thermographs were plotted by using temperature increments recorded by temperature sensors, placed inside the phantom, during microwave radiation (300 s), and temperature sensor position (next to the antenna, at 0.5 cm, 1.0 cm and 1.5 cm). The cubic spline interpolation function of Matlab (Matworks inc. USA) was used to plot the thermograph; the values of the interpolation function were calculated every 0.1 cm. A thermochromatic sheet was placed close to the phantom to observe whether the radiation generated from the antenna was radial. Microwave radiation was applied five times for all the phantoms, and the temperatures with and without the MNPs were acquired every second during the experiments using True Temp software (Luxtron, USA). None of the phantoms was reused for the same experiment so that their electromagnetic and thermal properties were not affected.

3. RESULTS

3.1. Characterization of the Magnetic Nanoparticles

Figure 4 shows a TEM micrograph where one can observe the spherical shape of the magnetoliposomes (liposomes were not stained with uranyl acetate and, hence, only the magnetic particles inside the liposome are visualized)and the average diameter of 15 nm and 150 nm of the particles of ferrofluid and MLs, respectively.

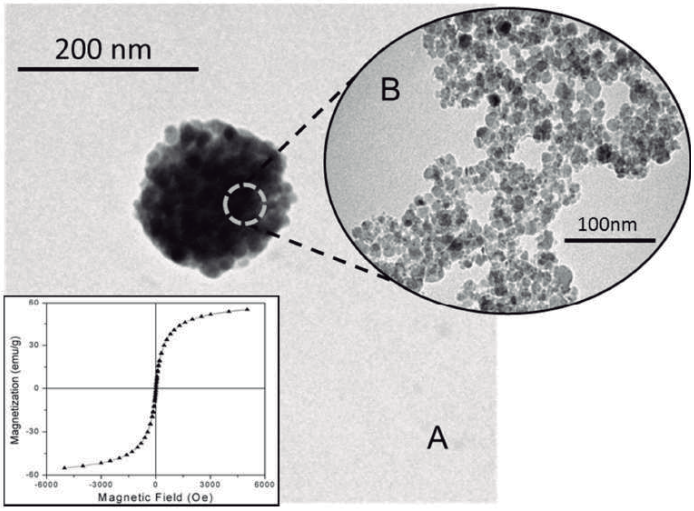

Figure 4. TEM image of: A) MLs and B) ferrofluid, shows the size and shape of particles. Inset: Magnetization curve for ferrofluid as a function of applied magnetic field.

The hydrodynamic diameter of the ferrofluid and MLs obtained by dynamic light scattering (DLS) was 52 ± 1 nm and 190 ± 1 nm, respectively. Both types of particles are nearly monodisperse: polydispersity index (PI) $= 0.181 \pm 0.003$ for ferrofluid, and 0.153 ± 0.015 for MLs. The average diameter obtained using this technique was much larger than that observed using TEM. This is because magneto static (magnetic dipole-dipole) interactions between particles can cause agglomeration even in the absence of any external magnetic field.

The Fe_3O_4 content of the ferrofluid and MLs was 22 mg/mL and 1.2 mg/mL, respectively. From these concentrations, the ferrofluid used in this study was diluted to see its thermal behavior at different concentrations.

The room temperature magnetization curve of the ferrofluid is shown in the inset of Figure 4. No hysteresis loop was observed, which indicated superparamagnetic behavior with a saturation magnetization of 52 emu/g. Furthermore, the coercive field was closed to zero.

3.2. Characterization of Agarose Tumor Phantoms

The tumor phantoms presented a permittivity of 55.88 and a conductivity of 2.88 S/m at 2.45 GHz. The reported dielectric constant of cancerous tissue was around 59 and its conductivity was about 2.5 S/m at 2.45 GHz [22]. As can be seen, the properties achieved in phantom showed similar values to those reported in the literature. The differences in the relative permittivity and conductivity observed were 3.12 units and 0.38 S/m, respectively.

3.3. Temperature Measurements in the Agarose Tumor Phantoms

Once a set of reference values was obtained, the effect of ferrofluid concentration on temperature was evaluated using the same experiment setup and conditions as for the reference assay.

3.4. Implant of Ferrofluid

Figure 5 shows the experimental results for the temperature rise as a function of time for various concentrations of ferrofluid.

The main parameter used to determine the heating of the tissue was the SAR, which is defined as the rate at which electromagnetic energy is absorbed by unit mass of a biological material and is proportional to the rate of the temperature increase ($\Delta T/\Delta t$) for adiabatic processes. From the initial slopes of the curves, SAR values

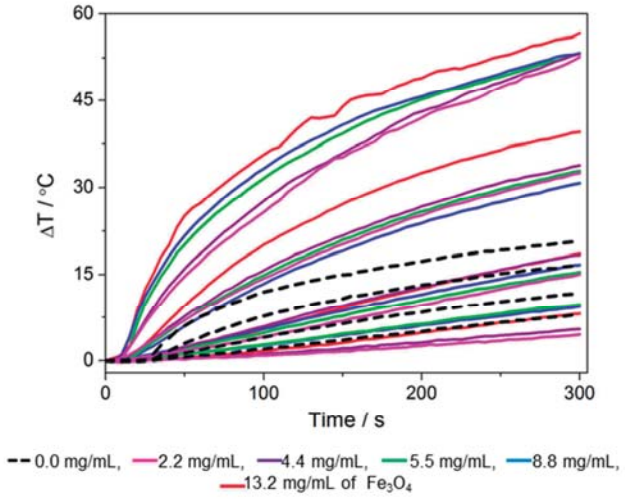

Figure 5. Temperature increments measured with the four fiber-optic sensors, placed inside the phantom, for each of the four concentrations of magnetite (in spheres of 1.5 cm) and in absence of MNPs. For each concentration, 4 time-dependent curves are displayed. Temperature was measured at the center of tumor phantom (highest temperatures for each concentration), next to the antenna, at 0.5 from the antenna, but still inside the tumor phantom, and at 1.5 cm and 2.0 from the antenna, both outside the tumor phantom (lowest temperatures for each concentration).

were calculated using

$$SAR = C_e \left(\frac{\Delta T}{\Delta t} \right)_{t=0}, \tag{5}$$

where C_e is the specific heat capacity of the sample. We used the specific capacity of a high water content tissue (3470 J/K kg) [23] because our phantom mimics this kind of tissue. The obtained SAR values for spheres of 2.5 mL were 1090 W/kg (2.2 mg/mL), 1166 W/kg (4.4 mg/mL), 1454 W/kg (5.5 mg/mL), 1544 W/kg (8.8 mg/mL), and 1697 W/kg (13.2 mg/mL). These values were plotted as a function of FF concentration, Figure 6; from this figure, it is evident the rise of SAR values associated with FF concentration.

Temperature increase distribution as a function of time, at the end of each test, is shown in Figure 7. Interpolation, in time and space, was used to make a graphical representation of the evolution in time of the four temperatures measured inside the phantom; the same method was carried out for Figures 8 and 9. As indicated above, it was verified, by means of a thermochromic paper, that the temperature gradient was radial. Then, by using the cubic spline interpolation function of

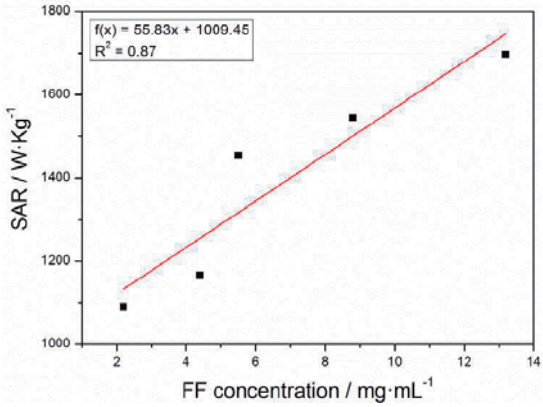

Figure 6. Plot of SAR as a function of ferrofluid concentration for 2.5 mL spheres.

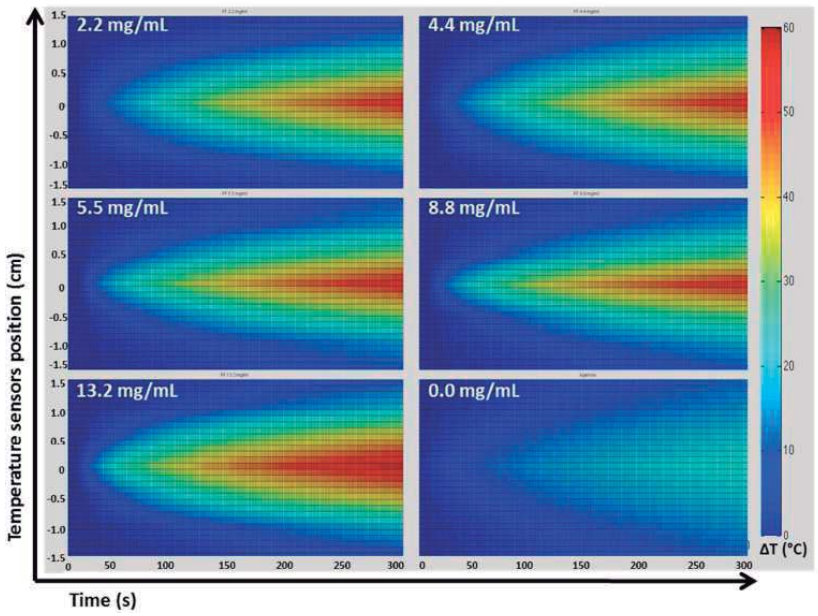

Figure 7. Temperature increase distribution as a function of time during 5 min at 10 W irradiation in phantoms with 2.5 mL spheres containing ferrofluid at different concentrations, from 0 to 13.2 mg/mL.

Matlab (Mathworks inc., USA) the figure was plotted. As can be seen, the increase in heating was concomitant with an increase in ferrofluid concentration. Maximum temperature increase was observed in the presence of ferrofluid at a concentration of 13.2 mg/mL of magnetite. Table 1 summarizes the temperature increments recorded at the end of each test for different positions of the fiber sensors with respect to the antenna for ferrofluid.

Table 1 shows that the same concentration of MNPs (8.8 mg/mL) but in a larger sphere (5 mL instead of 2.5 mL) resulted in a smaller increase in temperature. The corresponding thermograms show the difference in heat distribution clearly (Figure 8): with a sphere of 5 mL, the heat generated was distributed more homogenously throughout the phantom.

Table 1. Temperature increases in phantoms with different concentrations of ferrofluid and ML after 5 min of microwave irradiation. The volume used was 2.5 mL; *except for this case, 5 mL. ** Phantom without MNPs.

	Concentration /mg mL^{-1}	Sensor next to the antenna/°C	Sensor at 0.50 cm/°C	Sensor at 1.00 cm/°C	Sensor at 1.50 cm/°C
FF	13.2	56.64	39.57	18.62	8.13
	8.8	53.28	30.76	16.66	9.38
	8.8 *	32.29	21.46	19.26	7.27
	5.5	53.25	32.81	15.42	9.78
	4.4	53.19	33.78	18.36	5.40
	2.2	52.63	32.51	15.06	4.52
ML	1.2	53.44	32.64	14.64	5.35
	1.2*	23.13	18.37	17.90	11.00
	0**	20.78	16.65	11.75	7.99

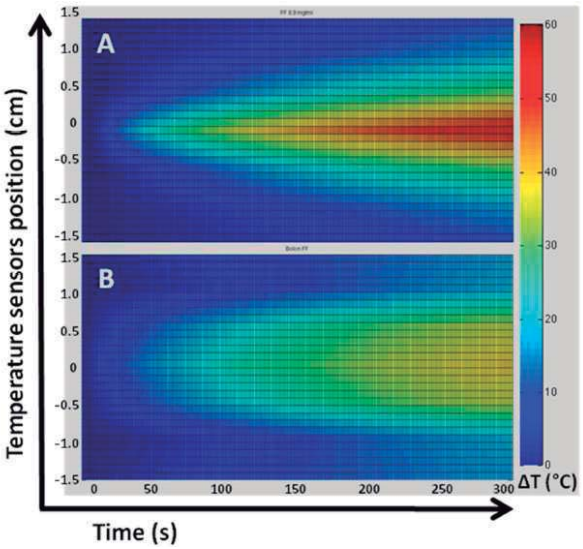

Figure 8. Temperature increase distribution as a function of time during 5 min at 10 W irradiation in phantoms with 8.8 mg/mL of magnetite containing ferrofluid: A) ferrofluid was inserted in a 2.5 mL sphere and B) ferrofluid was inserted in a 5 mL sphere.

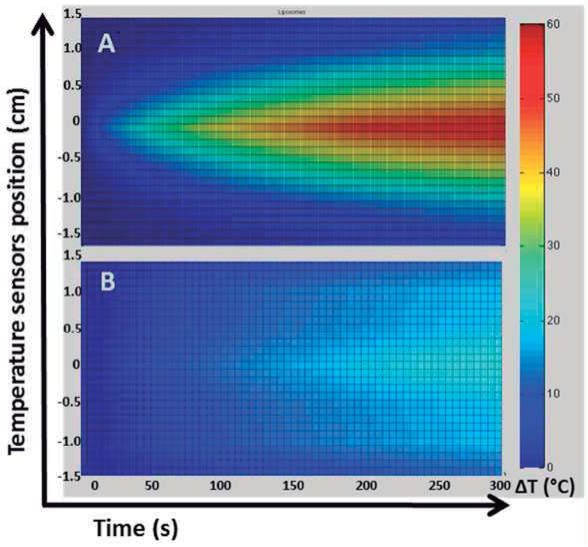

Figure 9. Temperature increment distribution as a function of time during 5 min at 10 W irradiation in phantom with MLs 1.2 mg/mL of magnetite A) MLs were inserted in a sphere of 2.5 mL and B) MLs were inserted in a sphere of 5 mL.

3.5. Implant of MLs

Values of SAR corresponding to magnetoliposomes were calculated by using Eq. [5] and were 1603 W/kg for a sphere of 2.5 mL, and 562 W/kg for one of 5 mL. The temperature distribution, in tumor phantom with MLs inside, is displayed in Figure 9. It is noteworthy that in spite of having encapsulated a lower concentration of magnetite (1.2 mg/mL), temperature increments were greater than those obtained with ferrofluid at a concentration of 8.8 mg/mL. A comparison of temperature distributions in spheres of different volumes showed similar behavior to the one observed for the ferrofluid. Table 1 shows the temperature increments recorded at the end of each test for different positions of the fiber sensors with respect to the antenna for MLs.

4. DISCUSSION

The heating effect caused by iron oxide nanoparticles subjected to an alternating magnetic field is caused by a combination of several different mechanisms: hysteresis loss, and Néel and Brownian relaxation. MNPs with a core diameter of less than 20 nm [24] have a single magnetic domain and have superparamagnetic properties. Under these particular conditions, the heating mechanism is dominated

by Brownian and Néel relaxation.

In hyperthermia treatment, controlling electromagnetic energy delivery to tumors is still a great challenge. This paper reports the heating effects in a tissue-mimicking phantom. In this study, ferrofluid and MLs were used as MNPs to focus EM energy in tumors [25]. The temperature recorded during treatment increased, although not in a linear way, with the increase of the concentration of MNPs into the sphere. The temperature increment was independent of concentration between 2.2–8.8 mg/mL; there were no differences between the final temperatures recorded with the different probes, but we observed little differences in the kinetics of heating: the final temperature for concentrations of 8.8 mg/mL and 5.5 mg/mLwas reached faster than for the concentrations of 4.4 mg/mL and 2.2 mg/mL. With a concentration of 13.2 mg/mL of magnetite, the highest temperature was achieved by the probe close to the antenna. The temperature difference between the probe that was next to the antenna and the one which was 2 cm from the antenna, outside the phantom that contained the nanoparticles, was approximately 50°C. The recorded temperature decreased with a decreasing concentration of nanoparticles and distance from the antenna. We observed that when the concentration was 0.0 mg/mL, there was no thermal ablation because the achieved temperature was lower than 50°C. We obtained a temperature increment of 20.78°C in the reference phantom, whose initial temperature was 25°C. When nanoparticles were used, we obtained greater increments in temperature than those observed in a reference phantom. Hence, nanoparticles do contribute to temperature increments. It is worth mentioning that the temperature may have increased more if radiation had been applied for longer times or at higher power rates. On the other hand, SAR determination showed the utility of the use of MNPs, since higher values of SAR were associated with an increase of FF concentration. The heating in the MLs was significantly higher for the same concentration of FF inside the liposome than for the FF alone. It has been described that the increase of thermal conductivity of nanoparticles in comparison to the macroscopic materials arises from the clustering of nanoparticles [26]. FF inside a liposome forms clusters and the effective volume of a cluster, i.e., the volume from which other clusters are excluded, can be much larger than the physical volume of the particles. Within such clusters, heat can move very rapidly and this produces a significantly increase of the thermal conductivity.

With this study we have demonstrated the feasibility of improving temperature increment and of focusing heat into the phantom using nanoparticles. Moreover, the physical properties of MNPs are such that they interact with the magnetic field generated by the antenna.

In consequence, the experimental results show that the use of MNPs is promising for *in vivo* treatments and justify further research to validate the techniques *in vitro* and *in vivo*. The phantom is only a model, and the propagation losses of body implanted antennas are different depending on the kind of tissue [27]. Hence, more research is still needed to establish how to guide the particles inside tumor cells; continued progress in nanotechnology research should result in this soon.

The antenna used in this study generated electric and magnetic fields; in conventional ablation treatment, only the electric field is taken into account because tissues interact weakly with magnetic fields. However, this situation changes dramatically when nanoparticles with superparamagnetic properties are present inside the tissue. In such a case, the electric field interacts with the electrical properties of the tissue (permittivity and conductivity) and the magnetic field interacts with the permeability of the MNPs. For this reason, it is possible to say that the presence of MNPs enhances the effect of the antenna by taking advantage of the magnetic fields. This allows more effective SAR distributions and hence requires lower power levels. Therefore, the use of MNPs in ablation therapy using microwaves is a good option as a method of focusing thermal energy.

5. CONCLUSION

By using ferrofluid and magnetoliposomes, it is possible to focus the heat in a tumor region until the appropriate therapeutic temperature is reached. The magnetic nanoparticles used in this study in combination with a microwave applicator enhance the temperature increment in order to produce therapeutic ablation in the tissue model. Comparing the behavior of both types of nanoparticles, magnetoliposomes achieved the desired temperature rise at a lower magnetite concentration than the ferrofluid.

ACKNOWLEDGMENT

Authors are grateful for the financial support given by the Spanish Ministerio de Ciencia e Innovación (MICINN) to the project MAT2009-13155-C04-03. Authors thank J. H. Zepeda Peralta for his invaluable technical assistance.

REFERENCES

1. Miltenyi, S., W. Muller, W. Weichel, and A. Radbruch, "High gradient magnetic cell separation with MACS," *Cytometry*, Vol. 11, 231–238, 1990.
2. Radbruch, A., B. Mechtold, A. Thiel, S. Miltenyi, and E. Pfluger, "High-gradient magnetic cell sorting," *Methods in Cellular Biology*, Vol. 42, 387–403, 1994.
3. Safarik, I. and M. Safarikova, "Use of magnetic techniques for the isolation of cells," *Journal of Chromatography B: Biomedical Sciences and Applications*, Vol. 722, 33–53, 1999.
4. Swan, H., *Thermoregulation and Bioenergetics*, Elsevier, Amsterdam, 1974.
5. Suit, H. and M. Shwayder, "Hyperthermia: Potential as an antitumour agent," *Cancer*, Vol. 34, 122–129, 1974.
6. Hahn, G., *Hyperthermia and Cancer*, Plenum Press, New York, 1982.
7. Kettering, M., J. Winter, M. Zeisberger, S. Bremer-Streck, H. Oehring, C. Bergemann, C. Alexiou, R. Hergt, K. J. Halbhuber, W. A. Kaiser, and I. Hilger, "Magnetic nanoparticles as bimodal tools in magnetically induced labeling and magnetic heating of tumour cells: An *in vitro* study," *Nanotechnology*, Vol. 18, 175101, 2007.
8. Simon, C. J., D. E. Dupuy, and W. W. Mayo-Smith, "Microwave ablation: Principles and applications," *Radio Graphics*, Vol. 25, S69–S83, 2005.
9. Safarik, I. and M. Safarikova, "Magnetic nanoparticles in biosciences," *Monatschefte für Chemie*, Vol. 133, 737–759, 2002.
10. Saiyed, Z. M., S. D. Telang, and C. N. Ramchand, "Application of magnetic techniques in the field of drug discovery and biomedicine," *BioMagnetic Research and Technology*, Vol. 1, 2, 2003.
11. Diederich, C. J., "Thermal ablation and high-temperature thermal therapy: Overview of technology and clinical implementation," *International Journal of Hyperthermia*, Vol. 21, 745–753, 2005.
12. Oura, S., T. Tamaki, I. Hirai, T. Yoshimasu, F. Ohta, R. Nakamura, and Y. Okamura, "Radiofrequency ablation therapy in patients with breast cancers two centimeters or less in size," *Breast Cancer*, Vol. 14, 48–54, 2007.
13. Rosensweig, R. E., "Heating magnetic fluid with alternating magnetic field," *Journal of Magnetism and Magnetic Materials*,

Vol. 252, 370–374, 2002.

14. Rovers, S. A., R. Hoogenbomm, M. F. Kemmere, and J. T. F. Keurentjes, "Relaxation processes of superparamagnetic iron oxide nanoparticles in liquid and incorporated in poly (methyl methacrylate)," *Journal of Physical Chemistry C*, Vol. 112, 15643–15646, 2008.
15. Pankurst, Q. A., J. Connolly, S. K. Jones, and J. Dobson, "Applications of magnetic nanoparticles in biomedicine," *Journal of Physics D: Applied Physics*, Vol. 36, R167–R181, 2003.
16. Huang, H., F. H. Xue, B. Lu, F. Wang, X. L. Dong, and W. J. Park, "Enhanced polarization in tadpole-shaped (Ni, Al)/Aln nanoparticles and microwave absorption at high frequencies," *Progress In Electromagnetics Research B*, Vol. 34, 31–46, 2011.
17. Hergt, R. and W. Andrä, "Magnetic hyperthermia and thermoablation," *Magnetism in Medicine*, 2nd Edition, W. Andrä and H. Nowak, editor, Wiley-VCH, Berlin, 2007.
18. Lai, J. C. Y., C. B. Soh, E. Gunawan, and K. S. Low, "Homogeneous and heterogeneous breast phantoms for ultra-wideband microwave imaging applications," *Progress In Electromagnetics Research*, Vol. 100, 397–415, 2010.
19. Sabaté, R, R. Barnadas-Rodríguez, J. Callejas-Fernández, R. Hidalgo-Álvarez, and J. Estelrich, "Preparation and characterization of extruded magnetoliposomes," *International Journal of Pharmaceutics*, Vol. 347, 156–162, 2008.
20. Cepeda, M. F. J., A. Vera. and L. Leija, "Coaxial antenna for microwave coagulation therapy in ex vivo swine breast tissue," *7th International Conference on Electrical Engineering, Computing Science and Automatic Control (CCE 2010)*, Tuxtla Gutiérrez, Chiapas, México, Sept. 8–10, 2010.
21. Trujillo-Romero, C. J., S. García-Jimeno, A. Vera, L. Leija, and J. Estelrich, "Using nanoparticles for enhancing the focusing heating effect of an external waveguide applicator for oncology hyperthermia: Evaluation in muscle and tumor phantoms," *Progress In Electromagnetics Research*, Vol. 121, 343–363, 2011.
22. Lazebnik, F. M., D. Popovic, L. McCartney, C. B. Watkins, M. J. Lindstrom, J. Harter, et al., "A large-scale study of the ultrawideband microwave dielectric properties of normal, benign and malignant breast tissues obtained from cancer surgeries," *Physics in Medicine and Biology*, Vol. 52, 6093–6115, 2007.
23. Guy, A. W., "Analysis of electromagnetic fields induced in biological tissues by thermographic studies on equivalent

phantom models," *IEEE Transactions in Microwave Theory and Techniques*, Vol. 19, 205–214, 1971.

24. Leslie-Peleckie, D. L. and R. D. Rieke, "Magnetic properties of nanostructured materials," *Chemistry of Materials*, Vol. 8, 1770–1783, 1996.
25. Iero, D., T. Isernia, A. F. Morabito, I. Catapano, and L. Crocco, "Optimal constrained field focusing for hyperthermia cancer therapy: A feasibility assessment on realistic phantoms," *Progress In Electromagnetics Research*, Vol. 102, 125–141, 2010.
26. Keblinski, P., S. R. Phillpot, S. U. S. Choi, and J. A. Eastman, "Mechanisms of heat flow in suspensions of nano-sized particles (nanofluids)," *International Journal of Heat and Mass Transfer*, Vol. 45, 855–863, 2002.
27. Gemio, J., J. Parrón, and J. Soler, "Human body effects on implantable antennas for ISM bands applications: Models comparison and propagation losses study," *Progress In Electromagnetics Research*, Vol. 110, 437–452, 2010.

Artículo 4.

External magnetic field-induced selective distribution of magnetoliposomes in mice.

Nanoscale Research Letters, 7 (1): 452.

Se ha estudiado el efecto de un imán externo sobre la biodistribución de magnetoliposomas que han sido administrados por vía intravenosa en ratones (8 mg de hierro / kg) con y sin inflamación aguda inducida. Los resultados muestran que debido a la mayor permeabilidad vascular, los magnetoliposomas se acumulan en la zona inflamada en ausencia de un campo magnético externo, pero la cantidad de hierro presente en la inflamación aumenta bajo el efecto de un imán. Este aumento depende del tiempo de exposición del campo magnético externo (20 min o 60). También se observó que la presencia del imán estaba asociada a que hubiera menor cantidad de hierro en el hígado, el bazo y plasma, comparándolo con el que hay en los ratones a los que no se les había aplicado ningún campo magnético externo. Los resultados de este estudio confirman que es posible dirigir fármacos encapsulados en partículas magnéticas por medio de un imán externo.

García-Jimeno et al. Nanoscale Research Letters 2012, 7:452
http://www.nanoscalereslett.com/content/7/1/452

Nanoscale Research Letters
a SpringerOpen Journal

NANO EXPRESS Open Access

External magnetic field-induced selective biodistribution of magnetoliposomes in mice

Sonia García-Jimeno[1], Elvira Escribano[2,4], Josep Queralt[3,4] and Joan Estelrich[1,4*]

Abstract

This study looked at the effect of an external magnet on the biodistribution of magnetoliposomes intravenously administrated in mice (8 mg iron/kg) with and without induced acute inflammation. Our results showed that due to enhanced vascular permeability, magnetoliposomes accumulated at the site of inflammation in the absence of an external magnetic field, but the amount of iron present increased under the effect of a magnet located at the inflammation zone. This increase was dependent on the time (20 or 60 min) of exposure of the external magnetic field. It was also observed that the presence of the magnet was associated with lower amounts of iron in the liver, spleen, and plasma than was found in mice in which a magnet had not been applied. The results of this study confirm that it is possible to target drugs encapsulated in magnetic particles by means of an external magnet.

Keywords: magnetoliposomes, magnetic nanoparticles, inflammation, biodistribution, external magnetic field

Background

The use of materials in nanoscale provides unparallel freedom to modify fundamental properties such as solubility, diffusivity, blood circulation half-life, drug release characteristic, and immunogenicity. In the last two decades, nanoparticles have attracted widespread attention due to the rapidly increasing number and variety of their applications in the biomedical sciences, including imaging and therapy [1,2]. Indeed, they possess unique nanoscale size-dependent physical and chemical properties that can be controlled in a manner that is not possible with bulk materials [3]. There are several nanoparticle platforms: liposomes, polymeric conjugates, polymeric nanoparticles, micelles, nanoshells, dendrimers, engineered viral nanoparticles, albumin-based nanoparticles, polysaccharide-based nanoparticles, ceramic nanoparticles, and magnetic nanoparticles.

Among the aforementioned particles, iron oxide-based magnetic nanoparticles (MNs) have been developed and represent promising new systems in biomedical sciences, especially in therapy and imaging [4]. Medical applications of MNs require that such nanoparticles possess superparamagnetic properties at room temperature. This property is displayed in small subdomain particles (of the order of tens of nanometers or less; 10 to 15 nm for magnetite). Superparamagnetic particles have fast relaxation times and, consequently, show neither remanence nor coercivity. Thus, these nanoparticles are nonmagnetic in the absence of an external magnetic field, but they do develop a mean magnetic moment in an external magnetic field [5].

Therapeutic application of MNs is when they are used for the site-specific delivery of therapeutic payloads. The goal of any drug delivery system is to ensure that the drugs are administered into the body correctly and reach the target area. Targeting a drug delivery system can be divided into two general categories: passive and active. Although both approaches are used, the technical demands of the two are considerably different. Passive targeting exploits the natural distribution pattern, i.e., the tendency of unmodified particles to accumulate in certain tissues, which occurs because nanoparticles are quickly removed from circulation by the cells of the mononuclear phagocyte system (MPS), in particular, the resident macrophages of the liver (Kupfer cells), spleen, lung, and bone marrow [6]. Hence, this strategy serves to target diseases that affect the MPS. Active targeting involves modifying the basic structure of nanoparticles by attaching a homing device to the carrier. Examples of

* Correspondence: joanestelrich@ub.edu
[1]Departament de Fisicoquímica, Facultat de Farmàcia, Universitat de Barcelona, Avda. Joan XXIII, Barcelona, Catalonia 08028, Spain
[4]Institut de Nanociència i Nanotecnologia de la Universitat de Barcelona (IN2UB), Barcelona, Catalonia 08028, Spain
Full list of author information is available at the end of the article

particle modifications include the attachment of ligands such as antibodies - which allow it to complex with the cell that contains the receptor for the interaction - and the incorporation of molecules that make the particles susceptible to pH or temperature changes [7].

MNs share the main advantages of both types of targeting; as with passive targeting, modification of the nanoparticle surface is not necessary, and like active targeting, they can be directed to the area of interest. This is due to the fact that MNs respond strongly to time-modulated magnetic fields, and in turn, magnetic fields can penetrate human tissues without impediment. Thus, MNs can be used as a tool for targeting drugs, such as anticancer or radionuclide atoms, which could be co-encapsulated within the magnetic nanoparticles and then carried within the nanoparticle structure under the influence of an external magnetic field to a targeted area in the human body. As with MNs, magnetoliposomes (MLs) formed by encapsulating iron oxide nanoparticles within liposomes have the advantage of being nontoxic and biocompatible and displaying magnetophoretic mobility [8,9]. Magnetoliposomes play an important role in the wide variety of MNs, which are routinely used as magnetic resonance imaging contrast agents [10,11] and for controlled drug release [12].

In this paper, we assess the effect of a magnetic field, generated outside the body, on the biodistribution of magnetoliposomes after intravenous administration in mice to which an inflammatory focus on their back has been induced. Cancer and inflammation are related by epidemiology, histopathology, and inflammatory profiles [13]. For this reason, the development of an experimental model to study *in vivo* whether the drug correctly reaches and concentrates at the target site is of great interest. The distribution of MNs within different organs and timescales (20 and 60 min) was examined by determining the amounts of the iron accumulated in the tissues.

Methods

Materials

Soybean phosphatidylcholine (PC), a zwitterionic phospholipid (Lipoid S-100), was donated by Lipoid (Ludwigshafen, Germany). Nanoparticles of magnetite stabilized with anionic coating (EMG 707) were purchased from FerroTec (Bedford, NH, USA). The particles had a nominal diameter of 10 nm, which was determined by transmission electron microscopy (TEM); a stock solution has a coefficient of viscosity of less than 5 mPa·s at 27°C and a magnetite volume content of 1.8%. Neodymium-iron-boron ($Nd_2Fe_{12}B$) magnet discs (N35D2510, 25×10 mm, of 600 mT by side) were obtained from Halde GAC (Barcelona, Spain). Reagents were of analytical grade.

Preparation and characterization of magnetoliposomes

Magnetoliposomes were obtained using a modified version of the phase-reverse method followed by extrusion at room temperature into a Liposofast device (Avestin, Inc., Ottawa, Canada) through two polycarbonate membrane filters of 0.2-μm pore size, a minimum of nine times both ways [14]. Ferrofluid was diluted with 0.16 M NaCl until an iron concentration of 1.12 mg mL^{-1} was achieved, and with this aqueous suspension, the phospholipid layers were hydrated. Ferrofluid particles no longer entrapped were removed by size exclusion chromatography on Sepharose 4B (GE Healthcare, Chalfont Saint Giles, UK). A total of 250 μL of magnetoliposomes was applied to a 1×30-cm column saturated with lipids before sample elution with 0.16 M NaCl. Magnetoliposomes were then separated from empty liposomes by means of a MACS separation column (Miltenyi Biotech, Bergisch Gladbach, Germany). The morphology of magnetoliposomes was observed by TEM using a JEOL 1010 microscope (JEOL Ltd., Akishima, Tokyo, Japan) operating at 80,000 V. A drop of the aqueous dispersion of magnetoliposomes was placed onto a 400-mesh copper grid coated with a carbon film with a Formvar membrane and then allowed to air dry before being inserted into the microscope. Images were recorded with a Megaview III camera (Arecont Vision, Glendale, CA, USA), and the acquisition was accomplished using Soft-Imaging software (SIS, Münster, Germany). The iron content of the magnetic particles was determined on the basis of the ferrous ion using *o*-phenanthroline [15]. The phospholipid content was determined by the Stewart-Marshall method [16]. The hydrodynamic diameter of magnetoliposomes was determined by dynamic light scattering (DLS) at 90° with the Zetasizer Nano (Malvern Instruments Ltd., Malvern, Worcestershire, UK) at a temperature of 25°C. The particle size distribution was designated by the polydispersity index (PI), which ranged from 0.0 for an entirely monodisperse sample to 1.0 for a polydisperse sample. The ζ-potential measurements of magnetoliposomes were performed at 25°C using the Zetasizer Nano ZS (Malvern Instruments Ltd., Malvern, Worcestershire, UK).

Animal and biological methods

Experiments were performed on 8-week-old female CD-1 mice with a body weight of 28 to 32 g (Harlam Ibérica, Sant Feliu de Codines, Barcelona, Spain). Animals were provided with food and tap water *ad libitum* and allowed a 1-week acclimation period after arrival to the animal facilities of the Faculty of Pharmacy. The animals were then allowed an additional week to adjust to restraining conditions. The study was conducted under a protocol approved by the Animal Experimentation

Ethics Committee of the University of Barcelona, Barcelona, Spain.

Mice were randomly divided into four groups (between seven and eight animals per group): (a) healthy control saline (C): animals with back air pouch receiving saline i.v. (0.1 mL/10 g body weight); (b) inflammation control group (I): animals with carrageenan-induced inflammation in the air pouch receiving saline i.v.; (c) inflammation magnetoliposomes (IN): animals with carrageenan-induced inflammation receiving magnetoliposomes i.v.; and (d) inflammation magnetoliposomes with magnet (INM): as in the previous group (IN), but under the effect of a magnet located just above the inflammatory pouch for 20 or 60 min. All injections and painful procedures were performed under isoflurane (Laboratorios Esteve, Barcelona, Spain) anesthesia (4% induction and 3% maintenance).

The method used to induce acute inflammation was similar to that described by Romano et al. [17]. Briefly, sterile air pouches were produced by injecting 5 mL of air subcutaneously (s.c.) through a disposable disc filter (EPS® Inc., Ivyland, PA, USA; 2 μm) into the back of the mouse (day 0); the pouches were injected again with 3 mL of air on day 3. On day 4, the pouches from the mice in group C received 1-mL saline (B Braum Medical, Barcelona, Spain), and the pouches from the mice in groups I, IN, and INM received 1-mL carrageenan lambda 1.2% s.c. (Sigma-Aldrich, St. Louis, MO, USA).

On day 5, 24 h after the phlogogen injection, the animals received 0.1 mL/30 g saline (group C) or magnetoliposomes (8 mg of iron/kg body weight) in saline (groups I, IN, and INM) i.v. through a jugular vein and were placed in restrained Plexiglas cages with air holes. Some mice did not have disc magnets on their backs (groups C, I, and IN) while some did for 20 or 60 min. Before i.v. administration, a small incision was made in the neck to one side of the midline. A 30-G needle was used for the injection (Becton Dickinson D Ultra-Fine U-100 insulin Syringe, USA) and was inserted into the vein through the pectoral muscle at an approximate angle of 10°, pointing toward the head. The muscle acts as a seal when the needle is withdrawn. To close the skin incision, one or two sterile silk suture 4/0 points were applied (Laboratorios Aragó, Barcelona, Spain).

After 20 or 60 min of i.v. dosing, mice were anesthetized, thoracotomy was performed, and the blood was harvested by cardiac puncture using a 27-G Becton Dickinson tuberculin syringe with needle. Plasma was obtained by centrifugation (10,000 × *g* for 5 min) (Heraeus Biofuge Pico, Hanau, Germany). When the heart

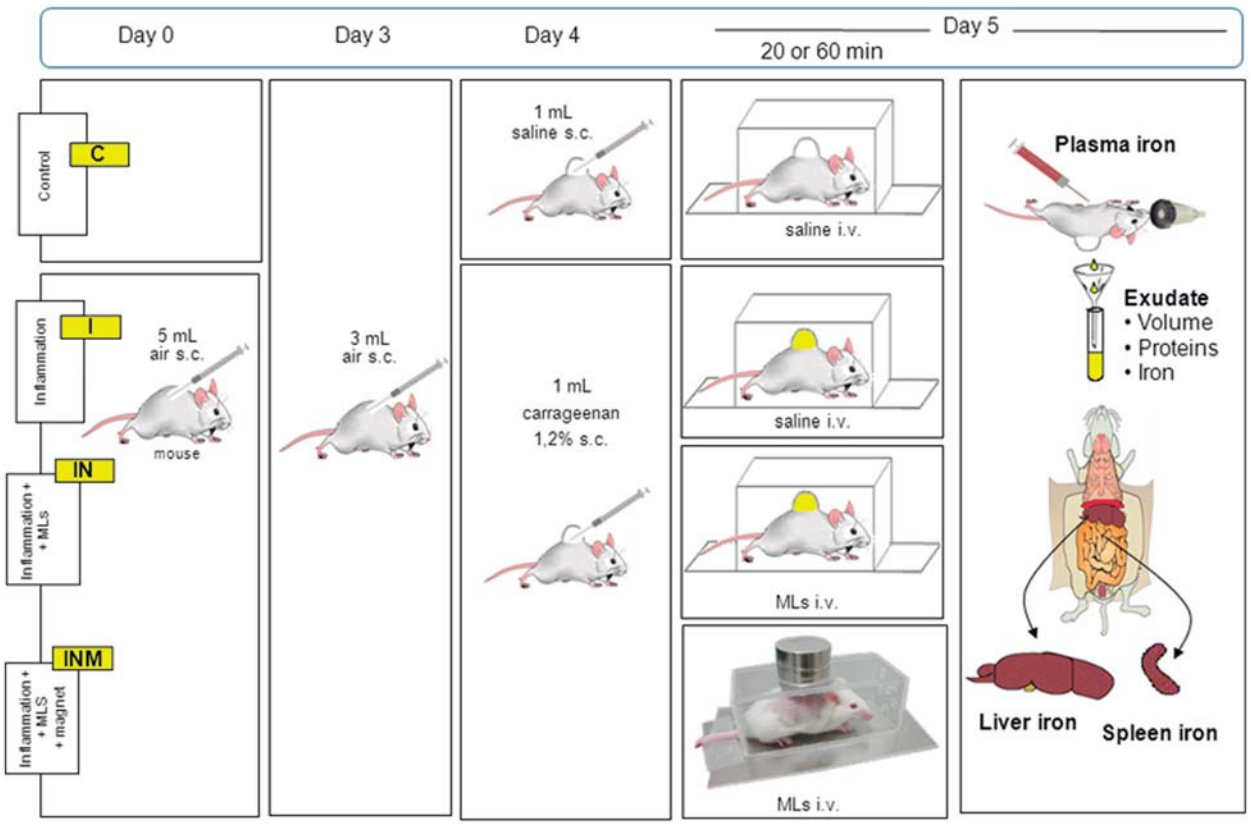

Figure 1 Experimental procedure performed to establish the effect of external magnet on biodistribution of MLs.

stopped beating, 2.5 mL of ultrapure water (Purelab® ultra analytics system, ELGA, Veolia Water, Barcelona, Spain) was injected into the pouch. The pouch was gently massaged, and the mouse was placed in the supine position on the top of a plastic funnel. An incision was made in the pouch, and the exudates were collected in 5-mL polyethylene tubes and weighed. The liver and spleen were harvested and dried by placing the samples in a laboratory heater at 60°C for 24 h. Figure 1 shows a schematic of the experimental procedure carried out.

Analytical determinations

To control inflammation, the volume (in milliliters) and protein content (in milligrams per milliliter) of the exudate were determined. The volume was determined by weighing the exudates, and the protein content was measured using the bicinchoninic acid assay [18]. The iron content in the plasma, exudates (pouch), and organs was analyzed by inductively coupled plasma optical emission spectrometry (Perkin-Elmer Optima 3200RL, Massachusetts, USA) after acid digestion of the organic material in closed systems. Microwave digestion (210°C, 1 h) was performed on organs, and digestion for plasma and exudates was carried out in Teflon vessels (90°C, 24 h).

The results are expressed as micrograms of iron per gram of dried tissue. The statistical significance of iron concentrations was analyzed using ANOVA followed by the post hoc Fisher's LSD test. Statistical significance was accepted at the 5% level ($P \leq 0.05$).

The presence of magnetoliposomes in the exudate was observed by TEM. To obtain the magnetoliposomes from the exudate, the exudate was eluted through the MACS separation column, and a drop of the aqueous dispersion after air drying was observed into the microscope as previously explained.

Results

The obtained magnetoliposomes contain 0.135 ± 0.005 g Fe^{3+} per mmol of phospholipid. The size of the magnetoliposomes determined by DLS ranged from 150 to 190 nm (Figure 2) with a single peak centered at 183 nm. This is consistent with our earlier results [12]. As can be observed, the magnetoliposomes are arranged in a monomodal distribution (PI < 0.2). The MLs captured within the phospholipid bilayer appear as clusters of ferrofluid particles (inset of Figure 2). At pH 7.4, a ζ-potential value of -23.5 ± 2.4 mV was obtained. This negative charge is conferred by the external phospholipid monolayer. Although PC is electrically neutral, the distribution of charges in its polar head region is asymmetrical. The negative ζ-potential of the liposomes is caused by the orientation of PC molecules in the liposome membrane.

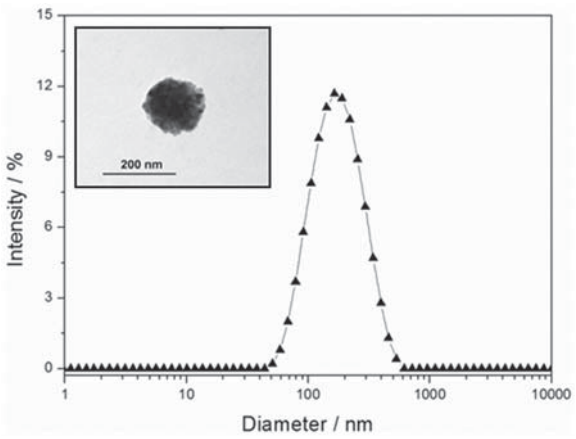

Figure 2 Size distribution expressed as *z*-diameter of magnetoliposomes after purification by size exclusion chromatography. Inset: TEM micrograph of non-stained magnetoliposomes.

The tissue distribution of iron oxide entrapped in magnetoliposomes and injected intravenously into mice from the four groups was studied 20 and/or 60 min after the injection. The presence of magnetoliposomes in the exudate is due to the hyperpermeability of the microvasculature in the inflammatory process. Therefore, in order to evaluate the biodistribution of magnetoliposomes, only those mice that demonstrated a protein concentration in exudates between 3.5 and 8.5 mg mL^{-1} as well as a similar volume of exudates for the animals induced with inflammation (2.6 ± 0.2 mL) were considered Values from 0.2 to 1.0 mg mL^{-1} are characteristic of an absence of inflammation.

Tables 1 and 2 summarize the results obtained for volume and protein content in the pouch, as well as for the iron content in the exudates, plasma, liver, and spleen 20 and 60 min after the injection of magnetoliposomes. The amount of iron determined in biological liquids and organs was higher after 60 min than after 20 min. The absence of a magnet resulted in a preferential accumulation of magnetoliposomes in the spleen and liver, consistent with the uptake of such particles by the mononuclear phagocyte system. The presence of the magnet (INM) resulted in a decrease in the iron present in the liver ($P < 0.05$) in comparison with group IN (a reduction of 23% after 20 min of the injection and of 25% after 60 min). In the plasma, the external magnet provoked a significant reduction of 30% and 31% for 20 and 60 min, respectively ($P < 0.05$). In the spleen, the reduction was less pronounced (13% and 16% for 20 and 60 min, respectively). Such reductions can be explained by the increase in iron content in the exudates. Table 1 shows how the levels of iron in the inflammatory focus

Table 1 Volume and protein content of the exudates and iron concentration in exudates, plasma, liver, and spleen

Groups	Pouch		Iron concentration (μg g^{-1})			
	Volume (mL)	Protein (mg mL^{-1})	Exudates	Plasma	Liver	Spleen
C	1.96 ± 0.24	0.61 ± 0.37	0.04 ± 0.04	4.04 ± 1.02	621 ± 310	665 ± 180
I	2.38 ± 0.33[a]	5.69 ± 2.01[a]	0.26 ± 0.13[a]	4.01 ± 1.27	712 ± 224	836 ± 278
IN	2.74 ± 0.24[a]	5.23 ± 1.43[a]	0.33 ± 0.11[a]	4.12 ± 1.07	873 ± 99[a]	1,446 ± 390[a,b]
INM	2.57 ± 0.05[a]	4.63 ± 0.21[a]	0.56 ± 0.12[a,b,c]	2.89 ± 0.42	674 ± 64[c]	1,264 ± 35[a,b]

The values are expressed as mean ± SD and were obtained 20 min after the injection of magnetoliposomes. [a,b,c] Significant differences ($P < 0.05$) with groups C, I, and IN, respectively ($n \geq 5$).

increased 1.7 times (after 20 min) and three times (after 60 min) after the injection.

As we have considered that the biodistribution of the MNs was in equilibrium with the distribution of iron, an increase in iron concentration in exudates in the IM and IMN groups was attributed to the presence of MNs in the target. To confirm this hypothesis, we determined whether MNs were present in exudates by visualizing them using TEM.

To determine whether magnetoliposomes were present in exudates, we separated them from the liquid using a magnetic separator. They can also be separated by centrifugation due to the high density of such liposomes, caused by iron loading. However, the magnetic separator allows us to concentrate on them. After this, they were visualized using TEM. Figure 3 shows the presence of magnetoliposomes in the exudates. The majority of the magnetoliposomes maintained their original form and size.

Discussion

The aim of this study was to determine whether magnetoliposomes could be directed *in vivo* to target sites under the effect of an external magnet, consequently avoiding modification of the liposomes. There are reports in the literature that this external stimulus actively locates and accumulates the drug at the targeted region [19]. It is known that liposomes (and therefore magnetoliposomes) can be directed through the functionalization of the external layer. For instance, liposomes with the RGD peptide exposed on their surface are able to bind vascular endothelial cells at inflammation sites [20]. The inflammatory reaction is one of the body's defense mechanisms. When damage occurs, blood flow is firstly increased at the point of injury, and blood vessels widen to allow oxygen, clotting agents, and white blood cells to penetrate the damaged tissues. Since the size of white blood cells is ranging from 7 to 20 μm, any nanoparticles can easily pass through the vessels and locate in the inflammation zone. To achieve an inflammation zone, we used mice with induced air pouches. Among many animal models of inflammation (sponge implant, paw edema, peritoneal, pleurisy, and air pouch), the air pouch model has the advantage of not involving internal organs, which can be damaged or perforated during sampling [21]. On the other hand, we have used a strong magnet (600 mT of surface strength of magnetic field) to assure that the magnetic field lines are penetrating the body deeply, that is, the technique is not only applicable for tissues located at the body's surface. However, the strength of the magnetic field falls off very quickly as the surface of the magnet is moved away from the target area. Besides the material of the magnet, the mass of the magnet has an important effect on its overall strength. The larger the mass of the magnet, the stronger and more effective (more uniform magnetic field) it will be. For this reason, we have used two magnets above one another (see Figure 1).

Conclusions

By using this approach (model of inflammation and strong magnet) and excluding animals with levels of iron and volumes of exudates out of the range of average values observed during inflammation, we secured a fairly

Table 2 Volume and protein content of the exudates and iron concentration in exudates, plasma, liver, and spleen

Groups	Pouch		Iron concentration (μg g^{-1})			
	Volume (mL)	Protein (mg mL^{-1})	Exudates	Plasma	Liver	Spleen
C	2.14 ± 0.02	0.63 ± 0.20	0.19 ± 0.12	4.45 ± 0.33	547 ± 91	914 ± 403
I	2.80 ± 0.23[a]	5.90 ± 2.53[a]	0.50 ± 0.10	4.12 ± 0.68	605 ± 114	1,039 ± 227
IN	2.85 ± 0.13[a]	5.20 ± 1.60[a]	0.64 ± 0.27	4.25 ± 1.43	1,174 ± 134[a,b,c]	1,611 ± 378[a,b]
INM	2.77 ± 0.18[a]	4.95 ± 1.01[a]	1.92 ± 1.44[a,b,c]	2.94 ± 0.38[a,b,c]	880 ± 97[a,b,c]	1,354 ± 260[a,b]

Values are expressed as mean ± SD and were obtained 60 min after the injection of magnetoliposomes. [a,b,c] Significant differences ($P < 0.05$) with groups C, I, and IN, respectively ($n \geq 5$).

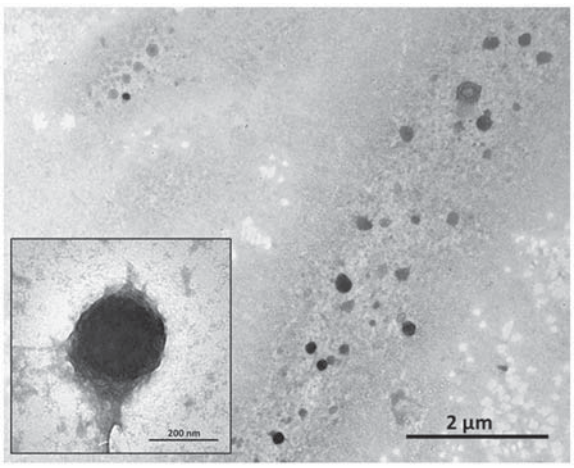

Figure 3 TEM micrograph of non-stained magnetoliposomes found in exudates of a mouse (IMN). The magnetoliposomes were found 20 min after intravenously injecting the particles. Inset: an enlarged image of a magnetoliposome.

homogeneous population in which to study the effect of an external magnetic field on the distribution of magnetoliposomes after injecting them intravenously. We observed the accumulation of magnetoliposomes at the site of inflammation (exudates) and, at the same time, the removal from the blood compartment, and the decrease in the liver and spleen. As shown in Tables 1 and 2, the increase in iron levels in exudates depends on the time of exposure of the external magnetic field; when comparing IN and INM groups, an increase of 70% and 200% was observed for 20 and 60 min, respectively. After this point, the magnetic field efficiently retains MNs. This method can also be used to enhance the accumulation of a certain drug (i.e., corticosteroid, hyaluronic acid) after an intra-articular injection, thus avoiding the need of repeated injections due to rapid clearance from the joint [22]. The fact that magnetoliposomes remain intact in the exudates 20 min after the injection is not surprising since with a diameter close to 12 nm, the magnetite particles are too large to passively cross the phospholipid bilayer. Only after the action of destabilizing agents, such as opsonins and cells of the mononuclear phagocyte system, the iron content may leave the interior of the magnetoliposomes. In conclusion, this study has demonstrated the efficacy of the magnet method. We have shown that when loaded with a suitable therapeutic agent, an anti-inflammatory in this case, magnetoliposomes, under the effect of a magnetic field can be used to treat the inflammatory process or other pathologies, and in doing so, it can reduce the drug dose administered and increase the efficacy of the treatment. Moreover, the observed reduction in the levels in the blood could prevent side effects.

Competing interests
The authors declare that they have no competing interests.

Authors' contributions
SD-J carried out the nanoparticle synthesis, participated in the biodistribution study, and performed the analysis of the samples. EE participated in the design of the study and performed the biological and analytical determinations. JQ participated in the design of the study, carried out the animal and biological studies, and contributed to the interpretation of data. JE participated in the design of the study and drafted the manuscript. All authors read and approved the final manuscript.

Acknowledgments
The authors thank Roser Estelrich for her work on the Plexiglas cages. We are also grateful for the financial support given by the Spanish Ministerio de Ciencia e Innovación (MICINN) to project MAT2009-13155-C04-03.

Author details
[1]Departament de Fisicoquímica, Facultat de Farmàcia, Universitat de Barcelona, Avda. Joan XXIII, Barcelona, Catalonia 08028, Spain. [2]Departament de Farmàcia i Tecnologia Farmacèutica, Facultat de Farmàcia, Universitat de Barcelona, Avda. Joan XXIII, Barcelona, Catalonia 08028, Spain. [3]Departament de Fisiologia, Facultat de Farmàcia, Universitat de Barcelona, Avda. Joan XXIII, Barcelona, Catalonia 08028, Spain. [4]Institut de Nanociència i Nanotecnologia de la Universitat de Barcelona (IN2UB), Barcelona, Catalonia 08028, Spain.

Received: 22 June 2012 Accepted: 27 July 2012
Published: 10 August 2012

References

1. Zhang L, Gu FX, Chan JM, Wang AZ, Langer RS, Farokhzad OC: **Nanoparticles in medicine: therapeutic applications and developments.** *Nat Clin Pharm Ther* 2008, **5**:761–769.
2. Ali Z, Abbasi AZ, Zhang F, Arosio P, Lascialfari A, Casula MF, Wenk A, Kreyling W, Plapper R, Seidel M, Niesser R, Seubert A, Park WJ: **Multifunctional nanoparticles for dual imaging.** *Anal Chem* 2011, **8**:2877–2882.
3. Leslie-Pelecky DL, Rieke RD: **Magnetic properties of nanostructured materials.** *Chem Mater* 1996, **8**:1770–1783.
4. Arruebo M, Fernández-Pacheco R, Ibarra MR, Santamaría J: **Magnetic nanoparticles for drug delivery.** *NanoToday* 2007, **2**:22–32.
5. Pankhurst QA, Connolly J, Jones SK, Dobson J: **Applications of magnetic nanoparticles in biomedicine.** *J Phys D* 2003, **36**:R167–R181.
6. Owens DE III, Peppas NA: **Opsonization, biodistribution and pharmacokinetics of polymeric nanoparticles.** *Int J Pharm* 2006, **307**:93–102.
7. Han Bae Y, Park K: **Targeted drug delivery to tumors: myths, reality and possibility.** *J Controlled Rel* 2011, **153**:198–205.
8. De Cuyper M, Joniau M: **Magnetoliposomes. Formation and structural characterization.** *Eur Biophys J* 1988, **15**:311–319.
9. Soenen SJ, Hodenius M, De Cuyper M: **Magnetoliposomes: versatile innovative nanocolloids for use in biotechnology and biomedicine.** *Nanomedicine* 2009, **4**:177–191.
10. Plassat V, Martina MS, Barratt G, Méneger C, Lesieur S: **Sterically stabilized superparamagnetic liposomes for MR imaging and cancer therapy: pharmacokinetics and biodistribution.** *Int J Pharm* 2007, **344**:118–127.
11. Soenen SJ, Vande Velde G, Ketkar-Atre A, Himmelreich U, De Cuyper M: **Magnetoliposomes as magnetic resonance imaging contrast agents.** *WIREs Nanomed Nanobiotechnol* 2011, **3**:197–191.
12. Nappini S, Baldelli Bombelli F, Bonini M, Nordèn B, Baglioni P: **Magnetoliposomes for controlled drug release in the presence of low-frequency magnetic field.** *Soft Matter* 2010, **6**:154–162.
13. Rakoff-Nahoum S: **Why cancer and inflammation?** *Yale J Biol Med* 2006, **79**:123–130.
14. García-Jimeno S, Escribano E, Queralt J, Estelrich J: **Magnetoliposomes prepared by reverse-phase followed by sequential extrusion: characterization and possibilities in the treatment of inflammation.** *Int J Pharm* 2011, **405**:181–187.
15. Kiwada H, Sato J, Yamada S, Kato Y: **Feasibility of magnetic liposomes as a targeting device for drugs.** *Chem Pharm Bull* 1986, **34**:42534258.
16. Stewart-Marshall JC: **Colorimetric determination of phospholipids with ammonium ferrothiocyanate.** *Anal Biochem* 1980, **104**:10–14.

17. Romano M, Faggioni R, Sironi M, Sacco S, Echtenacher B, Di Santo E, Salmona M, Ghezzi P: **Carrageenan-induced acute inflammation in the mouse air pouch synovial model.** *Mediat Inflamm* 1997, **6**:32–38.
18. Smith PK, Krohn RI, Hermanson GT, Mallia AK, Gartner FH, Provenzano MD, Fujimoto EK, Goeke N, Olson BJ, Klenk DC: **Measurement of protein using bicinchoninic acid.** *Anal Biochem* 1985, **150**:76–85.
19. Arias JL, López-Viota M, López-Viota J, Delgado AV: **Development of iron/ethylcellulose (core/shell) nanoparticles loaded with diclofenac sodium for arthritis treatment.** *Int J Pharm* 2009, **382**:270–276.
20. Koning GA, Schiffelers RM, Wauben MHM, Kok RJ, Mastrobattista E, Molema G, ten Hagen TLM, Storm G: **Targeting of angiogenic endothelial at sites of inflammation by dexamethasone phosphate-containing RGD peptide liposomes inhibits experimental arthritis.** *Arthritis Reum* 2006, **54**:1198–1208.
21. Jukanti R, Devaraj G, Devaraj R, Apte S: **Drug targeting to inflammation: studies on antioxidant surface loaded diclofenac liposomes.** *Int J Pharm* 2011, **414**:179–185.
22. Butoescu N, Seemayer CA, Palmer G, Guerne P-A, Gabay C, Doelker E, Jordan O: **Magnetically retainable microparticles for drug delivery to the joint: efficacy studies in an antigen-induced arthritis model in mice.** *Arthritis Res Ther* 2009, **11**:R72.

doi:10.1186/1556-276X-7-452
Cite this article as: García-Jimeno *et al.*: External magnetic field-induced selective biodistribution of magnetoliposomes in mice. *Nanoscale Research Letters* 2012 **7**:452.

4. Discusión

4. Discusión

El trabajo de esta tesis puede desglosarse en dos fases. En la primera, se seleccionó y optimizó un método de síntesis para dos tipos de nanopartículas magnéticas (NPMs): magnetoliposomas y ferrofluido, y se realizó la caracterización correspondiente a fin de asegurar su validez en aplicaciones biomédicas. En la segunda fase, se estudiaron dos aplicaciones terapéuticas de las partículas sintetizadas: como sistemas adecuados para terapia hipertérmica, y como sistemas transportadores de fármacos dirigidos bajo la acción de un campo magnético.

4.1. Síntesis y caracterización de nanopartículas magnéticas

En la síntesis de las NPMs se han utilizado diferentes montajes experimentales a pequeña escala con la finalidad de determinar el efecto de diversas variables experimentales sobre una serie de características (tamaño, magnetización y estabilidad) del producto finalmente obtenido. Como premisas de partida, se ha fijado que cualquier muestra obtenida de tener las siguientes características: tamaño inferior a 200 nm, estabilidad mínima de 24 horas, y un comportamiento propio de los ferrofluidos ante un campo magnético. Sobre aquellos productos que cumplían los citados requisitos se han ido introduciendo modificaciones en las variables experimentales hasta obtener un producto estable, con propiedades magnéticas y con un tamaño propio de las nanopartículas.

Uno de los métodos más usuales de estabilizar las partículas magnéticas es recubriéndolas con polímeros. Para obtener nanopartículas con aplicaciones biomédicas es preciso que el ferrofluido sea biocompatible y biodegradable. Uno de los polímeros más utilizados es el dextrano y sus derivados (Kawaguchi 2001; Paul et al. 2004; Chan et al. 2006, Jarrett et al., 2007). El polietilénglicol (PEG) también ha sido utilizado (Larsen et al. 2009, Barrera et al. 2009, Yue-Jian et al. 2010, Zhou et al. 2011, Schweiger et al. 2011, Brullot et al. 2012). Sin embargo, en estas ocasiones, el PEG utilizado estaba derivatizado y la unión con la magnetita implicaba un proceso químico.

En este trabajo se sintetizó un ferrofluido estabilizado con PEG sin modificar. Se determinaron las condiciones idóneas de concentración (relación Fe^{2+}/PEG) así como de masa molecular del polímero (entre 2000 y 10.000 Da). Se obtuvo una dispersión de ferrofluido de pH ≈ 5.0, con un contenido de hierro de ≈ 16 $mg \cdot mL^{-1}$, y un potencial-ζ de + 19 mV. El diámetro de las partículas sin recubrimiento se determinó por TEM y fue de unos 12 nm, valor idóneo para su uso en terapia de hipertermia ya que asegura una excelente biodisponibilidad y propiedades superparamagnéticas. El recubrimiento con PEG aumenta el tamaño de las partículas (un diámetro de 56 nm se observó para

la menor relación de PEG / hierro). El análisis de TGA mostró que el contenido de PEG en el ferrofluido va desde 6,5 hasta 23,8%, en función de los diferentes pesos moleculares y la cantidad de PEG utilizada. La interacción de PEG con magnetita puede ser debida a la unión dipolo-catión entre el grupo éter del polímero y la carga positiva de la magnetita. Se debe remarcar especialmente que el ferrofluido se ha obtenido mediante un método fácil, rápido (consta de un solo paso), totalmente reproducible, y experimentalmente benigno ya que el uso de reactivos está muy limitado y las condiciones son casi ambientales (se trabaja a un máximo de 40 ^{o}C). En la figura 1 se sintetizan alguna de las propiedades presentes en estos ferrofluidos.

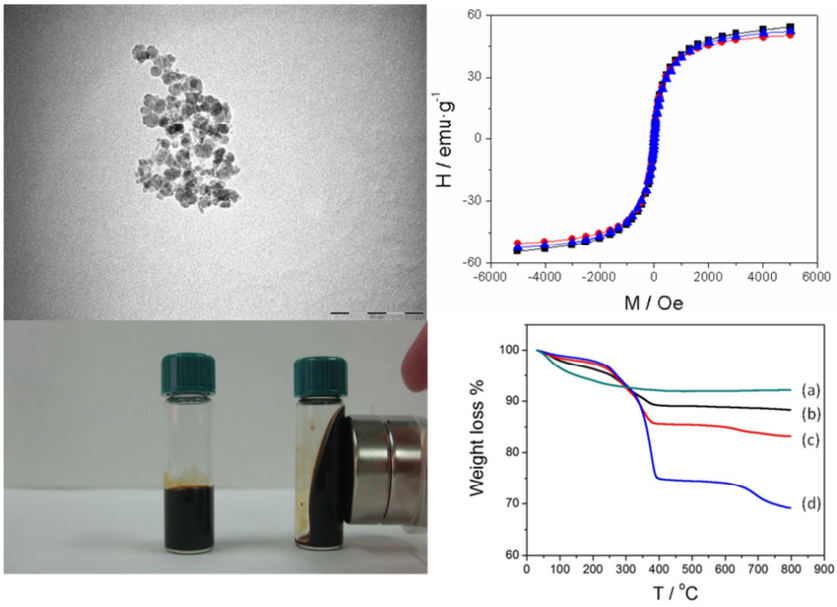

Figura 1. Propiedades del ferrofluido obtenido con PEG y empleado en el trabajo relacionado con la terapia hipertérmica. El ferrofluido de la imagen está formado por 3,0 g de PEG 6000 y 0,16 g de $FeCl_2{\cdot}4H_2O$ y 0,435 g $FeCl_3{\cdot}6H_20$. A: Micrografía de microscopia de transmisión electrónica de las partículas de ferrofluido. B: Respuesta del ferrofluido a la acción de un imán externo. C: Magnetización másica en función del campo magnético externo aplicado de un ferrofluido obtenido con PEG 6000. La ausencia de histéresis demuestra el carácter paramagnético de la preparación. D: Análisis termogravimétrico de tres muestras de ferrofluido obtenido con PEG 6000 con tres cantidades diferentes de polímero y la misma cantidad de sales férricas. b) 1,5 g, c) 3,0, y d) 4,5. Para comparar, se ha incluido el termograma de la magnetita pura (a).

Otro aspecto importante a destacar acerca del ferrofluido obtenido es su estabilidad. En ausencia de sales, el ferrofluido mantenido a temperatura ambiente y en el refrigerador a tres pH diferentes (5,0, 6,0 y 7,0) se ha mantenido estable durante un período cercano a tres años. El seguimiento de la estabilidad se ha establecido determinando periódicamente el radio hidrodinámico, no observando cambio alguno en este valor ni la existencia de floculación o precipitación. La magnetización también

se ha mantenido sin cambios significativos. El ferrofluido también ha sido estable en disoluciones amortiguadoras de Good, tales como el HEPES. Sin embargo, se observa agregación del ferrofluido en presencia de NaCl 37,5 mM. Es importante indicar que la tolerancia a la sal de las partículas magnéticas no estabilizadas es muy baja (Tombácz et al. 2008). Este hecho que, en un principio, podría constituir una desventaja, le confiere, en sí, un gran valor añadido, ya que si este ferrofluido se ha de encapsular en liposomas, la purificación de los magnetoliposomas, usualmente realizada por diálisis o por cromatografía de exclusión molecular (con el consiguiente consumo de tiempo y dilución de la muestra) se simplifica enormemente ya que la simple adición de NaCl a los magnetoliposomas sin purificar, precipita el ferrofluido no encapsulado dejando intactos los liposomas que encapsulan las partículas magnéticas. La separación se consiguirá simplemente mediante una centrifugación suave.

Por lo que respecta al otro tipo de partícula magnética sintetizada, los magnetoliposomas, se ha estudiado la optimización de la encapsulación de un ferrofluido aniónico comercial y del ferrofluido obtenido con PEG en liposomas. Se han utilizado dos métodos de síntesis: hidratación de la película y posterior extrusión por filtros de policarbonato, el primero, y técnica de evaporación en fase reversa seguida de extrusión, el segundo. El segundo método ha producido las tasas de encapsulación más elevadas y es el método que, desde el estudio realizado, se utiliza en nuestro grupo. Además, se ha determinado la composición de fosfolípido/magnetita óptima, y, posteriormente a los trabajos publicados, se ha comprobado que la inclusión de colesterol favorece el proceso de extrusión. En cualquiera de los dos métodos estudiados, los magnetoliposomas purificados son de tamaño alrededor de 200 nm. Así, en el método escogido de fase reversa + extrusión, se observó después de la extrusión un único pico centrado en 187 nm, y después de la purificación, la distribución se estrechó y se desplazó hacia 218 nm, coincidiendo con el valor del tamaño que se determino por TEM, indicando que se ha eliminado el ferrofluido no encapsulado de la muestra de magnetoliposomas, y que la distribución obtenida de la muestra sin purificar es el resultado de la superposición de las distribuciones de ferrofluido y los liposomas.

4.2. Aplicaciones biomédicas de las nanopartículas magnéticas: hipertermia y termoablación

El reto en los tratamientos terapéuticos de procesos cancerosos mediante hipertermia/ablación es lograr el calentamiento local del tumor hasta temperaturas terapéuticas (paradójicamente las que producen la muerte celular), sin dañar el tejido sano que se encuentra alrededor. Las nanopartículas de magnetita generan calor

cuando éstas se someten a un campo magnético externo. El calor se produce por la combinación de diferentes mecanismos, perdidas de histéresis, relajaciones de Néel y Brown. Con las nanopartículas magnéticas (magnetoliposomas y ferrofluido) se realizaron dos estudios basados en los procesos de terapia hipertérmica: la hipertermia propiamente dicha y la termo-ablación. El sistema utilizado para generar calor fue, por una parte, un aplicador de radiofrecuencia (guía de onda de RF) y, por otra, una antena de microondas. Teniendo en cuenta de que la temperatura corporal media es de 37 ˚C, cualquier incremento de temperatura igual o mayor a 7 ˚C, se considera capaz de generar los efectos terapéuticos deseados. En el caso de ablación, un incremento por encima de los 13˚C se considera adecuado para la ablación térmica. Los aplicadores, tanto la antena de microondas como la guía de onda de RF, son capaces de generar campo eléctrico y magnético; el primero interactúa con las propiedades dieléctricas de los tejidos modificando la permitividad y la conductividad de los mismos. Contrariamente, las propiedades magnéticas de los tejidos son muy débiles e incapaces de producir una respuesta a la acción de los aplicadores de radiofrecuencias o microondas. Sin embargo, la presencia de las nanopartículas magnéticas permite que, a través de la interacción del aplicador con estas, se genere una cantidad adicional de calentamiento; es decir, actúan como potenciadores del efecto de calentamiento y, además, sólo actúan en la zona inmediatamente circundante a las partículas, concentrando el efecto en el tumor.

Tal como se ha indicado, para medir los incrementos de temperatura producidos por la guía de onda o por la antena se utilizaron sustitutos de tejidos semisólidos, conocidos como *phantoms*. Este tipo phantoms se utilizan para evitar pérdidas de calor debidas al fenómeno de convección (debido al transporte de calor de las corrientes ascendentes y descendentes del fluido) que se presentan en phantoms líquidos.

De acuerdo con los procedimientos de diseño de phantoms descritos en los artículos 2 y 3, se realizaron diversas pruebas para observar el comportamiento de las propiedades dieléctricas al incorporar la agarosa (es utilizada para solidificar el phantom) y añadiendo las cantidades adecuadas del agua destilada, etanol y NaCl, obtener la permitividad relativa y la conductividad eléctrica semejantes a los tejidos reales a simular para cada experimento. Se diseñaron también los phantoms de carcinoma con NPMs que fueron incrustados en el interior del phantom de músculo. Estos son el resultado de mezclar las NPMs con agarosa, con la finalidad de proporcionar las propiedades del carcinoma a las NPMs y además para facilitar su manejo y la colocación en el lugar deseado dentro del phantom.

En el artículo 2 se muestra que se realizó un estudio previo en el que se determinó la frecuencia de trabajo. La frecuencia escogida fue de 224 MHz, ya que fue la frecuencia que concentró una mayor energía sobre el ferrofluido, y los incrementos de temperatura alcanzados fueron mayores que los obtenidos con las otras dos

frecuencias. Los resultados obtenidos de los incrementos de temperatura en función del tiempo para cada una de las diferentes concentraciones de magnetita utilizadas, y colocadas a diferentes distancias del aplicador, muestran que los incrementos de temperatura fueron progresivamente menores conforme incrementaba la distancia del ferrofluido al aplicador.

En el artículo 3 se realizó un estudio de focalización de la energía generada mediante una antena de microondas de dos sistemas de NPMs diferentes; magnetoliposomas y ferrofluido. La temperatura registrada durante el tratamiento aumentó, aunque no de forma lineal, cuando se aumentó la concentración de NPMs dentro de la esfera. Por otro lado, el cálculo de la SAR demuestra la utilizad de las NPMs, ya que los valores más altos de la SAR van asociados al incremento de concentración de ferrofluido. Comparando los dos tipos de nanopartículas, los magnetoliposomas logran el aumento de la temperatura deseada a una concentración de magnetita menor que el ferrofluido solo.

4.3. Aplicaciones biomédicas de las nanopartículas magnéticas: Biodistribución y direccionalidad magnética

En los artículos 1 y 4, se ha estudiado la biodistribución de los magneto liposomas, en ausencia de campo magnético (artículo 1), y en presencia de un campo magnético externo, un campo magnético de 600 mT (artículo 4). En ambos casos el modelo animal han sido ratones hembra a los que se había inducido un foco inflamatorio en el lomo. Los magnetoliposomas se administraron intravenosamente por la vena yugular.

La reacción inflamatoria es uno de los mecanismos de defensa del cuerpo. Cuando ocurre el daño, el flujo sanguíneo se incrementa primero en el punto de la lesión, y los vasos sanguíneos se ensanchan para permitir que el oxígeno, agentes de coagulación y los glóbulos blancos de la sangre puedan penetrar en los tejidos dañados. Dado que el tamaño de los glóbulos blancos oscila entre 7 y 20 micras, las nanopartículas pueden pasar fácilmente a través de los vasos y llegar a la zona de la inflamación.

Mediante el uso de este modelo de inflamación y excluyendo a los animales con niveles de hierro y volúmenes de exudados que están fuera del rango de valores medios observados durante la inflamación, se aseguró una población bastante homogénea para el estudio del efecto de un campo magnético externo en la distribución de magnetoliposomas después de su inyección intravenosa.

Se observó la acumulación de magnetoliposomas en el foco de inflamación (exudados) y, al mismo tiempo, la disminución en el plasma, hígado y el bazo. Esta distribución se acentuó más en presencia de campo magnético externo, validando el uso de este tipo de NPMs, los magnetoliposomas, como partículas con propiedades de ser dirigidas

hacia zonas determinadas mediante agentes externos. Así, pueden diseñarse NPMs que contengan un fármaco, y éstas se pueden concentrar en el lugar deseado con la ayuda de la aplicación de un campo magnético externo. Los fármacos pueden ser entonces liberados en la zona deseada durante un largo periodo de tiempo. Esto mejoraría la eficacia del tratamiento permitiendo la administración de dosis más bajas y reduciendo la toxicidad sistémica.

Finalmente, es conveniente citar dos aspectos de las NPMs indicados que no han quedado reflejadas en los artículos presentados y sobre los que se hicieron unos estudios previos que, por diversos motivos, no se concluyeron o están en fase de realización por otros miembros del grupo. Por una parte, las NPMs sirven como modelo físico en donde estudiar procesos como la agregación, y, por otra parte, las NPMs pueden interaccionar con las plaquetas, y esta interacción puede dar lugar a un número importante de aplicaciones.

En el primer caso, se ha realizado un estudio cinético y estructural a fin de investigar la respuesta de las nanopartículas ante un campo magnético controlable (García-Jimeno et al. 2010). Mediante dispersión elástica y dinámica de la radiación se comprobó la cinética de agregación y la estructura del agregado de NPMs inducido por un campo magnético de magnitud controlable. Se demostró que la estructura final del agregado era fractal, con una dimensión fractal que decrecía al incrementar la intensidad del campo magnético. La cinética de agregación también dependió de la intensidad de campo magnético presentando un comportamiento inicial escalado que se acopló a la estructura fractal. Finalmente, la evolución temporal del tamaño del agregado mostró efectos de fragmentación. Mientras que la agregación inducida por un campo magnético de baja intensidad era reversible, la provocada por un campo magnético de elevada intensidad fue irreversible. Por medio de microscopia óptica se demostró la estructura lineal de los agregados de NPMs inducidos por el campo magnético (Figura 2).

En el segundo caso, se comprobó que las NPMs sintetizadas son un sistema muy adecuado para marcar plaquetas (marcaje magnético), evitando el uso de radiomarcadores para hacerlo. Las plaquetas pueden incorporar NPMs por endocitosis, y una vez en el interior las NPMs pueden servir para visualizar células in vivo por análisis de MRI. Las imágenes que se han obtenidos después de incubar plaquetas con nuestras NPMs (Figura 3) posibilitan el inicio de estudios encaminados a profundizar en la interacción plaqueta-NPMs.

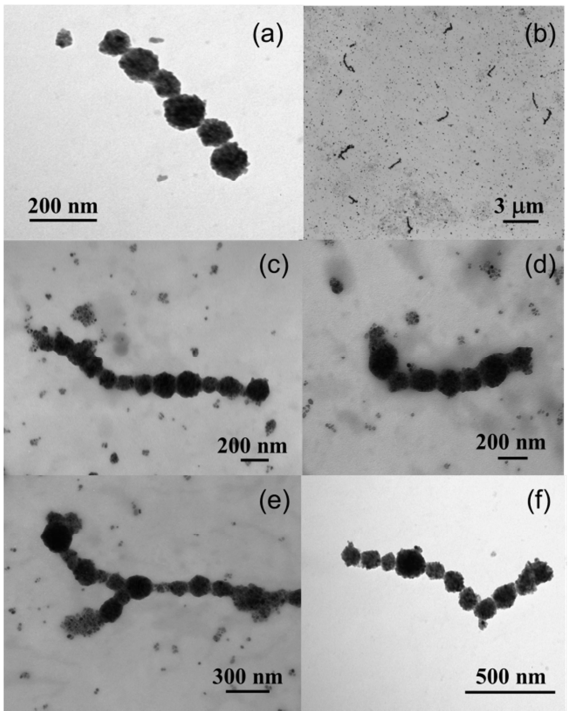

Figura 2. Agregados micrométricos inducidos por un campo magnético intenso (80 mT). La agregación fue irreversible ya que las micrografías fueron tomadas después de quitar el campo magnético. Esta agregación permanente se fundamenta en la fuerte atracción de Van der Waals entre las bicapas fosfolipídicas. Aunque se observan algunas figuras ramificadas (e.g. Fig (e)), los agregados presentan esencialmente una estructura lineal de acuerdo con las medidas de dispersión estática de la radiación.

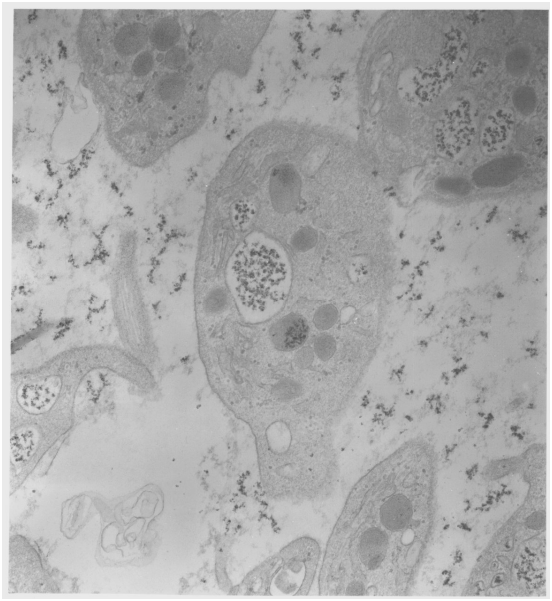

Figura 3. Micrografía de TEM de plaquetas incubadas con magnetoliposomas. Se observa la presencia de las partículas magnéticas principalmente en el sistema canalicular abierto (Micrografía obtenida por Ginés Escolar del Servei d'Hemostàsia i Hemoteràpia del Hospital Clínic de Barcelona).

5. Conclusiones

5. Conclusiones

Se han obtenido magnetoliposomas por encapsulación de un ferrofluido en liposomas empleando el método de fase reversa seguida de extrusión. Estos liposomas presentaban un diámetro de partícula de unos 200 nm, eran superparamagnéticos, y muy estables.

Se ha obtenido un ferrofluido por co-precipitación de sales férricas en presencia de PEG en medio básico. El PEG no estaba modificado y su interacción con la magnetita es de tipo físico. Se ha establecido el papel que juegan tanto la cantidad y el peso molecular del PEG como los parámetros asociados al proceso de síntesis. Se han obtenido nanopartículas de magnetita con un tamaño medio de 15 nm, observándose que el tamaño de partícula aumenta cuanto mayor es la cantidad de PEG utilizada (menor relación Fe:PEG).

Se ha estudiado el efecto de hipertermia y termo-ablación inducida de estas NPMs en phantoms, que constituyen sustitutos de tejido con propiedades dieléctricas y de permitividad semejantes a los tejidos reales. Se comprobó el funcionamiento de los aplicadores, guía de onda y antena de microondas, así como, el uso de las NPMs como potenciadores y como agentes para focalizar la energía en la zona deseada. Se demostró, que utilizando en conjunto el aplicador con las NPMs es posible focalizar la energía sobre el tumor evitando el calentamiento del tejido sano circundante, lograr incrementos de temperatura en el rango terapéutico y controlar los incrementos de temperatura en el tejido.

Se ha estudiado la biodistribución de los magnetoliposomas sintetizados en ratones a los que se les había inducido inflamación. Se confirmó que las NPMs se acumulan principalmente en foco inflamatorio sin la necesidad de dirigirlos mediante un campo magnético externo. En un segundo estudio se observo que, además, si se le aplica en la zona inflamatoria un campo magnético externo, la cantidad de NPMs aumenta en el exudado, y disminuye en sangre, hígado, y bazo. Esto demuestra que los magnetoliposomas pueden ser utilizados como vehículo de transporte, para dirigir fármacos a zonas de interés terapéutico, con lo que podríamos reducir la dosis de fármaco administrada y aumentar la eficacia del tratamiento y prevenir los efectos secundarios.

6. Referencias

6. Referencias

Akbarzadeh A., Samiei M., Davaran S., 2012. Magnetic nanoparticles: preparation, physical properties, and applications in biomedicine. *Nanoscale Res Lett*, **7**:144.

Arruebo M., Fernández-Pacheco R., Ibarra M.R., Santamaría J., 2007. Magnetic nanoparticles for drug delivery. *NanoToday*, 2, 22-32.

Azaroff L.V., Elements of X-ray Crystallography. McGraw-Hill: New York, USA, 1968.

Barrera C., Herrera A.P., Rinaldi C., 2009. Colloidal dispersions of monodisperse magnetite nanoparticles modified with polyethylene glycol. *J Colloid Interface Sci.*, **329**:107.

Batlle X. y Labarta A., 2002. Finite-size effects in fine particles: Magnetic and transport properties. J Phys D, 35, R15-R42.

Brullot W., Reddy N.K., Wouters J., Valev V.K., Goderis B., Vermant J., Verbiest T., 2012. Versatile ferrofluids based on polyethylene glycol coated iron oxide nanoparticles. *J Magn Magn Mater*., **324**:1919.

Butler R.F., Banerjee S.K., 1975. Theoretical single-domain grain size range in magnetite and titanomagnetite. *J Geophys Res*, 80, 4049-4058.

Chan H.T., Do Y.Y., Huang P.L., Chien T.S., Chan R.S., Liu C.Y., Huang S.Y., Yang H.E., Horng J., 2006. Preparation and properties of bio-compatible magnetic Fe_3O_4 nanoparticles. *J Magn Magn Mate*r., **304**:e415.

Choi H.S., Liu W., Misra P., Tanaka E., Zimmer J.P., Itty Ipe, B., Bawendi M.G., Frangioni J.V., 2007. Renal clearance of quantum dots. *Nat Biotechnol*, 25, 1165-1170.

Coey J.M.D., Magnetic properties of iron in soil iron oxides and clay minerals. In *Iron in soils and clay minerals*, (Dirigida por Stucki J.W., Goodman B.A. y Schwertmann U.), Reidel Publ., pp 397-466 (1988).

Cornell R.M. y Schwertmann U., *The Iron Oxides: Structure, Properties, Reactions, Occurrence and Uses*. Wiley VCH: Weinheim, Germany (1996).

Corot C., Robert P., Idee J.M., Port M., 2006. Recent advances in iron oxide nanocrystal technology for medical imaging. *Adv Drug Deliv Rev*, 58, 1471-1504.

Cullity B.D. *Introduction to Magnetic Materials*. Addison-Wesley: (EEUU) (1972).

Diederich C.J., 2005. Thermal ablation and high-temperature thermal therapy: overview of technology and clinical implementation. *Int J Hyperthermia*, 21, 745-753.

Duguet E., Vasseur S., Mornet S., Devoisselle J.M., 2006. Magnetic nanoparticles and their applications in medicine. *Nanomed*, 1, 157-168.

Frenkel J. y Dorfman J., 1930. Spontaneous and induced magnetisation in ferromagnetic bodies. *Nature,* 126, 274-275.

García-Jimeno S., Estelrich J., Callejas-Fernández, J., Roldán-Vargas, S., 2010. Aggregation of magnetic liposomes: A structural and kinetic study. En *International Soft Matter Conference 2010*, pp. 224. Universidad de Granada.

Gupta A.K., Wells S., 2004. Surface-modified superparamagnetic nanoparticles for drug delivery: preparation, characterization, and cytotoxicity studies. IEEE NanoBiosci, 3, 66-73.

Hanini A., Schmitt A., Kacem K., Chau F., Ammar S., Gavard J., 2011. Evaluation of iron oxide nanoparticle biocompatibility. *Int J Nanomed*, 6, 787-794.

Hergt R., Dutz S., Röder M., 2008. Effects of size distribution on hysteresis losses of magnetic nanoparticles for hyperthermia. *J Phys Condens Matter*, 20, 385214.

Ho D., Sun X., Sun S., 2011. Monodisperse magnetic nanoparticles for theranostic applications. *Acc Chem Rev* 44, 875-882.

Hildebrandt B., Wust P., Ahlers O., Dieing A., Sreenivasa G., Kerner T., Felix R., Riess H., 2002. The cellular and molecular basis of hyperthermia. *Crit Rev Oncol Hematol*, 43, 33-56.

Huber D.L., 2005. Synthesis, properties, and applications of iron nanoparticles. *Small*, 1, 482-501.

Jarrett B.R., Frendo M., Vogan J., 2007. Size-controlled synthesis of dextran sulfate coated iron oxide nanoparticles for magnetic resonance imaging. *Nanotechnology*, **18**:35603.

Jeng H.A., Swanson, J., 2006. Toxicity of metal oxide nanoparticles in mammalian cells. *J Environ Sci Health A*, 41, 2699-2711.

Jiles D., *Introduction to Magnetism and Magnetic Materials*. Taylor&Francis (EEUU). (1991)

Jordan A., Scholz R., Wust P., Fahling H., Felix R., 1999. Magnetic fuid hyperthermia (MFH): Cancer treatment with AC magnetic feld induced excitation of biocompatible superparamagnetic nanoparticles. *J Magn Magn Mater*, 201, 413-419.

Kawaguchi T., Hanaichi T., Hasegawa M., Maruno S., 2001. Dextran magnetite complex: conformation of dextran chains and stability solution. *J Mater Sci: Mater Med*., **12**:121.

Kittel C, 1946. Theory of the structure of ferromagnetic domains in films and small particles. *Phys. Rev*. 70, 965-971.

Larsen E.K., Nielsen T., Wittenborn T., Birkedal H., 2009. Size-dependent accumulation of PEGylated silane-coated magnetic iron oxide nanoparticles in murine tumors. *ACS Nano*, **3**:1947.

Laurent S., Dutz S., Hafeli U.O., Mahmoudi M., 2011. Magnetic fluid hyperthermia: focus on superparamagnetic iron oxide nanoparticles. *Adv. Colloid Interface Sci*, 166, 8-23.

Leslie-Pelecky D.L., Rieke R.D., 1996. Magnetic properties of nanostructured materials. *Chem Mater* 8, 1770-1783.

Lu A.H., Salabas E.L., Schuth F., 2007. Magnetic nanoparticles: synthesis, protection, functionalization, and application. *Angew Chem, Int Ed*, 46, 1222-1244.

Maeda H., Wu J., Sawa T., Matsumura Y., Hori K., 2000. Tumor vascular permeability and ttics: a rehe EPR effect in macromolecular therapeuview. *J Control Rel*, 65, 271-284.

Mailander V., Landfester K., 2009. Interaction of nanoparticles with cells. *Biomacromolec*, 10, 2379-2400.

Mitchell D., *MRI principles*. W. B. Saunders Company. Philadelphia, PA (2004).

Mornet S., Vasseur S., Grasset F., Duguet E., 2004. Magnetic nanoparticle design for medical diagnosis and therapy. *J Mater Chem*, 14, 2161-2175.

Nam J.M., Thaxton C.S., Mirkin, C.A., 2003. Nanoparticle-based bio-bar codes for the ultrasensitive detection of proteins. *Science* 301, 1884-1886.

Naqvi S., Samim M., Abdin M., Ahmed F.J., Maitra A., Prashant C., Dinda A.K., 2010. Concentration-dependent toxicity of iron oxide nanoparticles mediated by increased oxidative stress. *Int J Nanomed*, 5, 983-989.

Pankhurst, Q.A., Connolly, J., Jones, S.K., Dobson, J., 2003. Applications of magnetic nanoparticles in biomedicine. *J Phys D,* 36, R167-R181.

Paul K.G., Frigo T.B., Groman J.Y., Groman E.V., 2004. Synthesis of ultrasmall superparamagnetic iron oxides using reduced polysaccharides. *Bioconjugate Chem*., **15**: 394.

Raikher Y.L. y Shliomis M.I., 1974. Limiting Viscosity of Ferromagnetic Suspensions in a Strong Magnetic Field. *O predel ´Noi Vyazkosti Ferromagnitnykh Suspenzii V Sil´Nom Magnitnom Pole, 4*, 41-48.

Roca, A.G., 2009. Preparación de nanopartículas magnéticas uniformes y de alta cristalinidad para biomedicina. Tesis doctoral. Universidad Complutense de Madrid.

Rosensweig R.E., 2002. Heating magnetic fluid with alternating magnetic field. *J Magn Magn Mater*, 252, 370-374.

Saiyed Z., Telang S., Ramchand C., 2003. Application of magnetic techniques in the field of drug discovery and biomedicine. *Biomagn Res Technol*, 1, 2.

Schipper M.L., Iyer G., Koh A.L., Cheng Z., Ebenstein Y., Aharoni A., Keren S., Bentolila L.A., Li J., Rao J., Chen X., Banin U., Wu A.M., Sinclair R., Weiss S., Gambhir S.S., 2009. Particle size, surface coating, and PEGylation influence the biodistribution of quantum dots in living mice. *Small,* 5, 126-134.

Schweiger C., Pietzonka C., Heverhagen J., Kissel T., 2011. Novel magnetic iron oxide nanoparticles coated with poly(ethylene imine)-g-poly(ethylene glycol) for potential medical application: Synthesis, stability, cytotoxicity and MR imaging. *Int J Pharm.*, **408**:130.

Shubayev V.I., Pisanic II T.R., Jin S., 2009. Magnetic nanoparticles for theragnostics. *Adv Drug Deliver Rev,* 61, 467-477.

Weber C., Falkenhagen D. Specific blood purification by means of antibody-conjugate magnetic microspheres (pp. 371-378). En: *Scientific and clinical applications of magnetic carriers* (dirigida por U. Häfeli et al.). Plenum Press, New York (1997).

Weissleder R., Stark D.D., Engelstad B.L., Bacon B.R., Compton C.C., White D.L., Jacobs P., Lewis J., 1989. Superparamagnetic iron oxide: pharmacokinetics and toxicity. AJR *Am J Roentgenol*, 152, 167-173.

Yoo D., Lee J.-H., Shin T.-H., Cheon J., 2011. Theranostic magnetic nanoparticles. *Acc Chem Res*, 44, 863-874.

Yue-Jian C., Juan T., Fei X., Jia-Bi Z., Ning G., Yi-Hua Z., Ye D., Liang G., 2010. Synthesis, self-assembly, and characterization of PEG-coated iron oxide nanoparticles as potential MRI contrast agent. *Drug Dev Ind Pharm*, 36, 1235-1244.

Zhou H., Tao K., Ding J., Zhang Z., Sun K., Shi W., 2011. A general approach for providing nanoparticles water-dispersibility by grinding with poly (ethylene glycol). *Coll. Surf. A*., **389**:18.